

AD-A229 503

<b>REPORT DOCUMENTATION PAGE</b>			Form Approved OMB No. 0704-0188	
<small>Public reporting burden for this collection of information is estimated to average 1 hour per response, including the time for reviewing instructions, searching existing data sources, gathering and maintaining the data needed, and completing and reviewing the collection of information. Send comments regarding this burden estimate or any other aspect of this collection of information, including suggestions for reducing this burden, to Washington Headquarters Services, Directorate for Information Operations and Reports, 215 Jefferson Davis Highway, Suite 1204, Arlington, VA 22202-4302, and to the Office of Management and Budget, Paperwork Reduction Project (0704-0188), Washington, DC 20503.</small>				
AGENCY USE ONLY (Leave blank)	2. REPORT DATE 14 Nov 1990	3. REPORT TYPE AND DATES COVERED Final Report/1 Jul 87-30 Jun 90		
4. TITLE AND SUBTITLE EXPERIMENTAL RESEARCH ON HIGH GRADIENT ACCELERATION BY WAKEFIELDS IN AN ELLIPTIC CAVITY AT THE UTA WAKE FIELD TEST FACILITY		5. FUNDING NUMBERS 61102F 7301 AB		
6. AUTHOR(S) K. W. Chen		8. PERFORMING ORGANIZATION REPORT NUMBER AFOSR-TR-90-1153		
7. PERFORMING ORGANIZATION NAME(S) AND ADDRESS(ES) Texas A & M Research Center Box 3578 College Station, TX 77843		10. SPONSORING / MONITORING AGENCY REPORT NUMBER AFOSR-87-0290		
9. SPONSORING / MONITORING AGENCY NAME(S) AND ADDRESS(ES) AFOSR/NP Bolling AFB DC 20332-6448		11. SUPPLEMENTARY NOTES		
12A. DISTRIBUTION / AVAILABILITY STATEMENT Approved for public release; distribution is unlimited.		12B. DISTRIBUTION CODE		
13. ABSTRACT (Maximum 200 words)  An analytical method was developed to calculate the wake-fields in a metallic elliptical pillbox cavity. Results agreed well with computer simulations (3D) and with experimental data. A novel electrostatic probe to measure the wake-fields directly was also developed.				
14. SUBJECT TERMS		15. NUMBER OF PAGES 07		
		16. PRICE CODE		
17. SECURITY CLASSIFICATION OF REPORT UNCLASSIFIED	18. SECURITY CLASSIFICATION OF THIS PAGE UNCLASSIFIED	19. SECURITY CLASSIFICATION OF ABSTRACT UNCLASSIFIED	20. LIMITATION OF ABSTRACT UL GAD	

DTIC  
ELECTE  
NOV 29 1990  
S B D

FINAL TECHNICAL REPORT OF RESEARCH PERFORMED  
UNDER GRANT NO. AFOSR-87-0280

Submitted to the Air Force Office of Scientific Research

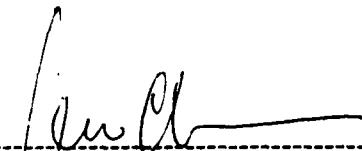
by

Center for Accelerator Science and Technology  
The University of Texas at Arlington  
Arlington, TX 76019

Submitted by 4FOSR-TR. 00 1153

K. W. Chen  
Principal Investigator

October 20, 1990

  
-----  
Authorizing Signature  
K. W. Chen  
The University of Texas at Arlington  
October 20, 1990

  
-----  
University of Texas at Arlington  
Date  
  
-----  
Texas A & M Research Foundation  
Date 11/02/90

## Table of Contents

### I. Research Summary

### II. Research performed by Category

- (1) A Study of Wake-Field Acceleration
- (2) A Study of Dielectric Wake-Field
- (3) Computer Code Development for an Elliptical Pillbox Cavity
- (4) Development of a Wake-Field Measurement System
- (5) Study of Soft x ray Free Electron Laser Scheme
- (6) Development of a Laser Photocathode for the Generation of High Current Short Electron Bunch

### III. Personel Working on the Program

### IV. Summary of Publications

- (1) Journal Publications
- (2) Conference Publications
- (3) Internal Reports
- (4) Thesis Completed

### V. Conclusions

### VI. Appendices

- (1) Particle Accelerator Journal Article
- (2) Journal of Applied Physics Article
- (3) Thesis



Accession For	
NTIS GRA&I	<input checked="" type="checkbox"/>
DTIC TAB	<input type="checkbox"/>
Unannounced	<input type="checkbox"/>
Justification	
By _____	
Distribution/	
Availability Codes	
Dist	Avail and/or Special
A-1	

## I. Research Summary

This final report summarizes research activities performed by the Center for Accelerator Science and Technology of the University of Texas at Arlington during the period of July 1, 1987 and June 30, 1990 under Grant No. AFOSR-87-0280. The main goals of the successful research program are to provide theoretical basis to analyze the wake-fields in the elliptically shaped wake-field cavity, and to examine the feasibility of applying the new idea of wake-field acceleration to beams of lasers. The theoretical research is very important due to the world-wide interest in finding new acceleration principles with higher accelerating gradients suitable for future particle accelerators. In particular, very exciting and new experimental results from Argonne National Laboratory seems to indicate that wake field acceleration is indeed a very viable alternative for this endeavor.

Although our own experimental work has not been completed in the period due to primarily an inadequate experimental support for the 20 MeV electron linac as noted on the technical report of July, 1990, a great deal was accomplished in the theoretical analysis. We hereby report the research activities undertaken during this period. The research performed under this contract is divided into six categories and main achievements in each category are as follows.

(1) Investigation of wake-field acceleration using the elliptical wake-field cavity.

Our theoretical works on this subject were very successful and major progress has been made. An analytical method was developed to calculate the wake-fields in a metallic elliptical pillbox cavity. By solving sets of the Maxwell's equations in the transformed plane, we were able to express the

wake-fields analytically. This analytic method simplifies the wake-fields calculation significantly, and we can readily optimize the cavity design without much computational efforts. Our analysis was shown to agree extremely well with data of existing 3-D computer code as well as with experimental data presented recently by the Argonne group. This work was well recognized and published in the refereed journal (Particle Accelerators). Modal analysis has been extended to include the effects of arbitrary sized beam aperture in a cavity. Excellent agreement between the experimental data and our analysis was demonstrated. The second work was also published in refereed journal (J. of Applied Physics, in progress).

(2) Theoretical study of dielectric wake-field cavity

It is found that the dielectric-lined elliptical wake-field cavity will yield an acceleration gradient of the same order of magnitude that can be obtained with a metallic cavity, and the deflection modes are suppressed if the energy of the driving beam is sufficiently high. This new acceleration scheme provides a simple solution to the transverse instability problem in the wake-field acceleration.

(3) Computer code development for a wake-field cavity analysis

Based on the theoretical analyses developed here, very efficient and time saving computer codes are developed.

(4) Development of wake-field measurement system

A novel electrostatic probe to measure the wake-fields directly was developed. It was shown that we can measure with reasonable accuracy the

strength of the wake potentials in a cavity without using an expensive energy analyzing magnet and beam manipulating equipments.

(5) Application of Wake field cavities: Study of a soft x-ray laser scheme

This work deals with an application of the elliptical wake-field cavity. We have performed pioneering analysis for applying the wake-fields generated in an elliptical cavity as an electric wiggler in free electron lasers. Theoretical study of a soft x-ray EFEL scheme using two-beam elliptical pillbox wake-field cavity has been conducted. It is found that the scheme provides sufficient gain as a coherent radiation source down to the x-ray regime. Our work was presented in a number of published and refereed articles.

(6) Development of a laser photocathode

The design and construction of a laser photocathode was conducted for a use as an intense, short electron beam source for the wake-field acceleration study. Numerical study of optimal cathode geometry was conducted and beam currents were measured. It was demonstrated that this type of photoemitter can be used as an efficient short, intense electron beam source for a compact linac design.

## II. Research Performed by Category

In the following, we describe in detail the six research tasks we accomplished. First we list the publications in which the results were presented in detail. A summary of the results is then given.

### Task 1:

#### Investigation of wake-field acceleration using the elliptical wake-field cavity.

Purpose: to develop a rigorous and theoretical basis to calculate the wake-fields in an elliptical cavity.

Publications to-date:

1. J. S. Yang and K. W. Chen, An analytical solution of wake-fields in an elliptical pillbox cavity, will appear on Particle Accelerators, Vol 23, 1990.

2. S. H. Kim, K. W. Chen and J. S. Yang, Madal analysis of wake-fields and its application to elliptical pillbox cavity with finite aperture, will appear on Nov. 1, 1990 issue of J. of Applied Physics.

3. J. S. Yang and K. W. Chen, Wake potential in a semi-elliptic pillbox cavity, on Advanced Accelerator Concepts, AIP conference proceedings 193, Lake Arrowhead, CA 1989.

4. K. W. Chen and S. H. Kim, Wake-field acceleration and compact accelerator considerations, SPIE Vol. 875 (SPIE, Bellingham, WA 1988), pp. 223-233.

### Results

Theoretical study on the wake-field generation using the elliptical cavity has been conducted. Major progress has been made in this study: development of an analytical method, and analysis of cavity with arbitrary sized aperture. It was known from theoretical and experimental works that the impedance, which

is the Fourier transformation of the wake-fields, of a closed cavity and that of a cavity with finite aperture are practically the same at the low frequencies. Therefore, the long range wake-fields of a short bunch or the wake-fields of a very long bunch are almost the same for these two different structures. Since the wake-field acceleration scheme requires a very short, intense driving bunch to excite acceleration fields of the order of 100 MeV/m and, furthermore, delay distance between the driving and trailing beam is very large compared to the bunch length, we can estimate with good accuracy the wake potentials of the most practical cavities by neglecting aperture effects. Under this assumption and using the coordinates transformation, we were able to express the wake-fields and wake potentials of an elliptical cavity analytically. With this analytical method, we can easily estimate maximum energy gain of the accelerated particles, and simplify the optimization of the cavity design without time consuming 3-dimensional computation. It is demonstrated that our analysis agrees extremely well with that of existing computer code WELL.

Although aperture effects are not serious for the long range wake-fields as long as aperture is small compared to the cavity cross section, we have to consider its effects to calculate the short range wake-fields or to estimate the energy loss of the driving beam and to consider the beam dynamics calculation. For this purpose, the theoretical analysis was expanded significantly to extend the modal analysis methods to include the effects of arbitrary apertures in the cavity. A complete modal analysis was carried out by using the Floquet's theorem and an obvious requirement that the energy gain over all acceleration cavity of repeating structure must be proportional to the number of pillboxes. In addition, by assigning proper boundary conditions on the apertures and considering the parity and continuity of the fields at the aperture, the formalism

to determine the Fourier coefficients for the repeating structure consisting of many pillbox cavities with arbitrary aperture was derived. The results of this analysis were compared with experiments done by the Argonne Group. An excellent agreement between the experiment data and our analysis was demonstrated as in publication 2.

## **Task 2**

### Study of wake-Fields excited in the dielectric structure

Purpose: to investigate the effects of dielectric material in the elliptical cavity for a use as a wake-field device.

Publications:

1. J. S. Yang and K. W. Chen, Wake-fields in a dielectric-loaded elliptical waveguide, submitted to Particle Accelerators for publication, July, 1990.

### Results

The wake-field acceleration scheme using dielectric-lined elliptical cavity was conducted. It is well known that the electron beam loses energy and excite slow EM waves (Cerenkov radiation) behind when it passes through a dielectric-lined structures. The dielectric structure can be used as a wake-field device as well as other applications such as storage cell, energy modulator, etc. It was shown experimentally by Argonne group that the dielectric-lined circular cavity has great advantages over other wake-field schemes; acceleration gradient is of the same order of magnitude that can be achieved with metallic cavity and the transverse wake potential can be made quite small for the ultra-relativistic driving beam. The proof-of-principle of acceleration by the wake-fields generated in the circular dielectric structure has been experimentally demonstrated by the Argonne group. However, it was not clear whether the

transverse modes are also suppressed in the elliptical dielectric cavity as in the circular cavity. Extraction and re-acceleration of driving beam can be simplified significantly if the driving beam and accelerated beam pass through different paths. Here, we extend the idea of acceleration using dielectric-lined elliptical cavity to suppress the transverse deflection modes and still provide staging capability. The investigation of the wake-fields excited in the elliptical dielectric cavity was carried out. Sets of the Maxwell's eqs. are solved analytically in the transformed plane. It was shown that only fundamental modes are excited in the dielectric structure, and all the higher modes and transverse deflecting modes are inversely proportional to the square of the driving beam energy. This property of lack of the transverse modes is a unique feature of a dielectric structures. The model calculation showed that this cavity can be used as a wake-field acceleration device which has a large acceleration gradient of the order of 100 MeV/m, no appreciable transverse forces, and still provides the easy staging capability. Excellent agreement with the Argonne wake-field experiment was demonstrated.

### **Task 3**

#### Computer Codes Development for an Elliptical Pillbox Cavity

Publications: J. S. Yang, Results of a PC-based wake-field code, CAST internal report CAST-89-0115

#### Results

As a result of the theoretical works developed here, a simple and efficient numerical code was developed to calculate all the resonant modes and loss parameters of an elliptical pillbox cavity. Excellent agreements with the 3-dimensional numerical code WELL as well as with experimental data were

demonstrated in publication 1.

#### **Task 4**

##### Development of a Wake-Field Measurement System

Purpose: to develop a method to measure the intensity of the wake-fields directly in an elliptical cavity.

Publications:

1. S. H. Kim and K. W. Chen, An electrostatic probe system for the measurement of wake-field in a two-beam elliptical pillbox cavity, submitted to Review of Scientific Instrumentation

##### Results

A unique system to measure the wake-fields generated in an elliptical cavity was developed. Utilizing the facts that wake-fields are predominated by a few lower order modes and the wavelength of the fundamental mode is of the order of the cavity size, an electrostatic probe with two conducting spheres can measure the longitudinal and transverse wake-fields of an elliptical cavity. The salient advantage of this probe system is deduced from the experimental result that the voltage amplitude at the oscilloscope is proportional to the wake-field amplitude. The wake-field is about 5 KV for 3 nC of driving charge for a cavity used in the Argonne group experiment. Since we can easily measure a 50 V pulse, which is the expected signal level from the probe for 0.03 nC driving charge of our linac, easily by an oscilloscope, this alleviates the need that a powerful buncher be installed to a system using a low-current injector or the need of a system using a witness bunch. This measurement procedure will simplify greatly the measurement and test system of the wake-field experiment.

## Task 5

### Theoretical Study of a Soft X-Ray Free Electron Laser Scheme

Purpose: to develop a soft x-ray laser

Publications:

1. S. H. Kim and K. W. Chen, Soft x-ray free electron laser using a two beam elliptical pill-box wake-field cavity, SPIE Vol. 875 (1988)
2. S. H. Kim, Free electron lasing in a longitudinal electric wave, Phys. Lett. 135A, 39 (1989)
3. S. H. Kim, Stimulated bremsstrahlung of soft x-ray in a two beam wake-field cavity, Proc. of International Conf. on Phenomena in Ionized Gases (ICPIG) XIX, Yugoslavia, 10-14 July (1989)
4. S. H. Kim, Free electron lasing in transverse undulating magnetic field, Phys. Lett. 135A, 44 (1989)

### Results

The lasing by stimulated bremsstrahlung of a relativistic dilute electron beam passing through a spatially periodic longitudinal electrostatic field (static electric wiggler) or a traveling undulating longitudinal electric field (traveling electric wiggler) was investigated. We found that the elliptical pillbox cavity is suitable to generate the traveling wiggler fields. If we inject the lasing electrons in the opposite direction of the driving beams which excite the wake-fields along the foci of the elliptic cavity, the lasing electrons are forced to emit the laser radiation by both the longitudinal and transverse wake-fields. This scheme is based on the fact that we can produce the longitudinal and transverse wake-fields whose amplitudes are more than 100 MeV/m in the elliptical pillbox cavity. Until the strength of the laser wave arrives that of the transverse wake-field excited by the driving beam, the transverse motion of the

lasing electrons is confined by the transverse wake-field, and both stimulated and unstimulated bremsstrahlung take place similar to the radiation in the conventional magnetic wiggler. It was shown that a laser using a traveling electric wiggler provides sufficient gain to be used as a coherent radiation source down to the soft x-ray regime. The gain increases with the inverse of the laser wavelength, while that of a conventional free electron laser using a transverse undulating magnetic field operating in the Compton regime decreases with the laser wavelength. This lasing scheme is entirely new and is quite important for workers in this field.

#### **Task 6**

##### Development of a laser photocathode for the generation of high current, short electron bunch

Purpose: To use in the wake-field acceleration and compact accelerator design study

Publications:

1. K. W. Chen, Y. C. Chae and J. Choi, Development of a laser photocathode for use in wake-field acceleration and compact accelerator design studies, SPIE Conf. on Innovative Science and Technology, Los Angeles, CA, SPIE Vol. 875 (SPIE, Bellingham, WA 1988)

#### Results

Experimental study of a back-illuminating short-pulse photocathode for a use as a short, intense electron source has been conducted. Thin films of Cs<sub>3</sub>Sb was deposited on the cathode using laser ablation method. The performance test of the constructed cathode was made with the Q-switched Nd-YAG laser pulse (532 nm) directed from the rear of the cathode surface. It was observed

that a current of  $2.5 \text{ mA/cm}^2$  is obtained at  $6 \text{ KV/cm}$  potential in a modest vacuum of  $10^{-7}$  torr. With subsequent improvements and refinements in design, it was demonstrated that use of this type can be extended to other compact linac designs for commercial applications.

### III. Personnel Participating in the AFOSR Program

Participants of the wake-field research program include: Dr. K. W. Chen, PI, and Dr. S. H. Kim, senior scientist and graduate students, Mr. J. S. Yang Y. C. Chae and J. Choi. Other research students involved in this program are T. Pham and N. Nguyen. Mr. Yang completed his Ph.D. degree in Mechanical Engineering in August 1990 with the support from this grant. Mr. J. Choi obtained a M.S. degree in Mechanical Engineering in 1988 and subsequently moved to the University of Wisconsin to pursue a Ph.D. degree. Mr. Chae has subsequently received a M.S. degree and has since moved to the University of Houston. He is currently pursuing his Ph.D. degree at the Argonne National Laboratory.

## V. Summary of Publications

### 1. Journal Publications

1. J. S. Yang and K. W. Chen, An analytical solution of wake-fields in an elliptical pillbox cavity, will appear on Particle Accelerators, Vol 23, 1990.
2. S. H. Kim, K. W. Chen and J. S. Yang, Madal analysis of wake-fields and its application to elliptical pillbox cavity with finite aperture, will appear on Nov. 1, 1990 issue of J. of Applied Physics.
3. S. H. Kim, Free electron lasing in a longitudinal electric wave, Phys. Lett. 135A, 39 (1989)
4. S. H. Kim, Free electron lasing in transverse undulating magnetic field, Phys. Lett. 135A, 44 (1989)
5. S. H. Kim and K. W. Chen, An electrostatic probe system for the measurement of wake-field in a two-beam elliptic pillbox cavity, submitted to Review of Scientific Instrumentation

### 2. Conference Publications

1. S. H. Kim, Stimulated bremsstrahlung of soft x-ray in a two beam wake-field cavity, Proc. of International Conf. on Phenomena in Ionized Gases (ICPIG) XIX, Yugoslavia, 10-14 July (1989)
2. J. S. Yang and K. W. Chen, Wake potential in a semi-elliptic pillbox cavity, on Advanced Accelerator Concepts, AIP conference proceedings 193, Lake Arrowhead, CA 1989.
3. K. W. Chen and S. H. Kim, Wake-field acceleration and compact accelerator considerations, SPIE Vol. 875 (SPIE, Bellingham, WA 1988), pp. 223-233
4. S. H. Kim and K. W. Chen, Soft x-ray free electron laser using a two beam elliptical pill-box wake-field cavity, SPIE Vol. 875 (1988)

5. K. W. Chen, Y. C. Chae and J. Choi, Development of a laser photocathode for use in wake-field acceleration and compact accelerator design studies, SPIE Conf. on Innovative Science and Technology, Los Angeles, CA, SPIE Vol. 875 (SPIE, Bellingham, WA 1988)

### 3. Internal Reports and Publications

1. CAST-88-0013, Status report on UTA Linac installation and testing
2. CAST-89-0810, Wake-fields in a dielectric loaded elliptic waveguide
3. CAST-88-0304, Radiation shielding structure design and radiation safety adequacy considerations
4. CAST-89-0115, Results of a PC-based wake-field code

### 4. Thesis Completed

1. J. Choi, M.S. Thesis, "Design and construction of a high current electron injector utilizing laser back-illuminated photoemission", June 1988, Mechanical Engineering Department.
2. J. S. Yang, Ph.D. Dissertation, "Wake-field Acceleration of Charged Particles With an Elliptical Cavity", August 1990, Mechanical Engineering Department.

## V. Conclusion

The research on the wake-field acceleration with an emphasis on the use of elliptical cavities has been conducted. Major progress has been made in the analysis of the wake-fields in elliptical structures and its application for generation of laser beams. It was demonstrated that the use of elliptically shaped wake-field cavity offers promising way for reaching acceleration gradients of a few hundreds MeV/m, which is suitable for applications such as compact, high brightness linacs. The elliptic geometry allows us to simplify multi-stage accelerator design and to overcome the low transformer ratio and transverse

wake-fields problem. We can achieve much higher acceleration gradients by selecting optimal cavity geometry and beam distribution. With our analytical method, we can simplify the optimization of the cavity design without time consuming computational work. To verify our theoretical analyses, we compared the results with experimental data in circular wake-field cavities obtained by the Argonne group, and excellent agreement are demonstrated. Furthermore, it was shown that we can obtain the wake- fields in a circular cavity exactly from our analytical formula for the wake-fields in an elliptical cavity. Also, the results of our analytical method were compared with existing numerical code and very good agreement between these two methods are demonstrated.

APPENDICS

## THE ANALYTICAL SOLUTION OF WAKE-FIELDS IN AN ELLIPTICAL PILLBOX CAVITY

J. S. YANG and K. W. CHEN

*Center for Accelerator Science and Technology, The University of Texas at Arlington,  
Arlington, TX 76019*

*(Received June 26, 1990)*

The wake potential of a bunch of relativistic charged particles traversing an elliptical pillbox cavity is derived analytically in the limit of vanishing aperture. It is found that the resonant modes of an elliptical cavity can be expressed in terms of Mathieu functions. Calculation results are presented and compared with numerical ones.

### 1. INTRODUCTION

The wake-field produced by a bunch of relativistic charged particles in an elliptical pillbox cavity is important not only for future high gradient electron accelerators<sup>1</sup>, but also for a use as an electric wiggler for some proposed free electron laser schemes<sup>2</sup>. The suitability is based on the estimation that the acceleration gradient will exceed 100 MeV/m per  $\mu\text{C}$  of driving bunch charge, and on wavelengths of the order of a few centimeters.

The principle of acceleration by the wake-field generated in a metallic cavity has been experimentally verified<sup>3</sup>. Also, other wake-field acceleration schemes using a plasma medium<sup>4</sup> or a dielectric-loaded cavity<sup>5</sup> have been experimentally investigated. However, these wake-field schemes have not been demonstrated to have significantly larger acceleration gradient than that in a metallic cavity. Elliptical cavities have been investigated by several authors<sup>1,2,6,9</sup>. It was shown<sup>6,9</sup> that in elliptical cavities the transformer ratios are rather limited, and that a strong transverse wake-field, which might lead to beam instabilities, is also excited. However, we can overcome the low transformer ratio and the transverse deflection problem by using multi-stage schemes. Although the transformer ratio would not be as high, a wake-field accelerator not based on the impedance transformation principle could be achieved by using multi-stage schemes with short stages; the driving beam is replaced with a new one or replenished in energy after each stage. By rotating subsequent groups of cavities, the overall transverse deflection of the accelerated beam can be minimized.

The wake potential in an elliptical cavity can be obtained either by modal analysis or by numerically solving Maxwell's equations in the time domain. In the previous modal analysis<sup>7,8</sup>, the wake-field is expressed in a Fourier series based on the vector eigenfunctions of the unit pillbox. For infinitely repeating structures, the problem for

the entire acceleration cavity is reduced to that in a pillbox cavity by using Floquet's theorem on the periodicity. The modal analysis can be generalized to a cavity of arbitrary shape when we can calculate the resonant modes. For a cavity with finite apertures we should use numerical methods to find resonant modes accurately. Previously the wake-fields in an elliptic pillbox cavity with finite aperture were calculated using the numerical code WELL<sup>9</sup>, which directly solves Maxwell's equations in the time domain.

In this article, we do not take into account the aperture effect. The analytic solution which will be formulated in this article exists and is of interest, even though it is an approximation for the cavity with beam holes, since we can readily estimate the maximum energy gain of the accelerated particle. In view of these considerations, we try to obtain an analytic expression for the resonant modes in an elliptical pillbox cavity in the limit of vanishing aperture. Using the mode analysis, the longitudinal and transverse wake potentials are derived in terms of Mathieu functions. It is also shown that we can derive exactly the same expressions for the wake potentials in a circular cavity as in Ref. 7 when the ellipse tends to a circle.

## 2. ELLIPTIC PILLBOX CAVITY

### 2.1. Solution of Homogeneous Helmholtz Equation in an Elliptic Cavity

Consider an elliptic pillbox cavity as shown in Fig. 1. For a cavity of elliptic cross section, the eigenfunctions can be found in terms of known functions by transforming the Cartesian coordinates to the confocal elliptic coordinates as shown in Fig. 2. In these coordinates, boundary conditions on the elliptic cavity are readily satisfied. The

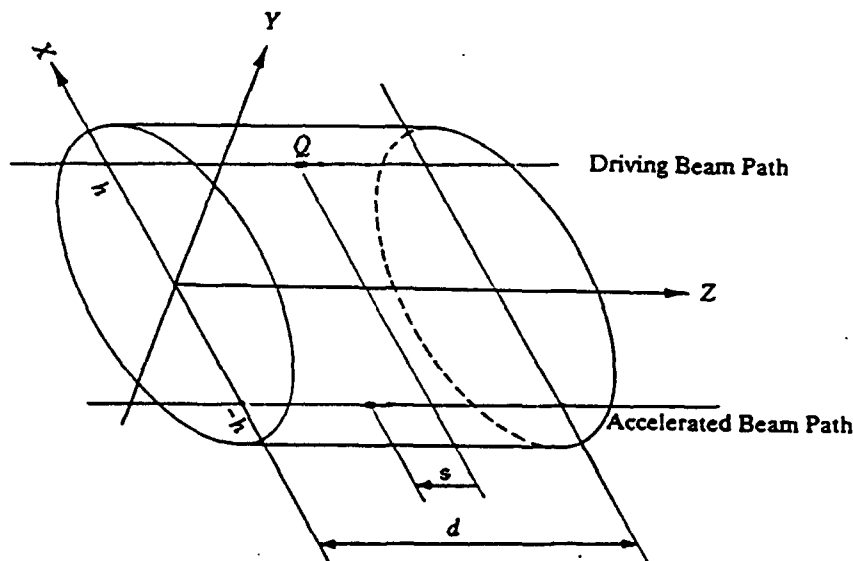


FIGURE 1 Elliptic pillbox cavity.

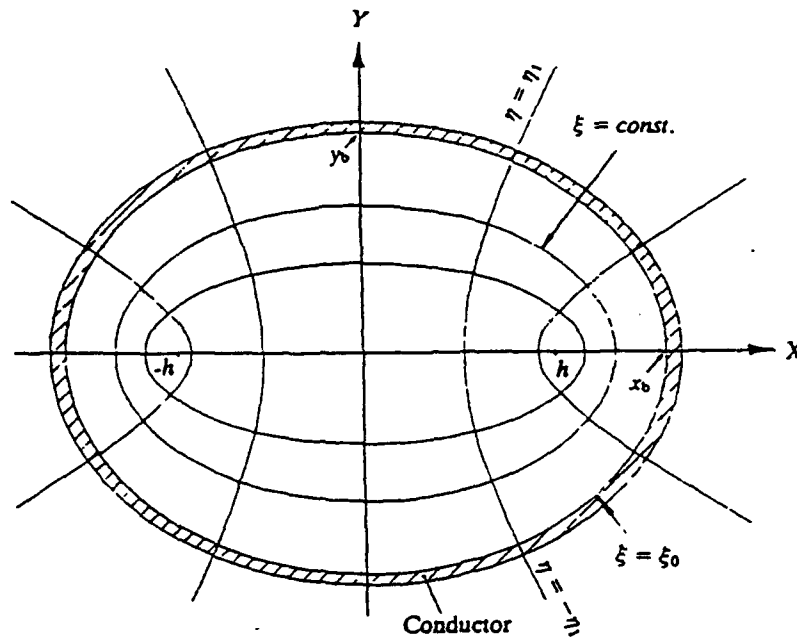


FIGURE 2 Confocal elliptical coordinates.

elliptic coordinate variables  $(\xi, \eta, z)$  are defined by<sup>10</sup>

$$\begin{aligned} X &= h \cosh \xi \cos \eta, \\ Y &= h \sinh \xi \sin \eta, \\ Z &= z, \end{aligned} \quad (1)$$

where  $h$  is the semi-interfocal distance.

The Helmholtz equation is then transformed to

$$\nabla^2 \Psi + \kappa^2 \Psi = \frac{1}{h^2(\sinh^2 \xi + \sin^2 \eta)} \left( \frac{\partial^2 \Psi}{\partial \xi^2} + \frac{\partial^2 \Psi}{\partial \eta^2} \right) + \frac{\partial^2 \Psi}{\partial z^2} + \kappa^2 \Psi = 0. \quad (2)$$

Following the method of separation of variables, we seek to find solutions of the form

$$\Psi(\xi, \eta, z) = f(\xi)g(\eta)w(z). \quad (3)$$

Substituting Eq. (3) into (2) and dividing by  $\Psi$ , Eq. (2) is split into three ordinary differential equations:

$$f''(\xi) - (a - 2q \cosh 2\xi)f(\xi) = 0, \quad (4)$$

$$g''(\eta) + (a - 2q \cos 2\eta)g(\eta) = 0, \quad (5)$$

$$w''(z) + \beta^2 w(z) = 0, \quad (6)$$

where  $2q = \gamma^2 h^2 / 2$ ,  $\gamma^2 = \kappa^2 - \beta^2$ , and  $a$  is an arbitrary separation constant. The above Eqs. (4) and (5) are called the Mathieu equations. The solutions of these equations are the Mathieu functions<sup>10</sup>.

## 2.2. Resonant Modes of a Cavity

For a closed elliptic pillbox cavity, we consider the solutions of

$$(\nabla_{\perp}^2 + \gamma^2)\psi(\xi, \eta) = 0 \quad (7)$$

in the region  $0 \leq \xi \leq \xi_0$  and  $0 \leq \eta \leq 2\pi$ , where  $\psi = E_z$  for a TM wave and  $H_z$  for a TE wave. Any combination of the product of the solution of Eqs. (4) and (5) is also the solution of Eq. (7). In addition to the boundary conditions, the following conditions must be satisfied:

(i) continuity of  $\psi$  on the interfocal line,

$$\psi(0, \eta) = \psi(0, -\eta), \quad (8)$$

(ii) continuity of gradient of  $\psi$  on the interfocal line,

$$\frac{\partial}{\partial \xi} (\psi(\xi, \eta))_{\xi=0} = -\frac{\partial}{\partial \xi} (\psi(\xi, -\eta))_{\xi=0}. \quad (9)$$

Among the possible combinations, the only permissible form of the solution which satisfies above two conditions is

$$\psi = \sum_{m=0}^{\infty} C_m C e_m(\xi, q) c e_m(\eta, q) + \sum_{m=1}^{\infty} S_m S e_m(\xi, q) s e_m(\eta, q), \quad (10)$$

with the factor  $\exp(j(\omega t - \beta z))$  being omitted. Here,  $C_m$  and  $S_m$  are arbitrary constants. The functions  $c e_m(\eta, q)$  and  $s e_m(\eta, q)$  are respectively the even and odd type Mathieu functions of the first kinds of integral order, and  $C e_m(\xi, q)$  and  $S e_m(\xi, q)$  are the modified Mathieu functions of the first kinds of integral order. These functions are given by<sup>10</sup>

$$c e_{2n}(\eta, q) = \sum_{r=0}^{\infty} A_{2r}^{(2n)} \cos 2r\eta, \quad (11)$$

$$c e_{2n+1}(\eta, q) = \sum_{r=0}^{\infty} A_{2r+1}^{(2n+1)} \cos (2r+1)\eta, \quad (12)$$

$$s e_{2n+2}(\eta, q) = \sum_{r=0}^{\infty} B_{2r}^{(2n+2)} \sin (2r+2)\eta, \quad (13)$$

$$s e_{2n+1}(\eta, q) = \sum_{r=0}^{\infty} B_{2r+1}^{(2n+1)} \sin (2r+1)\eta, \quad (14)$$

for  $n = 0, 1, 2, \dots$ , and the coefficients  $A$  and  $B$  are function of  $q$ . Modified Mathieu functions  $C e_m(\xi, q)$  and  $S e_m(\xi, q)$  have the same forms as in Eqs. (11)–(14) except  $\eta$ ,  $\sin$ , and  $\cos$  are replaced by  $\xi$ ,  $\sinh$ , and  $\cosh$  respectively.

We first notice that symmetry of  $\psi(\xi, \eta)$  is determined by  $c e_m(\eta, q)$  and  $s e_m(\eta, q)$ . From Eqs. (11)–(14) we see that the first term in Eq. (10) is an even function and the second term is an odd function with respect to  $\eta$ . Therefore, the second term in Eq. (10) is always zero on the median plane ( $y = 0$  plane) where wake potentials are to be evaluated, and does not contribute to the calculation of the longitudinal wake

potential. For this reason, we only consider the even-type modes of a TM wave,  $\psi_m = Ce_m(\xi, q)ce_m(\eta, q)$ , for the wake potential calculation.

The boundary conditions are:

$$\psi(\xi_0, \eta) = 0. \quad (15)$$

There remains the condition that no tangential component of electric field exists at the end-plate walls at  $z = 0$  and  $d$ , which is satisfied if we choose

$$\beta = \frac{p\pi}{d}, \quad p = 0, 1, 2, \dots \quad (16)$$

where  $d$  is the gap distance of the pillbox cavity shown in Fig. 1. From Eq. (15) we have

$$Ce(\xi_0, q) = 0. \quad (17)$$

Let  $q_{mn}$  be the  $n$ th root of Eq. (17) for mode  $m$ . Then we can calculate the resonant frequencies from the root  $q_{mn}$ . Combining  $2q = \gamma^2 h^2 / 2$  and  $\gamma^2 = \kappa^2 - \beta^2$ , the resonant frequencies are given by

$$\frac{\omega_{mnp}}{c} = \left\{ \frac{4q_{mn}^2}{h^2} + \left( \frac{p\pi}{d} \right)^2 \right\}^{1/2}. \quad (18)$$

The wavelength of the dominant mode is then given by

$$\lambda_{010} = \frac{\pi h}{\sqrt{q_{01}}} = \frac{\pi x_b e_c}{\sqrt{q_{01}}}, \quad (19)$$

where  $e_c$  and  $x_b$  are, respectively, the eccentricity and semi-major axis of the boundary ellipse. The ratio  $\lambda_{010}/x_b$  is plotted against  $e_c$  in Fig. 3. In this figure, we see that as  $e_c \rightarrow 0$ , i.e., as an ellipse tends to a circle, the ratio approaches 2.61, which is the ratio of wavelength to the radius,  $\lambda/r_0 = 2\pi/\chi_{01}$ , for the  $TM_{010}$  mode of a circular pillbox cavity of radius  $r_0$ , where  $\chi_{01}$  is the first zero of Bessel function  $J_0$ .

The field components are given by

$$E_{z_{mnp}} = Ce_m(\xi, q_{mn})ce_m(\eta, q_{mn}) \cos \frac{p\pi}{d} z, \quad (20)$$

$$E_{\xi_{mnp}} = -\frac{p\pi}{D_{mn}d} Ce'_m(\xi, q_{mn})ce_m(\eta, q_{mn}) \sin \frac{p\pi}{d} z, \quad (21)$$

$$E_{\eta_{mnp}} = \frac{p\pi}{D_{mn}d} Ce_m(\xi, q_{mn})ce'_m(\eta, q_{mn}) \sin \frac{p\pi}{d} z, \quad (22)$$

$$H_{\xi_{mnp}} = \frac{j\omega_{mnp}\epsilon_0}{D_{mn}d} Ce_m(\xi, q_{mn})ce'_m(\eta, q_{mn}) \cos \frac{p\pi}{d} z, \quad (23)$$

$$H_{\eta_{mnp}} = \frac{-j\omega_{mnp}\epsilon_0}{D_{mn}d} Ce'_m(\xi, q_{mn})ce_m(\eta, q_{mn}) \cos \frac{p\pi}{d} z, \quad (24)$$

$$H_z = 0, \quad (25)$$

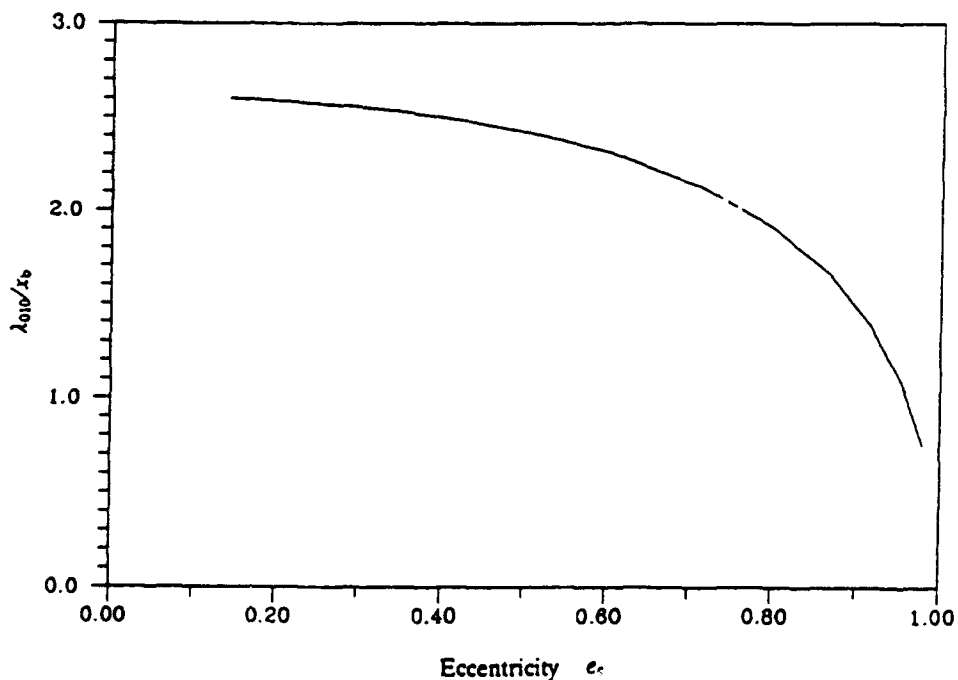


FIGURE 3 Plot of  $\lambda_{010}/x_b$  as a function of eccentricity.

where

$$D_{mn} = \frac{4q_{mn}}{h} \left\{ \frac{\cosh 2\xi - \cos 2\eta}{2} \right\}^{1/2} \quad (26)$$

The resonant mode patterns for some of the lower-order modes are shown in Fig. 4.

### 3. WAKE POTENTIAL CALCULATION

#### 3.1. Longitudinal Wake Potential

Consider the test charge which is traveling through the focus axis of an elliptic pillbox cavity ( $\xi = 0, \eta = \pi$ ) and trailing the driving charge  $Q$ , which is traveling through the other focus axis ( $\xi = \eta = 0$ ), by a fixed distance  $s$  in the  $z$ -direction. The delta function longitudinal wake potential  $W_z$  is defined as the energy gained by unit test charge. Bane et al.<sup>7</sup> obtained the wake potential as an infinite sum

$$\begin{aligned} W_z(s) &= 2 \sum_{\lambda} k_{\lambda} \cos \left( \frac{\omega_{\lambda} s}{c} \right) \\ &= \sum_{\lambda} \frac{V_{\lambda}^*(\mathbf{r}') V_{\lambda}(\mathbf{r})}{2u_{\lambda}} \cos \left( \frac{\omega_{\lambda} s}{c} \right), \quad \text{for } s > 0 \end{aligned} \quad (27)$$

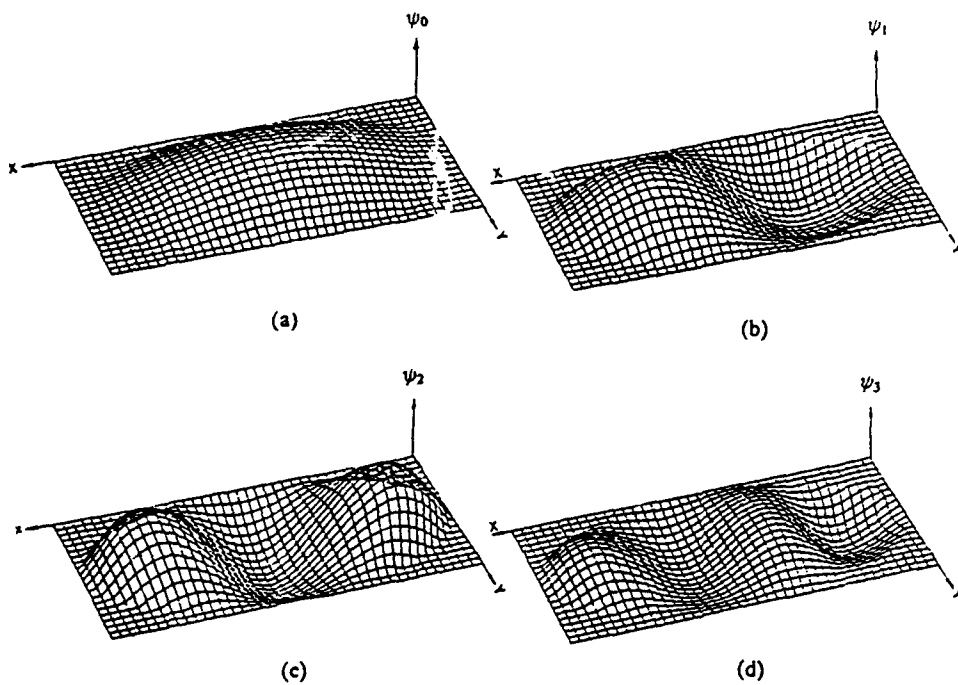


FIGURE 4 Configuration of resonant modes in an elliptic pillbox cavity. ((a)  $m = 0$ , (b)  $m = 1$ , (c)  $m = 2$ , (d)  $m = 3$ ).

where  $k_\lambda$  is the loss parameter and  $V_\lambda$  is the voltage induced by a point charge  $Q$ . The stored energy  $u_\lambda$  is given by

$$\frac{\epsilon_0}{2} \int \mathbf{a}_\lambda \cdot \mathbf{a}_{\lambda'} dV = u_\lambda \delta_{\lambda\lambda'}, \quad (28)$$

where  $\mathbf{a}_\lambda$  is the vector eigenfunction. The vectors  $\mathbf{r}'$  and  $\mathbf{r}$  represent, respectively, the transverse position of the path of the driving charge and that of the test charge. Using the field components in Eqs. (20)–(22), the voltage  $V_\lambda$  becomes

$$\begin{aligned} V_\lambda(\mathbf{r}) &= \int_0^d dz \exp\left(\frac{j\omega z}{c}\right) a_{\lambda_i}(0, 0, z) \\ &= C e_m(0, q_{mn}) c e_m(0, q_{mn}) \int_0^d dz \exp\left(\frac{j\omega z}{c}\right) \cos \frac{p\pi}{d} z, \end{aligned} \quad (29)$$

$$\begin{aligned} V_\lambda(\mathbf{r}) &= \int_0^d dz \exp\left(\frac{j\omega z}{c}\right) a_{\lambda_i}(\xi, \eta, z) \\ &= C e_m(\xi, q_{mn}) c e_m(\eta, q_{mn}) \int_0^d dz \exp\left(\frac{j\omega z}{c}\right) \cos \frac{p\pi}{d} z, \end{aligned} \quad (30)$$

and further

$$V_{\lambda}^* V_{\lambda} = \frac{2C_{mn} \left(\frac{\omega}{c}\right)^2}{\left(\left(\frac{\omega}{c}\right)^2 - \left(\frac{p\pi}{d}\right)^2\right)^2} \left(1 - (-1)^p \cos \frac{\omega_{mnp} d}{c}\right), \quad (31)$$

where  $C_{mn} = Ce_m(\xi, q_{mn}) Ce_m(0, q_{mn}) ce_m(\eta, q_{mn}) ce_m(0, q_{mn})$ .

The stored energy  $u_{\lambda}$  becomes

$$\begin{aligned} u_{mnp} &= \frac{\varepsilon_0}{2} \int \mathbf{a}_{\lambda} \cdot \mathbf{a}_{\lambda} dV \\ &= \frac{\varepsilon_0}{2} \frac{\left(\frac{\omega_{mnp}}{c}\right)^2}{\gamma_{mn}^2} \int Ce_m^2(\xi, q_{mn}) ce_m^2(\eta, q_{mn}) \cos^2\left(\frac{p\pi}{d} z\right) dV. \end{aligned} \quad (32)$$

After integration using  $dV = \frac{h^2}{2} (\cosh 2\xi - \cos 2\eta) d\xi d\eta dz$ , it is further reduced to

$$u_{mnp} = \frac{\varepsilon_0 \pi h^2 d}{8} \frac{\left(\frac{\omega_{mnp}}{c}\right)^2}{\gamma_{mn}^2} \int_0^{\xi_0} Ce_m^2(\xi, q_{mn}) \times (\cosh 2\xi - \Theta_m) d\xi, \quad (33)$$

where

$$\begin{aligned} \Theta_m &= \frac{1}{\pi} \int_0^{2\pi} ce_m^2(\eta, q_{mn}) \cos 2\eta d\eta \\ &= \begin{cases} A_0^{(m)} A_2^{(m)} + \sum_{r=0}^{\infty} A_{2r}^{(m)} A_{2r+2}^{(m)}, & \text{for } m = 0, 2, 4, \dots \\ \frac{1}{2}(A_1^{(m)})^2 + \sum_{r=0}^{\infty} A_{2r+1}^{(m)} A_{2r+3}^{(m)}, & \text{for } m = 1, 3, 5, \dots \end{cases} \end{aligned} \quad (34)$$

and  $A_r^{(m)}$  are the coefficients for the series representation of the Mathieu function  $ce_m(\eta, q)$  given in Eqs. (11) and (12).

Substituting Eq. (31) and (33) into (27), the delta function longitudinal wake potential on the accelerated beam path ( $\xi = 0, \eta = \pi$ ) becomes

$$W_{\lambda}(s) = \frac{2}{\varepsilon_0 \pi d} \sum_{m=0}^{\infty} \sum_{n=1}^{\infty} \sum_{p=0}^{\infty} \frac{\varepsilon_p C_{mn} \left(1 - (-1)^p \cos \frac{\omega_{mnp} d}{c}\right)}{q_{mn} N_{mn}} \cos\left(\frac{\omega_{mnp} s}{c}\right), \quad (35)$$

where  $\varepsilon_p = \frac{1}{2}$  for  $p = 0$  and 1 for  $p \neq 0$ .  $N_{mn}$  and  $C_{mn}$  in Eq. (35) are given by

$$N_{mn} = \int_0^{\xi_0} Ce_m^2(\xi, q_{mn}) \times (\cosh 2\xi - \Theta_m) d\xi, \quad (36)$$

$$C_{mn} = (Ce_m(0, q_{mn}))^2 ce_m(0, q_{mn}) ce_m(\pi, q_{mn})$$

$$= \begin{cases} \left( \sum_{r=0}^{\infty} A_{2r}^{(m)} \right)^4 & \text{for } m = 0, 4, \dots \\ - \left( \sum_{r=0}^{\infty} A_{2r+1}^{(m)} \right)^4 & \text{for } m = 1, 3, 5, \dots \end{cases} \quad (37)$$

For a circular pillbox cavity,  $W_z$  is expressed analytically<sup>7,8</sup> in the form of

$$W_z(s) = \frac{4}{\epsilon_0 \pi d} \sum_{n=1}^{\infty} \sum_{p=0}^{\infty} \epsilon_p \frac{\left( 1 - (-1)^p \cos \frac{\omega_{onp} d}{c} \right)}{\chi_{on} J_1^2(\chi_{on})} \cos \left( \frac{\omega_{onp} s}{c} \right), \quad (38)$$

where  $\chi_{on}$  is the  $n$ th zero of the Bessel function  $J_0$ .

When the boundary ellipse tends to a circle of radius  $r_0$ , the confocal hyperbolae in Fig. 2 become radii of the circle  $r$ , and the confocal ellipses become concentric circles of that radius. In this case, Eq. (35) is reduced exactly to Eq. (38). We can easily show this by using the limiting properties of Mathieu functions. The Mathieu functions  $ce_m(\eta, q)$  and  $Ce_m(\xi, q)$  degenerate into the following forms<sup>10</sup> as  $h \rightarrow 0$  and  $\xi \rightarrow \infty$ , while keeping the product  $h \cosh \xi \rightarrow r$ :

$$q \rightarrow 0 \quad \text{as } h \rightarrow 0, \quad (39)$$

$$ce_m(\eta, q) \rightarrow \begin{cases} \sqrt{\frac{1}{2}}, & \text{for } m = 0 \\ \cos m\phi, & \text{for } m \neq 0 \end{cases} \quad (41)$$

$$Ce_m(\xi, q) \rightarrow p_m J_m(\gamma r), \quad (41)$$

$$A_r^{(m)} \rightarrow 0 \quad (\text{except } A_m^{(m)} \rightarrow 1 \text{ for } m \neq 0, \text{ and } A_0^{(0)} \rightarrow \sqrt{\frac{1}{2}}), \quad (42)$$

where  $p_m$  is a constant multiplier, and  $J_m(x)$  is the Bessel function of the first kind. Then, Eq. (37) becomes

$$C_{mn} = (Ce_m(0, q_{mn}))^2 ce_m(0, q_{mn}) ce_m(\pi, q_{mn})$$

$$\rightarrow (p_m J_m(0) \cos m\phi)^2 = 0, \quad \text{for } m \neq 0$$

$$\rightarrow (p_0 J_0(0))^2 / 2 = p_0^2 / 2, \quad \text{for } m = 0. \quad (43)$$

It is apparent from Eq. (43) that contributions from  $m \neq 0$  modes become zero as expected as an ellipse tends to a circle. The denominator in Eq. (35) for  $m = 0$  becomes

$$q_{on} \int_0^{\xi_0} Ce_0^2(\xi, q_{on}) \cosh 2\xi d\xi \rightarrow \frac{(p_0 \gamma)^2}{2} \int_0^{r_0} J_0^2 J_0^2(\gamma r) r dr$$

$$\rightarrow \frac{p_0^2}{4} \chi_{on}^2 J_1^2(\chi_{on}), \quad (44)$$

where  $\gamma = \chi_{on}/r_0$ . Substituting Eqs. (43) and (44) into (35), we can get exactly the same expression for the wake potential in the circular pillbox cavity as in Eq. (38).

No closed expression is known for the infinite sum in Eqs. (35) and (38), and they must be evaluated numerically.

If the driving bunch has a Gaussian charge distribution

$$\lambda(z) = \frac{1}{\sqrt{2\pi}\sigma} \exp\left(\frac{-z^2}{2\sigma^2}\right), \quad (45)$$

then the bunch wake potential  $U_z$  becomes

$$\begin{aligned} U_z(s) &= \int_{-\infty}^s \lambda(z) W_z(s-z) dz \\ &= \frac{\sqrt{2/\pi}}{\varepsilon_0 \pi d \sigma} \sum_{m=0}^{\infty} \sum_{n=1}^{\infty} \sum_{p=0}^{\infty} \frac{\varepsilon_p C_{mn} \left(1 - (-1)^p \cos \frac{\omega_{mnp} d}{c}\right)}{q_{mn} N_{mn}} \\ &\quad \times \int_{-\infty}^s \exp\left(\frac{-z^2}{2\sigma^2}\right) \cos \frac{\omega_{mnp}(s-z)}{c} dz. \end{aligned} \quad (46)$$

When  $s \gg \sigma$ , the bunch wake potential becomes

$$\begin{aligned} U_z(s) &\approx \frac{2}{\varepsilon_0 \pi d} \sum_{m=0}^{\infty} \sum_{n=1}^{\infty} \sum_{p=0}^{\infty} \exp\left(-\left(\frac{\omega_{mnp}}{c}\right)^2 \sigma^2 / 2\right) \\ &\quad \times \frac{\varepsilon_p C_{mn} \left(1 - (-1)^p \cos \frac{\omega_{mnp} d}{c}\right)}{q_{mn} N_{mn}} \cos \frac{\omega_{mnp} s}{c}. \end{aligned} \quad (47)$$

From this equation, we can see that contributions from the modes whose resonant wavelengths are much shorter than the bunch length  $2\sigma$  become negligible. For the dominant mode, Eq. (47) can be conveniently written as

$$U_{z_{110}} \approx \frac{(1 - e_c^2)^{1/2} \lambda^2 C_{01}}{\varepsilon_0 \pi^2 d e_c^2 S N_{01}} e^{-1/2(2\pi\sigma/\lambda)^2} \left(1 - \cos \frac{2\pi d}{\lambda}\right) \cos \frac{2\pi s}{\lambda}, \quad (48)$$

where  $S = \pi x_b y_b$  is the cross sectional area of the cavity,  $\lambda$  is the wavelength of dominant mode, and  $e_c$  is the eccentricity of the boundary ellipse. From Eq. (48), we see that the wake potential scales as  $\omega_\lambda^{-2}$  and  $S^{-1}$ .

### 3.2. Transverse Wake Potential

From the Panofsky-Wenzel theorem, the transverse wake potential is related to the longitudinal wake potential by

$$\frac{\partial \mathbf{W}_\perp(s)}{\partial s} = \nabla_\perp W_z(s). \quad (49)$$

From this relation we can write the transverse delta function wake potential as<sup>7</sup>

$$\mathbf{W}_\perp(s) = \sum_\lambda c \frac{V_\lambda^*(\mathbf{r}) \nabla_\perp V_\lambda(\mathbf{r})}{2u_\lambda \omega_\lambda} \sin\left(\frac{\omega_\lambda s}{c}\right). \quad (50)$$

On the accelerating beam path ( $\xi = 0, \eta = \pi$ ), we have

$$V_{\lambda}^*(r)\nabla_{\perp} V_{\lambda}(r) = Ce_m(0, q_{\lambda})ce_m(0, q_{\lambda})ce_m(\pi, q_{\lambda})\nabla_{\perp} Ce_m(0, q_{\lambda}) \\ \times \left( \int_0^d dz \exp\left(\frac{j\omega z}{c}\right) \cos \frac{p\pi}{d} z \right)^2. \quad (51)$$

Since the driving charge and test charge are assumed to pass through each focus axis, only  $\hat{\xi}$ -component of the transverse wake potential exists at the foci of the elliptic cavity. Thus,

$$\nabla_{\perp} Ce_m(0, q_{\lambda}) = \hat{\xi} \lim_{\xi \rightarrow 0} \frac{1}{h \sinh \xi} \frac{\partial}{\partial \xi} Ce_m(\xi, q_{\lambda}) \\ = \hat{\xi} \begin{cases} \frac{1}{h} \sum_{r=0}^{\infty} (2r)^2 A_{2r}^{(m)}, & \text{for } m = 0, 2, 4, \dots \\ \frac{1}{h} \sum_{r=0}^{\infty} (2r+1)^2 A_{2r+1}^{(m)}, & \text{for } m = 1, 2, 5, \dots \end{cases} \quad (52)$$

Therefore, the transverse delta function wake potential is given by

$$W_{\perp}(s) = \frac{2c}{\epsilon_0 \pi d} \sum_{\lambda} \frac{\epsilon_p \bar{C}_{\lambda} \left( 1 - (-1)^p \cos \frac{\omega_{\lambda} d}{c} \right)}{\omega_{\lambda} q_{\lambda} N_{\lambda}} \sin \left( \frac{\omega_{\lambda}}{c} s \right), \quad (53)$$

where

$$\bar{C}_{\lambda} = Ce_m(0, q_{mn})ce_m(0, q_{mn})ce_m(\pi, q_{mn})\nabla_{\perp} Ce_m(0, q_{mn}) \\ = \begin{cases} \left( \frac{1}{h} \sum_{r=0}^{\infty} A_{2r}^{(m)} \right)^3 \left( \sum_{r=0}^{\infty} (2r)^2 A_{2r}^{(m)} \right) & \text{for } m = 0, 2, 4, \dots \\ \left( \frac{1}{h} \sum_{r=0}^{\infty} A_{2r+1}^{(m)} \right)^3 \left( \sum_{r=0}^{\infty} (2r+1)^2 A_{2r+1}^{(m)} \right), & \text{for } m = 1, 3, 5, \dots \end{cases} \quad (54)$$

For the driving bunch of a Gaussian charge distribution, the transverse bunch wake potential becomes

$$U_{\perp}(s) = \int_{-\infty}^s \lambda(z) W_{\perp}(s-z) dz \\ = \frac{c\sqrt{2/\pi}}{\epsilon_0 \pi d \sigma} \sum_{m=0}^{\infty} \sum_{n=1}^{\infty} \sum_{p=0}^{\infty} \frac{\epsilon_p \bar{C}_{mnp} \left( 1 - (-1)^p \cos \frac{\omega_{mnp} d}{c} \right)}{\omega_{mnp} q_{mnp} N_{mnp}} \\ \times \int_{-\infty}^s \exp\left(\frac{-z^2}{2\sigma^2}\right) \sin \frac{\omega_{mnp}}{c} (s-z) dz. \quad (55)$$

#### 4. NUMERICAL EXAMPLES AND DISCUSSIONS

The longitudinal and transverse wake potentials in an elliptic pillbox cavity are calculated by using Eqs. (46) and (55). We choose the same cavity dimensions and bunch length as in Ref. 9 to compare the results. The cavity dimensions and beam parameter are:

$$\begin{aligned} \text{major axis } 2x_b &= 10 \text{ cm,} \\ \text{minor axis } 2y_b &= 6 \text{ cm,} \\ \text{gap distance } d &= 2 \text{ cm,} \\ \sigma &= 5 \text{ mm.} \end{aligned}$$

The wavelength,  $\lambda_{mnp}$ , and the loss parameters of a Gaussian bunch,  $k_\lambda(\sigma)$ , for some of lower-order resonant modes are tabulated in Table I, while in Table II the

TABLE I

Wavelength  $\lambda_{mnp}$  and Loss Parameter  $k_{mnp}(\sigma)$  of an Elliptical Pillbox Cavity ( $x_b = 5 \text{ cm}$ ,  $y_b = 3 \text{ cm}$ ,  $d = 2 \text{ cm}$ ,  $\sigma = 5 \text{ mm}$ )

m	$q_{m1}$	$\lambda_{m10}$ (cm)	$\lambda_{m11}$ (cm)	$\lambda_{m12}$ (cm)	$k_{m10}(\sigma)$ (V/pC)	$k_{m11}(\sigma)$ (V/pC)	$k_{m12}(\sigma)$ (V/pC)
0	1.7353	9.5394	3.6883	1.9574	$3.2345 \times 10^{-2}$	$1.6366 \times 10^{-3}$	$6.8638 \times 10^{-5}$
1	3.3522	6.8634	3.4559	1.9201	$1.2629 \times 10^{-1}$	$1.2993 \times 10^{-2}$	$5.7848 \times 10^{-4}$
2	5.6530	5.2853	3.1895	1.8705	$2.2821 \times 10^{-1}$	$4.3203 \times 10^{-2}$	$2.0914 \times 10^{-3}$
3	8.6577	4.2708	2.9194	1.8112	$2.5776 \times 10^{-1}$	$8.4739 \times 10^{-2}$	$4.5668 \times 10^{-3}$
4	12.3689	3.5731	2.6648	1.7452	$2.0007 \times 10^{-1}$	$1.1262 \times 10^{-1}$	$6.9154 \times 10^{-3}$
5	16.7792	3.0678	2.4343	1.6754	$1.1060 \times 10^{-1}$	$1.0854 \times 10^{-1}$	$7.7733 \times 10^{-3}$

m	$q_{m2}$	$\lambda_{m20}$ (cm)	$\lambda_{m21}$ (cm)	$\lambda_{m22}$ (cm)	$k_{m20}(\sigma)$ (V/pC)	$k_{m21}(\sigma)$ (V/pC)	$k_{m22}(\sigma)$ (V/pC)
0	11.3563	3.7289	2.7276	1.7625	$2.8997 \times 10^{-6}$	$1.4188 \times 10^{-6}$	$8.4089 \times 10^{-8}$
1	14.6278	3.2856	2.5389	1.7084	$1.9755 \times 10^{-5}$	$1.4828 \times 10^{-5}$	$9.8517 \times 10^{-7}$
2	18.4878	2.9225	2.3598	1.6505	$6.1309 \times 10^{-5}$	$7.4392 \times 10^{-5}$	$5.6547 \times 10^{-6}$
3	22.9665	2.6221	2.1930	1.5902	$1.0984 \times 10^{-4}$	$2.3849 \times 10^{-4}$	$2.1224 \times 10^{-5}$
4	28.0957	2.3708	2.0395	1.5287	$1.1261 \times 10^{-4}$	$5.4398 \times 10^{-4}$	$5.8271 \times 10^{-5}$
5	33.9196	2.1577	1.8990	1.4668	$4.5322 \times 10^{-4}$	$9.1853 \times 10^{-4}$	$1.2279 \times 10^{-5}$

TABLE II

Wavelength  $\lambda_{0np}$  and Loss Parameter  $k_{0np}(\sigma)$  of a Circular Pillbox Cavity ( $r_0 = 3.873 \text{ cm}$ ,  $d = 2 \text{ cm}$ ,  $\sigma = 5 \text{ mm}$ )

n	$\lambda_{0n0}$	$\lambda_{0n1}$ (cm)	$\lambda_{0n2}$ (cm)	$k_{0n0}(\sigma)$ (V/pC)	$k_{0n1}(\sigma)$ (V/pC)	$k_{0n2}(\sigma)$ (V/pC)
1	2.405	10.118	3.720	1.962	$7.235 \times 10^{-1}$	$3.212 \times 10^{-2}$
2	5.520	4.408	2.962	1.821	$6.031 \times 10^{-1}$	$1.818 \times 10^{-1}$
3	8.654	2.812	2.300	1.630	$1.162 \times 10^{-1}$	$1.700 \times 10^{-1}$
4	11.792	2.064	1.834	1.436	$4.419 \times 10^{-4}$	$4.693 \times 10^{-2}$
5	14.931	1.630	1.509	1.263	$3.944 \times 10^{-3}$	$2.710 \times 10^{-3}$

same information is given for the circular pillbox cavity that has the same cross sectional area ( $r_0 = \sqrt{a_b b_b}$ ).

Figures 5 and 6 are, respectively, the curves of the longitudinal wake potential on the accelerated beam path and that on the driving beam path, in which different number of modes are included (solid lines for 24 modes and broken lines for 12 modes). From these figures, we see that the mode summation converges rapidly, indicating clearly that the wake potential is dominated by a few lower modes. It was pointed out that the wake potential inside the bunch is difficult to calculate because of the slow convergence of mode summation<sup>8</sup>. However, it is not clear in these figures whether the series converges rather slowly for positions inside the driving bunch.

On the accelerated beam path, we obtained about 125 MeV/m/ $\mu$ C acceleration gradient, while about 110 MeV/m/ $\mu$ C was obtained by Y. Chin<sup>9</sup> (see Fig. 7). The elliptical cavity in this example calculation does not represent the maximum acceleration gradient that can be achieved. As discussed earlier, the longitudinal wake potential is proportional to the number of particles in the driving bunch and inversely proportional to the cross sectional area of the cavity. Also, it is dependent on the distribution of charges within a bunch and the eccentricity of a cavity. By choosing appropriate parameters, one can achieve an even-higher acceleration gradient.

The transverse wake potentials on the accelerated beam path and driving beam path are shown in Figs. 8 and 9 by the broken lines. The corresponding longitudinal

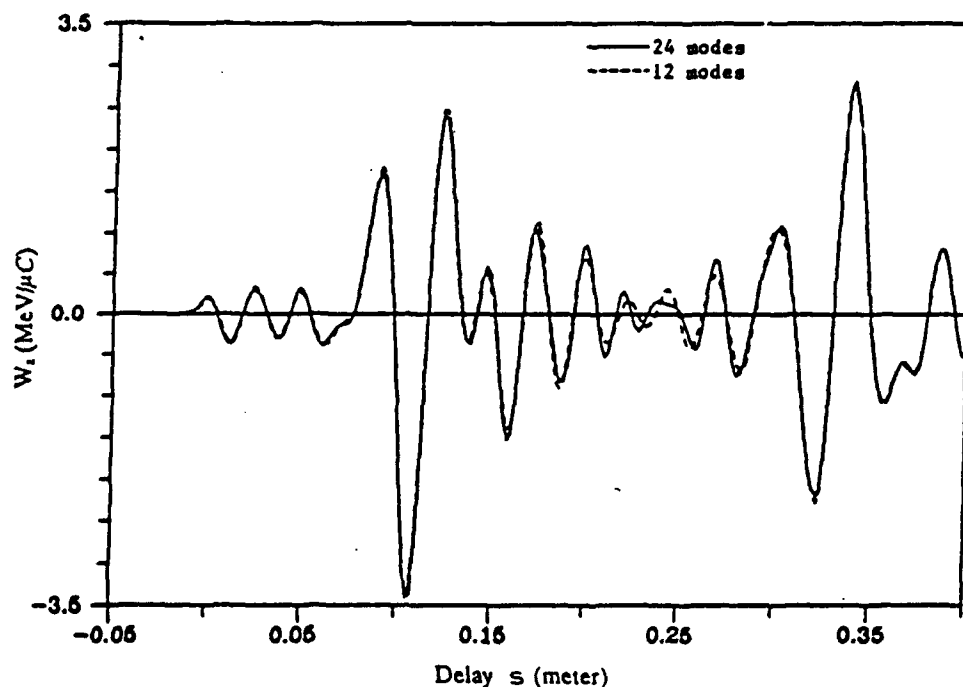


FIGURE 5 Plot of the longitudinal wake potential on the accelerated beam path (solid line: 24 modes sum; broken line: 12 modes sum).

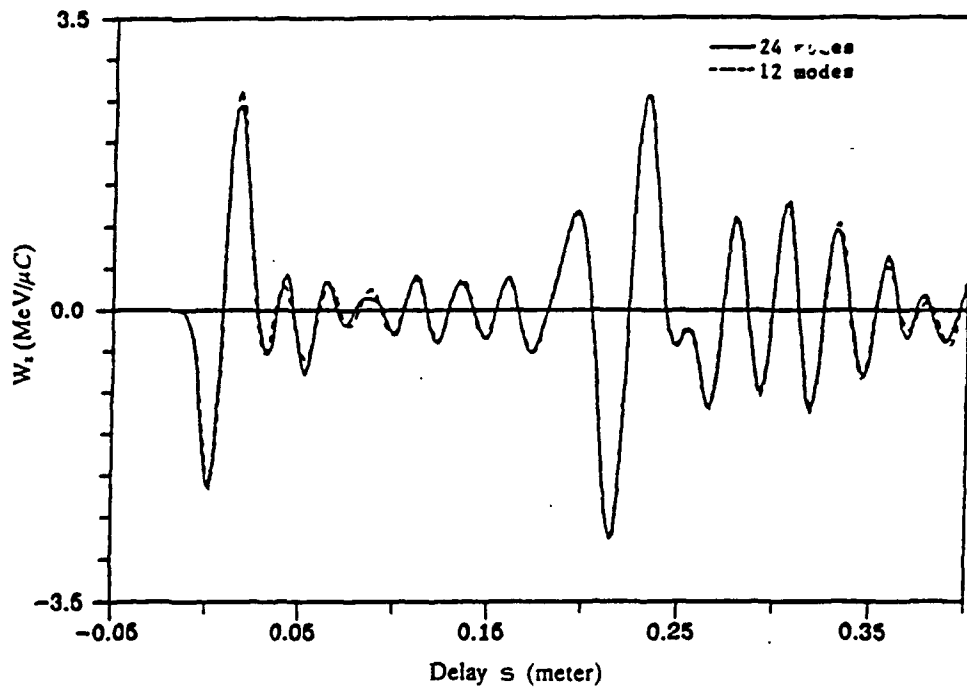


FIGURE 6 Plot of the longitudinal wake potential on the driving beam path (solid line: 24 modes sum; broken line: 12 modes sum).

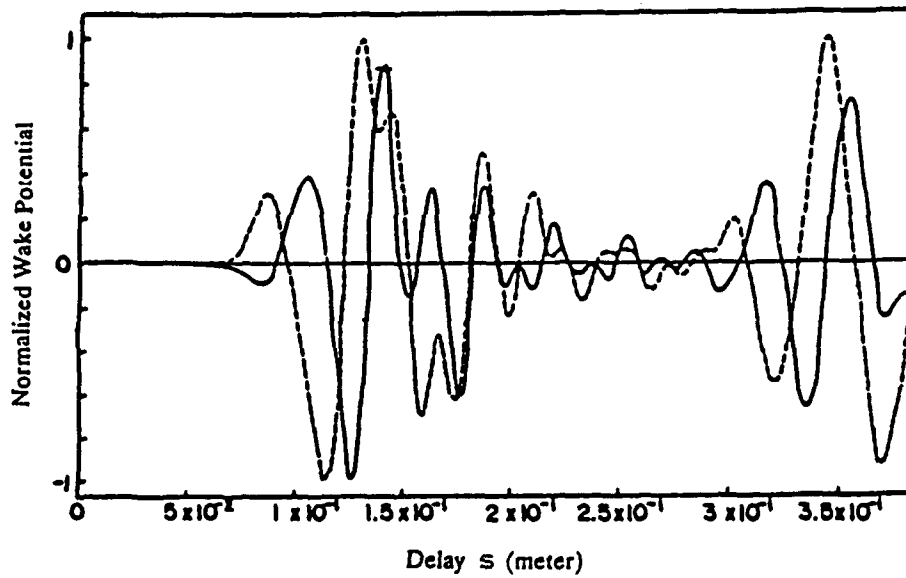


FIGURE 7 Plot of normalized wake potentials on the accelerated beam path (results of Ref. 9).

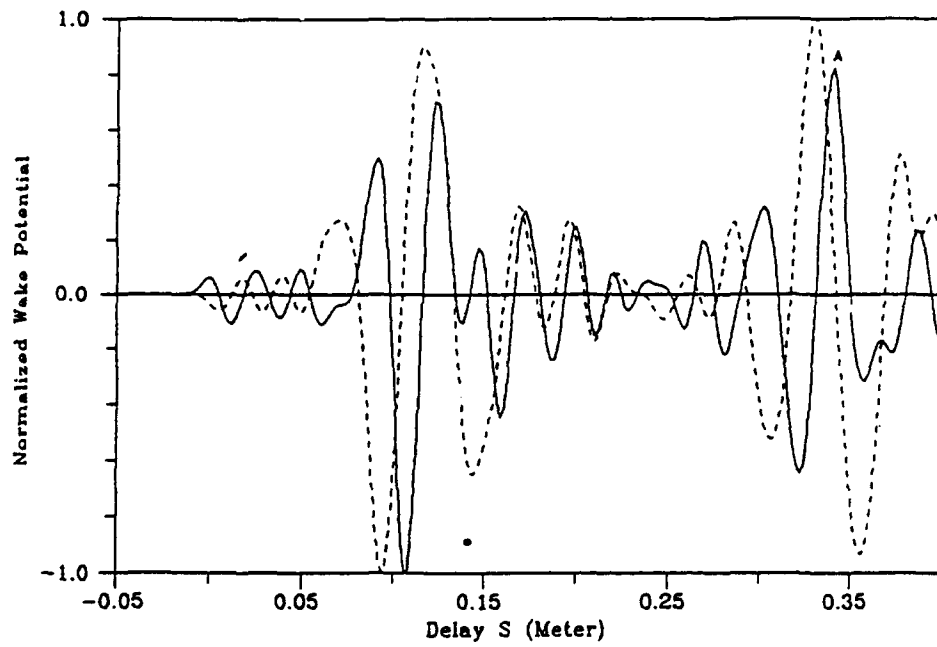


FIGURE 8 Plot of normalized wake potentials on the accelerated beam path (solid line: longitudinal wake potential; broken line: transverse wake potential).

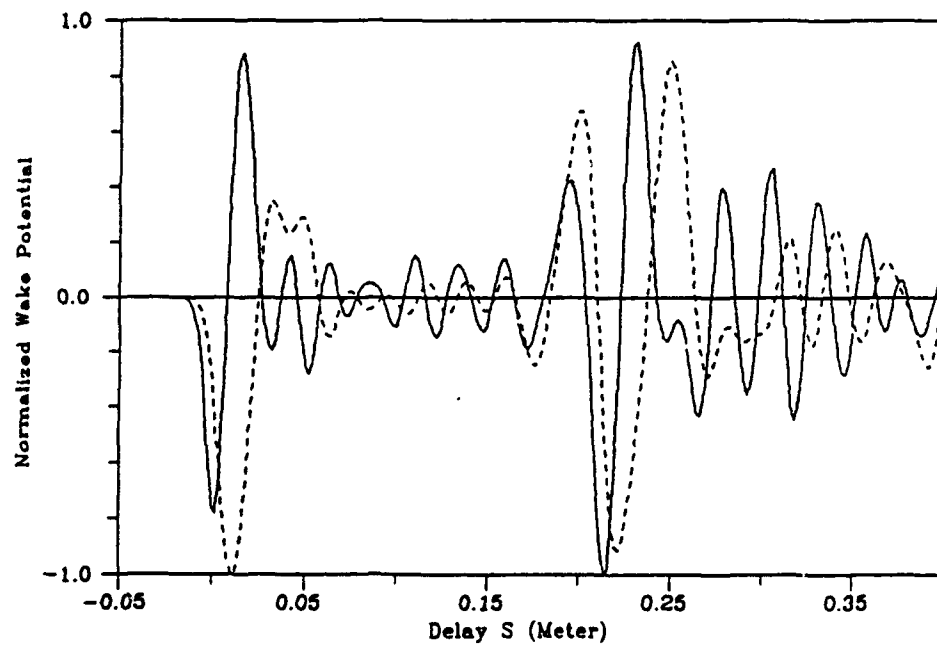


FIGURE 9 Plot of normalized wake potentials on the driving beam path (solid line: longitudinal wake potential; broken line: transverse wake potential).

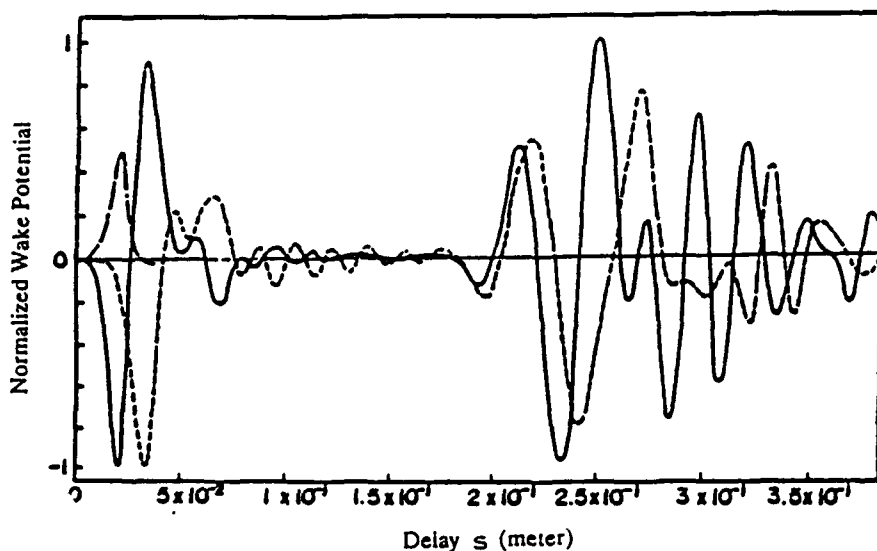


FIGURE 10 Plot of normalized wake potentials on the driving beam path (results of Ref. 9).

wake potentials are plotted together in order to see if we can find the positions, such as the point A in Fig. 8, at which the accelerating potential is large while the transverse potential is small. The charge to be accelerated should be positioned at such a point in order to avoid large transverse deflection during acceleration. Figures 7 and 10 are, respectively, the curves for the longitudinal and transverse wake potentials on the accelerated beam path and driving beam path calculated by the numerical code WELL<sup>9</sup>. In these calculations, the effect of beam apertures of 0.5 cm radius was considered. Comparing these analytical results (Figures 8 and 9) with numerical method (Figures 7 and 10), we found very good agreement in both magnitudes and frequencies. However, magnitude of the longitudinal and transverse wake potentials are higher for this analytical method which does not include the beam aperture effects.

#### ACKNOWLEDGMENTS

This work is supported in part by the U.S. Air Force Office of Science Research under grant no. AFOSR-87-0280.

#### REFERENCES

1. G. A. Voss and T. Weiland, DESY reports M82-10 (1982) and M82-074 (1982).
2. S. H. Kim, *J. Plasma Phys.* **36**, 195 (1986); *Corrigendum* **41**, 577 (1989); S. H. Kim, *Phys. Lett.* **135A**, 39 (1989).
3. H. Figueroa, W. Gai, R. Konecny, J. Norem, A. Ruggiero, P. Schoessow, and J. Simpson, *Phys. Rev. Lett.* **60**, 21 (1988).

4. J. B. Rosenzweig, D. B. Cline, B. Cole, H. Figueroa, W. Gai, R. Konecny, J. Norem, P. Schoessow and J. Simpson, *Phys. Lett.* **61**, 98 (1988).
5. W. Gai, P. Schoessow, B. Cole, R. Konecny, J. Norem, J. Rosenzweig, and J. Simpson, *Phys. Lett.* **61**, 2756 (1988).
6. K. W. Chen and S. H. Kim, *Proc. of 6th International Conference on High Power Particle Beams*, Kobe, Japan (June 1986).
7. K. L. F. Bane, P. B. Wilson, and T. Weiland, in *Physics of High Energy Particle Accelerators*, AIP Conf. Proc. No. 127, AIP, New York (1983).
8. T. Weiland and B. Zotter, *Part. Accel.* **11**, 143-151 (1981).
9. Y. Chin, KEK report 83-19 (1983).
10. N. W. McLachlan, *Theory and Application of Mathieu Functions*, Dover Publications, Inc., NY (1964).

# Modal analysis of wake fields and its application to elliptical pill-box cavity with finite aperture

S. H. Kim, K. W. Chen, and J. S. Yang

Center for Accelerator Science and Technology, University of Texas at Arlington, Arlington, Texas 76019

(Received 27 December 1989; accepted for publication 10 July 1990)

The potential of the wake-field produced by a bunch of relativistic charged particles passing through a pill-box cavity is expressed by using Floquet's theorem, and an obvious requirement that the energy gain over all acceleration cavity of many pill boxes must be proportional to the number of pill boxes, based on the previous modal approach (BWW theory). It is found that the wake-field is consisted of two classes of modes: the longitudinal modes which are independent of the aperture and the pill-box gap, the hybrid (pill-box) modes which are dependent of the pill-box gap. The wake field is predominated by the fundamental longitudinal mode whose wavelength is on the order of the effective diameter of the cavity, and its magnitude is inversely proportional to the cross sectional area of the cavity for practical cavities with small apertures. Both longitudinal and transverse wake-fields due to the longitudinal modes in an elliptical-pill box cavity are expressed analytically in a closed series form by solving exactly the longitudinal eigenmode-equation in the elliptical cylindrical coordinates in terms of Mathieu functions. It is found that both longitudinal and transverse wake-fields whose amplitudes per driving charge are greater than 100 MV/m/ $\mu\text{C}$  can be generated in an elliptical cavity.

## I. INTRODUCTION

Even though a charged particle in uniform motion on a straight line in free space of a pill-box cavity does not radiate (or does not produce "acceleration fields"), it can produce "velocity field," which are independent of acceleration. These velocity fields induce currents at the metallic surface of cylinder and disk plates, which in turn produce the electric and magnetic field, commonly called the wake field, behind the trajectory of the charged particle.

The wake fields produced by a bunch of relativistic charged particles in pill-box cavities are important not only for future high-current compact electron accelerators,<sup>1</sup> but also for a use as an electric wiggler for a proposed free electron laser scheme.<sup>2</sup> The suitability is based on an estimate that the wake electric field exceeds 100 MV/m per  $\mu\text{C}$  driving bunch charge, and the wavelength is on the order of a few centimeters. The principle of acceleration by the wake field in metallic cavities was experimentally verified.<sup>3</sup> Also, other wake fields in either plasma medium<sup>4,5</sup> or a dielectric cavity<sup>6</sup> have been experimentally investigated. The energy gain in the recent plasma wake experiment<sup>5</sup> is about 4 MeV whereas those in the previous wake field experiments<sup>3,4,6</sup> are on the order of 100 keV.

In the rf acceleration cavity, the current source is outside the cavity, and the phase velocity of an electromagnetic wave is determined entirely by the cavity structure. In contrast, the wake field is produced by the driving charge. Therefore, the phase velocities of the wake field modes are determined by both the velocity of the driving charge which produce the wake field, and the cavity structure.

The experiments<sup>3</sup> showed the predominance by the fundamental mode, indicating that the modal analysis is appropriate tool for the evaluation of the wake field. In the previous modal analysis,<sup>7</sup> the wake-field is expanded in a

Fourier series based on the scalar and vector eigenmode functions of the entire cavity. By the law of causality, Bane *et al.*<sup>7</sup> expressed the part of the Fourier series expanded on the scalar eigenmode functions in terms of the part on the vector eigenmode functions. Thus the wake field can be expressed in a Fourier series based on only the vector eigenmode functions so that the general formulation of the wake-field become much tractable. The synchronism between particle and mode was used to formulate implicitly the Fourier coefficients in a Fourier series expansion of the wake field.<sup>7</sup> So far, from the synchronism, only the acceleration gradient in a cavity in the limit of vanishing aperture has been explicitly calculated, and it was shown explicitly to be proportional to the inverse square of the pill-box gap.<sup>8</sup> This inverse square law is appropriate when the gap distance  $p$  is much longer than the thickness of the disks. When  $p \rightarrow 0$ , the pill-box cavity is same as a plain cylinder cavity with inner radius equal to the aperture radius (i.e., the inner radius of the disks). Thus, the wake field gradient approaches to the zero as  $p \rightarrow 0$ . In the above modal analysis, the disks are assumed to be infinitely thin so that the inverse square law holds for any  $p$ .

The principle of the modal analysis for a physical quantity is to determine the Fourier coefficients based on the complete basis functions. Since the basis functions are complete, the Fourier coefficients are uniquely determined. Therefore, once the Fourier coefficients are determined to satisfy some proper conditions pertinent to the physical quantity, there are no other proper Fourier coefficients than these coefficients. In this article, using an obvious attribute of the acceleration gradient in the periodic cavity, we show the formulation to determine the Fourier coefficients for any pill-box cavity of arbitrary aperture. Using the formulation, the wake-potential in a cavity of vanishing aperture is analytically expressed, and the result is exactly the same as the result from the synchronism.

To apply the modal analysis, we first find the basis functions (or the mode functions). By using Floquet's theorem on the periodicity, the problem all over the acceleration cavity can be reduced to that in a unit pill box. Since the mode functions satisfy the elliptic partial differential equations, we should specify boundary conditions all over the enclosing surface to determine mode functions uniquely. On the metallic surface, the infinite conductivity condition can be assigned as the pertinent boundary condition as usual. However, so far the problem as to what is the boundary condition on aperture has not been investigated; the previous modal analysis is applied to the cavity in the limit of vanishing aperture, which does not have such problem, and the numerical methods which solve directly the Maxwell equations and boundary conditions all over the entire cavity (not the unit pill-box) in the time- and space-mesh domain, e.g., the TBCI and T3 code, have been used for the cavities with nonzero aperture.<sup>7,9</sup> We show here how should the boundary condition on aperture be assigned by considering the parity and the continuity at the aperture. Even though the modal analysis, in principle, cannot take into account the effect of large aperture, the specification of the boundary condition is still of academic interest. For large apertures, we should use other methods.<sup>10</sup>

As is mentioned, one important application of the wake field in a pill-box cavity other than the acceleration is to use the wake field as a wiggler field for a free electron laser. For this application, the cavity should be a two-beam configuration such as an elliptic cavity<sup>2</sup> or an annular circular cavity<sup>7</sup> so that the lasing electrons can be injected in the opposite direction of the driving charge to be wiggled by the wake-field produced by the driving charge. Being an axi-symmetric configuration, the annular cavity cannot have the electric field in the transverse direction (i.e., the direction perpendicular to the cavity axis) along the cavity axis ("transverse wake field"). Therefore, as far as free electron lasing is concerned, the annular pill-box cavity is similar to the usual rf acceleration cavity in which the electric field undulating along the cavity axis can be routinely made more than 10 MeV/m. The rf cavity cannot support both a TM mode of the same wavelength which has an electric field in the transverse direction. Since the wake-field is produced by the driving charge moving inside the cavity as is already mentioned, the elliptic wake-field cavity have both the longitudinal electric field and the transverse electric field of the same wavelength. If we inject the lasing electrons in the opposite direction along the path passing through the foci of the elliptic disks on the other side of the foci through which the driving charge is passing, the lasing electrons are forced to emit the laser radiation by both the longitudinal wake-field and the transverse wake-field. Until the field-strength of laser wave arrives that of the transverse wake-field ("weak laser regime"), the transverse motions of the electrons are still confined by the transverse wake-field field. Similar to the present free electron lasing in the magnetic wiggler, both stimulated bremsstrahlung and unstimulated bremsstrahlung by the transversely bound electrons requires the transverse current produced by the transverse wake-field along, and take place at the same wavelengths.<sup>2</sup> A transverse wake

field whose amplitude and wavelength are on the order of 100 MV/m and 5 cm, respectively, is equivalent to a magnetic wiggler on the order of 3 kG and 5 cm, respectively, which are about the standard values for the magnetic wigglers used in the present free electron lasers. Therefore, even if we just consider the transverse wake-field, the elliptic wake-field cavity is superior to the conventional magnetic wiggler if we can produce the transverse wake fields whose amplitudes are more than 100 MV/m.

If we inject an electron beam in the direction of the longitudinal electric wiggler, the transverse motions of the electrons are not bounded by the electric field, which contrasts with the transverse motions of the electrons in the free electron laser using a magnetic wiggler. Also, the longitudinal motions of the electrons are not bounded by the longitudinal electric wiggler if the initial kinetic energies are sufficiently large which is the usual case in any free electron laser. Free electron lasing by the electrons whose transverse and longitudinal motions are not bound by the wiggler does not require a transverse current produced by the wiggler along. The transverse motion in the longitudinal electric wiggler is primarily governed by the incident electromagnetic wave, and the incident laser wave is the major field to drive the source current with the help from the longitudinal electric wave. Unlike transversely-bound FELs, stimulated emission in the longitudinal electric wiggler occurs as a two-quantum Stark emission<sup>11,12</sup> in which the electron make the transitions from a free state via a virtual free state. The two-quantum Stark emission by the bound electrons are used as a diagnostic means in plasma spectroscopy. By this two-quantum Stark emission, a light is emitted in the same direction as the applied electric field by either stimulated emission or spontaneous emission. It had been theoretically shown that the shorter the wavelength of the free electron laser which we want to create, the more advantageous is the longitudinal electric wiggler compared with the transverse magnetic wiggler.<sup>2</sup>

The emission in the so-called Smith-Purcell laser<sup>13</sup> is a spontaneous emission in both transverse and longitudinal wake fields generated by non-relativistic electron bunches when they pass over a ruled grating, which acts similarly as the pill box. Since the electrons are non-relativistic in this laser, they can experience the ripple of the wake field which they produce. We can guess that the electrons experience extraordinary large electric fields since the gap distance is extremely small in the ruled grating.

Previously, the wake fields in an elliptic pill-box cavity was calculated by solving directly the Maxwell equations and boundary conditions over the entire cavity in the time- and space-mesh points.<sup>9</sup> The advantage of the direct solution of the Maxwell equations is that the aperture effect can be taken into account. However, the direct solution requires a very large number of numerical processing. In contrast to the direct solution, any modal analysis, in principle, cannot take into account properly the aperture effect when the aperture is large. However, the experiment showed that the predominance of the wake field by the fundamental mode even for a cavity of considerably large aperture,<sup>3</sup> indicating that a modal analysis can render a reasonably good approximate

results unless high accuracy is demanded. Both longitudinal and transverse wake fields due to the longitudinal modes can be calculated to any degree of precision since we can express these fields analytically in closed series forms. This expression is possible by solving analytically the longitudinal eigenmode equation in the elliptical cylindrical coordinates in terms of Mathieu functions<sup>14</sup> as will be shown in this article.

## II. THE LONGITUDINAL WAKE POTENTIAL

For clarity, let us consider a wake-field consisting of a very large number of elliptic pill boxes. A point charge  $Q$  passes through one of the foci of the elliptic disks with a speed  $c$ . Let the transverse coordinates of these centers be  $r_1 = (x_0, 0)$  and  $(-x_0, 0)$ . The delta-function longitudinal wake potential  $W_z$  is defined as the energy gained by a unit negative point charge with a velocity  $c$  traveling in the path passing through the other elliptic foci, at a distance  $s$  in the  $z$  direction behind the accelerating point charge  $Q$ .

The pill-box cavity is a periodic structure, the wake field in this cavity should be very amenable to a modal analysis. However, since the wake field is consisted of both electromagnetic (vector) and electrostatic (scalar) fields, the complete basis functions for the Fourier series expansion should include both scalar and vector eigenmode functions. A tractable analysis of the Fourier analysis (or modal analysis) based on these two different classes of basis functions had been nearly impossible. This difficulty is resolved by Bane *et al.*<sup>7</sup> They found the relationship between the scalar wake field and the vector wake field, which is arisen by the causality. Accordingly, imposing the causality and using Maxwell's equations, they<sup>7</sup> (BWW theory) first obtained

$$W_z(s) = 4\pi Q \sum_{\alpha} \left| \int_0^L a_{\alpha z}(z) \exp(i\omega_{\alpha} z/c) dz \right|^2 \quad (1)$$

where  $a_{\alpha}$  is the normalized vector eigenfunctions given by the following equation and boundary conditions:

$$\nabla^2 a_{\alpha} + \frac{\omega_{\alpha}^2}{c^2} a_{\alpha} = 0 \quad (2)$$

and

$$\nabla \cdot a_{\alpha} = 0 \quad (3)$$

everywhere, and

$$a_{\alpha} \times \hat{n} = 0 \quad (4)$$

on the surface of the metallic enclosure of the accelerator cavity where  $\hat{n}$  is the normal vector of the surface.

From this point, the wake potentials is formulated by using an obvious attribute of the periodic structure which the previous BWW theory<sup>7</sup> has not used. Also, the mathematical treatment is different from that in the BWW theory.

From this point, the wake potentials is formulated by using an obvious attribute of the periodic structure which the previous BWW theory<sup>7</sup> has not used. Also, the mathematical treatment is different from that in the BWW theory.

Since the acceleration cavity is a repetitive structure with period  $p$ ,  $a_{\alpha}(z)$  is required by Floquet's periodicity theorem to satisfy

$$a_{\alpha z}(z + np) = \exp(in\beta_{\alpha}) a_{\alpha z}(z), \quad (5)$$

where  $\beta_{\alpha}$  is an arbitrary constant. By means of Eq. (5), we have

$$\int_0^L a_{\alpha z}(z) \exp(i\omega_{\alpha} z/c) dz = \int_0^p a_{\alpha z}(z) \exp(i\omega_{\alpha} z/c) dz \sum_{n=0}^{n_0} \exp[i(\beta_{\alpha} + \omega_{\alpha} p/c)n], \quad (6)$$

where  $n_0 = L/p - 1$ .

Even though any value of  $\beta_{\alpha}$  satisfies the geometric condition that the cavity is a periodic structure, only a particular value satisfies other physical requirements. An obvious requirement is that the energy gain over the entire cavity,  $W_z(s)$  is proportional to  $L$  (or the number of the pill boxes). To satisfy this requirement, we find from Eq. (6) that  $\beta_{\alpha}$  must be given by

$$\beta_{\alpha} = -\omega_{\alpha} p/c. \quad (7)$$

Substituting Eq. (7) into Eq. (6) and combining the resulting equation with Eq. (1), we derive the longitudinal wake potential (or the acceleration gradient) as

$$\frac{W_z}{L} = \frac{4\pi Q}{p^2} \sum_{\alpha} V_{\alpha}^*(x_0, 0, \lambda_{\alpha}) V_{\alpha}(-x_0, 0, \lambda_{\alpha}) \cos(s/\lambda_{\alpha}), \quad (8)$$

where

$$V_{\alpha}(x, y, \lambda_{\alpha}) = \int_0^1 a_{\alpha z}^p(x, y, z) \exp(iz/\lambda_{\alpha}) dz. \quad (9)$$

Here, all distances such as  $z$  and  $\lambda_{\alpha}$  are measured in units of the pill-box gap  $p$ , and  $a_{\alpha}^p = c_{\alpha} a_{\alpha}$  where  $c_{\alpha}$  is a constant such that

$$\int \int \int_{V_p} a_{\alpha}^p \cdot a_{\beta}^{p*} d^3r = \delta_{\alpha\beta}, \quad (10)$$

where  $V_p$  denotes the space in the pill-box. Equation (8) is a similar form of the Coulomb law in that the acceleration is inversely proportional to the square of a distance,  $p$ .

If the driving bunch has a Gaussian distribution

$$g(z) = (2\pi)^{-1/2} \exp(-z^2/2\sigma^2)/\sigma,$$

the wake potential for  $s \gg \sigma$  is given by

$$\frac{W_z(s)}{L} \sim \frac{4\pi Q}{p^2} \sum_{\alpha} V_{\alpha}^*(x_0, 0, \lambda_{\alpha}) V_{\alpha}^*(-x_0, 0, \lambda_{\alpha}) \times \exp(-\sigma^2/2\lambda_{\alpha}^2) \cos(s/\lambda_{\alpha}). \quad (11)$$

From Eq. (11), we find that the modes whose wavelengths are much shorter than the length of the Gaussian driving bunch,  $2\sigma$ , do not contribute significantly to the wake field, and the shorter the wavelength of a mode, the smaller is the contribution to the wake-field from this mode.

## III. CLASSIFICATION OF WAKE MODES AND BOUNDARY CONDITIONS

For brevity, we drop the superscript  $p$  which denotes the pill-box eigenfunction unless there is a chance of confusion, and choose the origin of the pill-box coordinates at the center of the pill-box. Then, the pill-box vector eigenfunctions  $a = a_1 + a_2 \hat{z}$  satisfy the following equations and boundary conditions:

$$\nabla^2 a_1 + a_1/\lambda^2 = 0, \quad (12)$$

$$\nabla^2 a_2 + a_2/\lambda^2 = 0, \quad (13)$$

$$\frac{\partial a_2}{\partial z} + \nabla_1 \cdot a_1 = 0 \quad (14)$$

in the pill box,

$$a_1 = 0 \quad (15)$$

on the disk plates at  $z = \pm p/2$ ,

$$a_1 \times \hat{n} = 0, \quad (16)$$

$$a_2 = 0 \quad (17)$$

on the periphery of the cross section (the side surface of the cylinder).

From Eqs. (14) and (15), we should impose

$$\frac{\partial a_2}{\partial z} = 0 \quad (18)$$

on the disk plates at  $z = \pm p/2$ .

We must impose a condition that  $a$  and its derivatives are continuous functions of  $z$  as  $z$  crosses an aperture to the next adjacent pill box.

Since  $a$  should satisfy Eqs. (12) and (13), and the pill box is symmetric with respect to the reflection about the center plane ( $z = 0$ ) of the pill box,  $a_2$  must be either symmetric (even parity with respect to  $z$ ) or anti-symmetric (odd parity with respect to  $z$ ). However, because of Eq. (14),  $a_1$  and  $a_2$  must have different parities (the pair of either  $a_2$  and  $\partial a_1/\partial z$  or  $a_1$  and  $\partial a_2/\partial z$  should have the same parity).

We need only to prescribe the mode functions in the region  $0 < z < p/2$ . The modes can be classified into following classes.

(i) The odd hybrid modes: These modes are dependent on the pill-box gap and aperture, and their  $a_2$  have the odd parity (consequently,  $\nabla a_1/\nabla z$  must have the odd parity). Accordingly,

$$a_{z, \text{hyb}}^{\text{odd}} = 0, \quad \frac{\partial a_{z, \text{hyb}}^{\text{odd}}}{\partial z} = 0 \quad (19)$$

at  $z = 0$  and on the aperture at  $z = p/2$ .

(ii) The even hybrid modes: These modes are dependent on the pill-box gap, but independent of the aperture. Their  $a_1$  and  $\partial a_2/\partial z$  have the odd parity. Equations (15), (18), and the continuity of the odd functions at the aperture are combined to

$$a_{z, \text{hyb}}^{\text{even}} = 0, \quad \frac{\partial a_{z, \text{hyb}}^{\text{even}}}{\partial z} = 0 \quad (20)$$

at  $z = 0$  and  $z = p/2$ .

(iii) The pure longitudinal ( $a_1 = 0$ ) modes: The wavelengths of these modes are completely independent of both the pill-box gap and the aperture. From the fact that  $a_1 = 0$  satisfies Eq. (12) for any  $\lambda$ , Eq. (15), and Eq. (16),  $a_{kmg} = f(r_1) \hat{z}$  are the eigenmode if

$$\nabla_1^2 f(r_1) + \frac{f(r_1)}{\lambda^2} = 0, \quad (21)$$

inside in the cross section

$$f(r_1) = 0, \quad (22)$$

on the periphery of the cross section, and

$$\iint_S f^2(r_1) dx dy = 1, \quad (23)$$

where  $S$  is the cross section of the pill box. These longitudinal modes are independent on the apertures, and their wavelengths are determined only by the cross section.

#### IV. WAKE POTENTIAL IN A CIRCULAR PILL-BOX CAVITY

The modal analysis presumes the periodicity of the acceleration cavity, and thus neglects the velocity field directly arrived at the accelerated charge compared to the electric and magnetic field produced by the currents, which are induced at the surface of the disk plates and the cylinder surface by the velocity field. This assumption can be approximately met when the aperture is much smaller compared to the cross section of the pill box for practical lengths of the cavity. Therefore, the modal analysis, in principle, renders more accurate values as the aperture becomes smaller, and should not be applied to the limit of no disks. The experimental results<sup>3</sup> showed that the wake-field is predominated by the fundamental longitudinal mode even when the ratio of the aperture radius ( $r_0$ ) to the cavity radius ( $R_0$ ) is considerably large ( $r_0/R_0 \approx \frac{1}{2}$  for cavity 1 in the experiment). Therefore, we can take the wake-field in the limit of vanishing aperture as a good approximation of the wake field for most practical cavities whose aperture radii are not greater than  $\frac{1}{2}$  of the cavity radius.

For a circular pill box with finite aperture radius,  $a_1 = a_r \hat{r}$  and Eq. (16) is automatically satisfied for this pill box.

Since in the cylindrical coordinate system, Eqs. (12) and (13) are written as

$$\frac{\partial^2 a_r}{\partial r^2} + \frac{1}{r} \frac{\partial a_r}{\partial r} - \frac{a_r}{r^2} + \frac{\partial^2 a_r}{\partial z^2} + \frac{a_r}{\lambda^2} = 0, \quad (24)$$

$$\frac{\partial^2 a_z}{\partial r^2} + \frac{1}{r} \frac{\partial a_z}{\partial r} + \frac{\partial^2 a_z}{\partial z^2} + \frac{a_z}{\lambda^2} = 0, \quad (25)$$

and  $a_r$  and  $a_z$  are finite at  $r = 0$ , we have

$$\frac{\partial a_z}{\partial r} = 0, \quad a_r = 0, \quad \frac{\partial a_r}{\partial r} = 0 \quad (26)$$

at  $r = 0$ .

Further, Eqs. (24) and (14) are combined a single second-order differential equation with respect to  $z$ :

$$\frac{\partial^2 a_r}{\partial z^2} + \frac{a_r}{\lambda^2} = \frac{\partial^2 a_z}{\partial z \partial r}. \quad (27)$$

For convenience, we will omit the superscripts "even" and "odd", and the subscript "hyb", where there will be no possible change of confusion.

##### A. Wake-field gradient from all even hybrid modes

Solving Eq. (25) with boundary conditions  $a_z(R_0, z) = 0$  [Eq. (17)],  $\partial a_z(0, z)/\partial r = 0$  [Eq. (26)], and

$$\frac{\partial a_z(r,0)}{\partial z} = \frac{\partial a_z(r,p/2)}{\partial z} = 0$$

[Eq. (20)], we obtain

$$a_z(r,z) = AJ_0(\nu_r r) \cos(\nu_z z), \quad (28)$$

where  $J_n(\xi)$  is Bessel function of order  $n$ ,  $\nu_r = \xi_n/R_0$  with  $\xi_n$  being the  $n$ th root of  $J_0(\xi) = 0$ ,  $\nu_z = 2n\pi/p$  with  $n = 1, 2, 3, \dots$ , and  $A$  is the normalization constant to be determined later.

Substituting Eq. (28) into Eq. (27), and solving the resulting equation with boundary condition  $a_r(r,0) = 0$ , which is derived from  $a_r$  being odd for  $z$ ,  $a_r(0,z) = 0$ ,  $\partial a_r(0,z)/\partial r = 0$  [Eq. (26)], and  $a_r(r,p/2) = 0$  [Eq. (20)], we obtain

$$a_r(r,z) = -A(\nu_z/\nu_r) J_1(\nu_r r) \sin(\nu_z z). \quad (29)$$

From Eqs. (28), (29), and (10), we find the normalization constant as

$$A = \sqrt{\frac{2}{\pi}} \frac{1}{R_0 J_1(\xi_n) \nu_{n,2m}}, \quad (30)$$

where  $\nu_{n,m} = [(\xi_n/R_0)^2 + (m\pi/p)^2]^{1/2}$ .

Combining Eqs. (8), (9), (28), and (30), we find that the wake field gradient from all even hybrid modes is given by

$$\frac{W_{z,\text{hyb}}^{\text{even}}(s)}{L} = \frac{16Q}{p^2} \sum_{n=1}^{\infty} \sum_{\substack{m=\text{even} \\ m>0}}^{\infty} \frac{[1 - (-1)^m \cos(\nu_{n,m} p)] \cos(\nu_{n,m} s)}{J_1^2(\xi_n) \xi_n^2}. \quad (31)$$

### B. Wake-field gradient from all longitudinal modes

The calculation of the longitudinal modes from Eqs. (21) to (23) is elementary. We find that the wake field gradient from all longitudinal modes is given by

$$\frac{W_{z,\text{long}}(s)}{L} = \frac{8Q}{p^2} \sum_{n=1}^{\infty} \frac{[1 - \cos(\nu_{n,0} p)] \cos(\nu_{n,0} s)}{J_1^2(\xi_n) \xi_n^2}. \quad (32)$$

### C. Wake-field gradient from all odd hybrid modes

For  $r_0 \neq 0$ ,  $a_z$  must satisfy Eq. (25) and the boundary conditions

$$a_z(r,0) = 0, \quad a_z(R_0, z) = 0,$$

$$a_z(r,p/2) = 0 \quad \text{for } 0 < r < r_0,$$

$$\frac{\partial a_z(r,p/2)}{\partial z} = 0 \quad \text{for } r_0 < r < R_0,$$

$$\frac{\partial a_z(0,z)}{\partial r} = 0, \quad (33)$$

and  $a_r$  should be determined by Eq. (27) and the boundary conditions

$$\frac{\partial a_r(r,0)}{\partial z} = 0, \quad \frac{\partial a_r(r,p/2)}{\partial z} = 0, \quad \text{for } 0 < r < r_0,$$

$$a_r(r,p/2) = 0 \quad \text{for } r_0 < r < R_0,$$

$$a_r(0,z) = \frac{\partial a_r(0,z)}{\partial r} = 0, \quad (34)$$

We can solve these equations only by the numerical methods.<sup>15</sup> The result from the numerical methods is not important. The reason is as follows. First, the modal analysis does not take into account properly the aperture effect as mentioned before. Therefore, the wake field gradient from all odd hybrid modes by means of a modal analysis is, in principle, appropriate only for small apertures where an analytical good estimate is readily available. Second, we can readily find that the wake field gradient from all odd hybrid modes from the above equations is anyhow negligible compared to that from all longitudinal modes for most practical cavities. In the limit of vanishing aperture (i.e.,  $r_0 \rightarrow 0$ ), the boundary condition at  $z = p/2$  is now

$$\frac{\partial a_z(r,p/2)}{\partial z} = 0, \quad a_r(r,p/2) = 0. \quad (35)$$

Then, the analytical solution for the wake-potential from the odd hybrid modes is given by

$$\frac{W_{z,\text{hyb}}^{\text{odd}}(s)}{L} = \frac{16Q}{p^2} \sum_{n=1}^{\infty} \sum_{\substack{m=\text{odd} \\ m>0}}^{\infty} \frac{[1 - (-1)^m \cos(\nu_{n,m} p)] \cos(\nu_{n,m} s)}{J_1^2(\xi_n) \xi_n^2}. \quad (36)$$

In the limit of no disks (i.e.,  $r_0 \rightarrow R_0$ ), the boundary condition at  $z = p/2$  is written as

$$a_z(r,p/2) = 0, \quad \frac{\partial a_r(r,p/2)}{\partial z} = 0. \quad (37)$$

Then, the wake-field gradient from all odd hybrid modes is given by

$$\frac{W_{z,\text{hyb}}^{\text{odd}}(s)}{L} = \frac{16Q}{p^2} \sum_{n=1}^{\infty} \sum_{\substack{m=\text{even} \\ m>0}}^{\infty} \frac{[1 - (-1)^m \cos(\nu_{n,m} p)] \cos(\nu_{n,m} s)}{J_1^2(\xi_n) \xi_n^2}. \quad (38)$$

This wake-field gradient in the limit of no disks has no appropriate physical meaning. Only the magnitude of this field can be used only a crude estimate of the component of the wake-field gradient which depends on the aperture.

Since the eigenmodes of the odd hybrid modes is in the range between the eigenmode in the limit vanishing aperture and that in the limit of no-disks, we find the largest eigenvalue ( $\lambda$ ) of the odd hybrid modes is about  $p/\pi$ .

The wake-potential from all modes in the limit of vanishing aperture is given, by adding Eqs. (31), (32), and (36), as

$$\frac{W_z(s)}{L} = \frac{8Q}{p^2} \sum_{n=1}^{\infty} \sum_{m=-\infty}^{\infty} \frac{[1 - (-1)^m \cos(v_{n,m}p)]}{J_1^2(\xi_n) \xi_n^2} \times \cos(v_{n,m}s). \quad (39)$$

This equation is the exactly same as Eq. (8) of Ref. 8 which is derived from the synchronism between the accelerated particle and the wake-field modes.

From the above equations, we find that the largest eigenvalue of the longitudinal mode is  $2\pi R_0/\xi_1 \approx 2.6R_0$ , while the largest eigenvalue of the hybrid modes is about  $p/\pi$ . This guarantees that the wake-field from all hybrid modes are small compared to those from the longitudinal modes for most practical cases. Further, if  $R_0/\sigma \gg 0.26$ , we have

$$\frac{W_z(s)}{L} \approx \frac{15Q}{R_0^2} \exp(-2.89\sigma^2/R_0^2) \cos(2.4s/R_0), \quad (40)$$

where  $Q$ ,  $R_0$ , and  $s$  are in Gaussian units.

To demonstrate the above features of the modal analysis, the wake potentials in a cavity of  $R_0 = 10$ ,  $r_0 = 3$ ,  $\sigma = 4$  are calculated. In Fig. 1, both the wake potential from the nine most dominant longitudinal modes and the one from the nine most dominant even hybrid modes, expressed by Eqs. (25) and (26) are drawn as the functions of  $s$ . The wake potential from the nine odd hybrid modes computed numerically by solving Eqs. (13), (24), and (25) by means of the finite difference method. The largest eigenvalues of the longitudinal modes, even hybrid modes, and odd hybrid modes are 4.158, 0.159, and 0.215, respectively. Therefore, for the driving-charge length of  $\sigma = 4$ , the wake potential from all hybrid modes are practically zero compared to that from the longitudinal modes as shown in Fig. 1. The wake potential

from the longitudinal modes clearly shows the predominance by the fundamental longitudinal mode.

In Fig. 2, the theoretical energy increments over the total acceleration length of a cavity with the same cavity geometry of cavity 1 used in the experiment<sup>3</sup> are drawn for both a driving charge having the length which makes the theoretical curve fit best the experimental one (curve *a*), and another driving charge having the same length as the experimental one (curve *b*). The contribution from all hybrid modes is not considered since it is theoretically negligible. Even though we do not see so remarkable predominance of the fundamental mode in curve *b* as in the experimental result. Therefore, we can conjecture that either the bunch length was not measured accurately in the experiment, or the aperture effect, which will be considerably large in the experimental case where  $r_0/R_0 \approx \frac{1}{3}$ , suppresses more strongly high-modes than the fundamental mode or the finite conductivity. The latter reason is more probable since the result from the TBCI code, which can calculate accurately the wake field for any aperture, is in excellent agreement with the experimental data.

## V. WAKE FIELDS IN AN ELLIPTIC PILL-BOX CAVITY

### A. The formula of the transverse wake potential

Consider again the exciting charge  $Q$  traveling the one foci of the elliptic cavity at  $v = c$ . The delta-function transverse wake potential  $U_1$  is defined as the transverse momentum kick experienced by a test charge following at a distance  $s$  in the  $z$  direction on the other foci and also at  $v = c$ . Bane *et al.*<sup>7</sup> derived

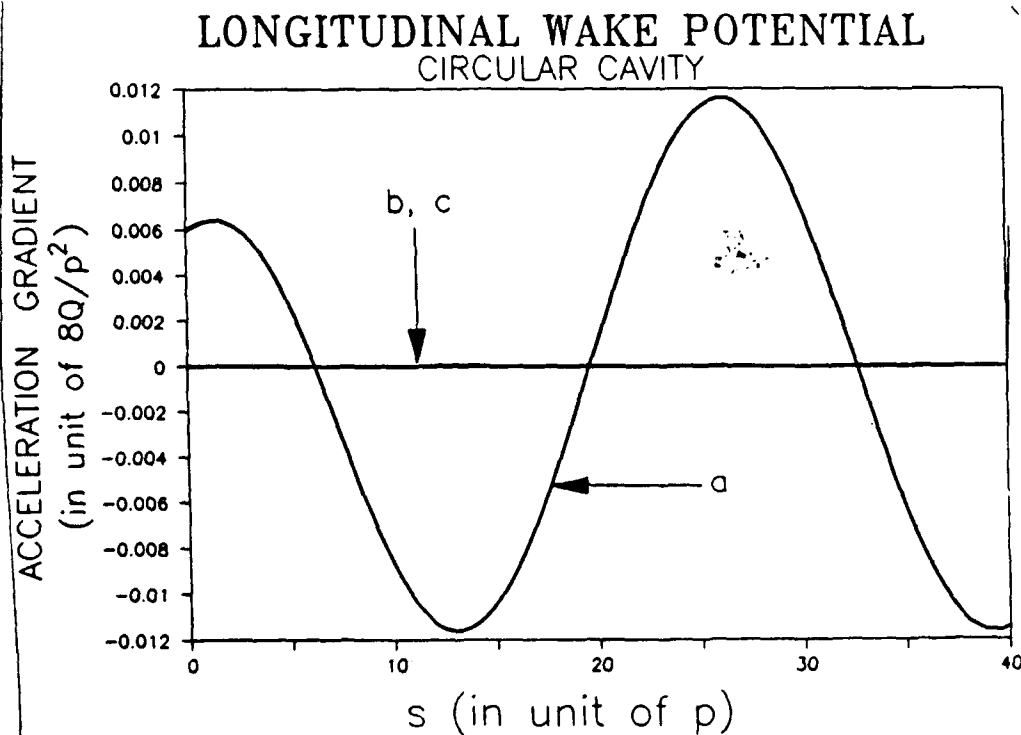


FIG. 1. Wake potentials in unit of  $8Q/p^2$  as the functions of the distance  $s$  between the driving charge and the accelerated charge in a cavity  $R_0 = 10$ ,  $r_0 = 3$ ,  $\sigma = 4$ . Here,  $p$ ,  $R_0$ ,  $r_0$ , and  $2\sigma$  are the cavity radius, the aperture radius, and the length of the driving charge in unit of the pill-box gap  $p$ , and  $Q$  is the driving charge. (a) The wake potential from the fifteen longest longitudinal modes. (b) The wake potential from the odd nine longest modes. (c) The wake potential from the even nine ( $m = 2, 4, 6$ ;  $n = 1, 2, 3$ ) longest hybrid modes.

# WAKE POTENTIAL

## Circular Cavity

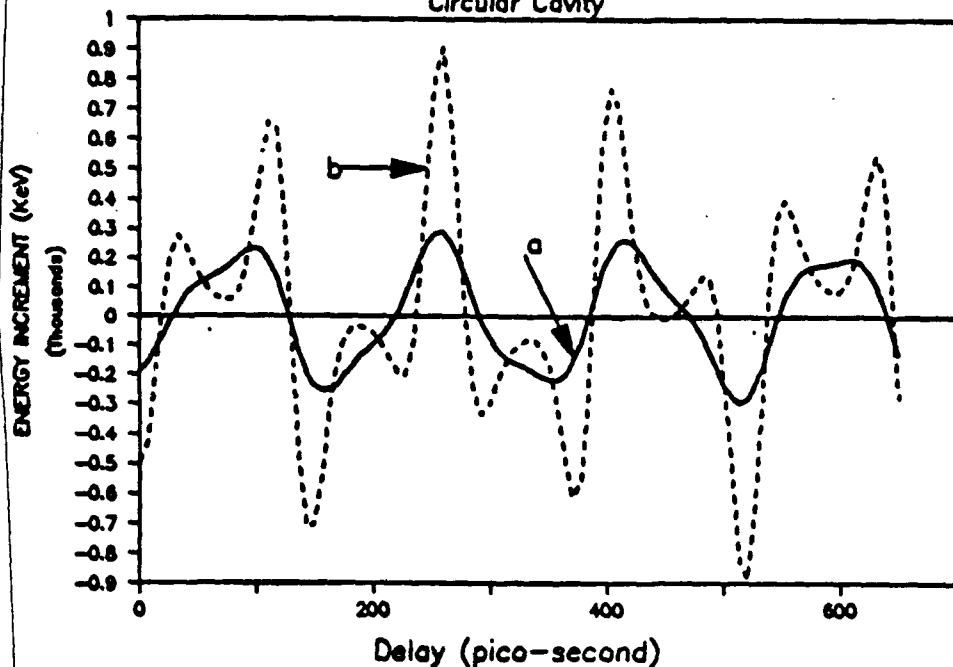


FIG. 2. Energy increment (in unit of KeV) over the total acceleration length as a function of the distance  $s$  between the accelerated charge and the driving charge in unit of picosecond. The cavity has the following parameters: cavity radius  $R_c = 19.5$  mm, aperture radius  $r_0 = 6.3$ , pill-box gap  $p = 6.3$  mm, driving charge  $Q = 3.1$  nC, number of pill boxes = 60, and rms length of the driving charge  $\sigma = 8, 4$  mm. The contributions from the fifteen most dominant longitudinal modes are considered. (a)  $\sigma = 8$  mm. (b)  $\sigma = 4$  mm.

$$\frac{U_1(s)}{L} = \frac{4\pi Q}{p^2} \sum_{\alpha} V_{\alpha}^*(x_0, 0, \lambda_{\alpha}) \nabla_1 V_{\alpha}(-x_0, 0, \lambda_{\alpha}) \lambda_{\alpha} \times \sin(s/\lambda_{\alpha}), \quad (41)$$

Accordingly, the transverse wake potential driven by the driving charge of an arbitrary charge distribution is defined by

$$U_1(s) = \int_{-s}^{\infty} U_1(s+s')g(s')ds', \quad (42)$$

where  $g(s)$  is the charge distribution of the driving bunch.

### B. The wake potentials in an elliptical cylindrical cavity

From the previous theoretical result (Fig. 1) and an experiment,<sup>2</sup> we found that the aperture of practical size does not affect significantly the wake field, and the wake field is predominated by the longitudinal modes. Therefore, we neglect the hybrid modes, and consider only the wake fields contributed from the longitudinal modes.

To obtain the wake fields from the longitudinal modes in an elliptical cavity whose periphery of the cross section is given by

$$\frac{x^2}{x_b^2} + \frac{y^2}{y_b^2} = 1, \quad (43)$$

we must solve Eq. (21) with the boundary condition such that  $f = 0$  on this periphery. We first note that the solution must be an even or odd function for  $y$  since both the equation [Eq. (21)] and the boundary condition are invariant when  $y$  is replaced by  $-y$ . However, the odd functions do not contribute to either longitudinal or transverse wake-potential at the foci whose  $y$  values are zero, and accordingly should be excepted. Also, we note that  $f$  and  $\nabla_1 f$  must be finite at the

foci since both the longitudinal and transverse wake-potentials are finite.

The solution can be found in terms of known functions by the transformation of the coordinates system to the elliptical cylindrical coordinates.<sup>14</sup>

The elliptical cylindrical coordinates  $(\xi, \eta)$  are related with the cartesian coordinates by the following equations:

$$\begin{aligned} x &= h \cosh \xi \cos \eta, \\ y &= h \sinh \xi \sin \eta, \end{aligned} \quad (44)$$

where  $2h$  is the distance between two foci, i.e.,  $h = \sqrt{x_b^2 - y_b^2}$ . Then, the problem is transformed to solve

$$\frac{\partial^2 f}{\partial \xi^2} + \frac{\partial^2 f}{\partial \eta^2} + 2k^2(\cosh 2\xi - \cos 2\eta)f = 0. \quad (45)$$

in the region  $0 < \xi < \xi_0, 0 < \eta < 2\pi$  with the boundary condition

$$f(\xi_0, \eta) = 0, \quad (46)$$

where  $k = h/2\lambda$  and  $\xi_0 = \cosh^{-1}(x_b/\sqrt{x_b^2 - y_b^2})$ .

By means of the separation of variables, we have  $f(\xi, \eta) = \phi(\xi)\psi(\eta)$  where  $\phi(\xi)$  and  $\psi(\eta)$  satisfy the following Mathieu equations:

$$\frac{d^2 \psi}{d\xi^2} - (a - 2k^2 \cosh 2\xi)\psi = 0, \quad (47)$$

$$\frac{d^2 \phi}{d\eta^2} + (a - 2k^2 \cos 2\eta)\phi = 0, \quad (48)$$

where  $a$  is the separation constant.

Since we consider only the even functions of  $y$ , we have that  $\phi(\eta) = \phi(2\pi - \eta)$ . From this parity consideration,  $f$  being finite at the foci and Eqs. (46)-(48), the solutions are expressed as

$$f(\xi, \eta) = \sum_m \sum_q N_{mq} C_{e_m}(\xi, q) c_{e_m}(\eta, q) + \sum_m \sum_q N'_{mq} S_{e_m}(\xi, q) c_{e_m}(\eta, q), \quad (49)$$

where  $q = k^2$ ,  $N_{mq}$  and  $N'_{mq}$  are the normalization constant, and

$$C_{e_m}(\xi_0, q) = S_{e_m}(\xi_0, q) = 0, \quad (50)$$

for any value of  $q$ .

Since  $\partial f / \partial x = \nabla_{\perp} f \cdot \hat{x}$  at the foci, i.e.,  $(\xi, \eta) = (0, 0)$  and  $(0, \pi)$ , is given by

$$\frac{\partial f(0, 0)}{\partial x} = \frac{1}{h} \lim_{\xi \rightarrow 0} \left( \frac{1}{\sinh \xi} \frac{\partial f(\xi, 0)}{\partial \xi} \right),$$

$$\frac{\partial f(0, \pi)}{\partial x} = -\frac{1}{h} \lim_{\xi \rightarrow 0} \left( \frac{1}{\sinh \xi} \frac{\partial f(\xi, 0)}{\partial \xi} \right), \quad (51)$$

the condition that the transverse wake-field is finite leads to the discard of all  $S_{e_m}(\xi, q) c_{e_m}(\eta, q)$  terms in Eq. (49). Further, we are concerned with large eigenvalue  $\lambda$ , which corresponds to small values of  $q$  under the condition Eq. (50). Accordingly, we can ignore the terms with  $m > 1$ . Therefore, we obtain

$$f(\xi, \eta) = \sum_q N_q C_{e_0}(\xi, q) c_{e_0}(\eta, q), \quad (52)$$

where  $q$ 's are the real roots of the following equation:

$$0 = 1 - \frac{1}{2} q \cosh 2\xi_0 + \frac{1}{32} q^2 \cosh 4\xi_0 - \frac{1}{73} q^3 (\frac{1}{2} \cosh 6\xi_0 - 7 \cosh 2\xi_0) + \frac{1}{73 \cdot 728} q^4 (\cosh 8\xi_0 - 320 \cosh 4\xi_0) + O(q^5), \quad (53)$$

and  $N_q$  is the normalization constant given by

$$\frac{1}{N_q^2} = \frac{h^2}{2} \int_0^{\xi_0} d\xi \int_0^{2\pi} d\eta (\cosh 2\xi - \cos 2\eta) [C_{e_0}(\xi, q) c_{e_0}(\eta, q)]^2. \quad (54)$$

If  $q$ 's and  $N_q$ 's are determined, then the longitudinal wake potentials on the same path as that of the driving bunch by a gaussian driving charge of length  $\sigma$  is, for  $s \gg \sigma$ ,

$$\frac{W_z(0, 0)}{L} = \frac{4\pi Q h^2}{p^2} \sum_q \frac{N_q^2}{q} \alpha^4(q) \sin^2(\sqrt{q}/h) \times \exp(-2q\sigma^2/h^2) \cos(2\sqrt{qs}/h), \quad (55)$$

and the longitudinal wake potential on the opposite path is

$$\frac{W_z(0, \pi)}{L} = \frac{4\pi Q h^2}{p^2} \sum_q \frac{N_q^2}{q} \alpha^4(q) \sin^2(\sqrt{q}/h) \times \exp(-2q\sigma^2/h^2) \cos(2\sqrt{qs}/h). \quad (56)$$

where

$$\alpha(q) = C_{e_0}(0, q) = c_{e_0}(0, q) = c_{e_0}(\pi, q) = 1 - \frac{1}{2} q + \frac{1}{32} q^2 + \frac{31}{73 \cdot 728} q^3 - \frac{319}{73 \cdot 728} q^4 + O(q^5).$$

Similarly, the transverse wake-potential on the same path as that of the driving charge is

$$\frac{U_x(0, 0)}{L} = \frac{2\pi Q h^2}{p^2} \sum_q \frac{N_q^2}{\sqrt{q}} \alpha^3(q) \beta(q) \sin^2(\sqrt{q}/h) \times \exp(-2q\sigma^2/h^2) \sin(2\sqrt{qs}/h), \quad (57)$$

$$\frac{U_y(0, 0)}{L} = 0, \quad (58)$$

and the transverse wake potential on the opposite path is

$$\frac{U_x(0, \pi)}{L} = -\frac{2\pi Q h^2}{p^2} \sum_q \frac{N_q^2}{\sqrt{q}} \alpha^3(q) \beta(q) \sin^2(\sqrt{q}/h) \times \exp(-2q\sigma^2/h^2) \sin(2\sqrt{qs}/h), \quad (59)$$

$$\frac{U_y(0, \pi)}{L} = 0, \quad (60)$$

where

$$\beta(q) = \frac{1}{q} \lim_{\xi \rightarrow 0} \left( \frac{1}{\sinh \xi} \frac{\partial C_{e_0}(\xi, q)}{\partial \xi} \right) = -2 + \frac{1}{2} q + \frac{3}{16} q^2 - \frac{79}{1152} q^3 + O(q^4).$$

From Eqs. (43) to (48), we find that the wake potential is symmetrical with respect to  $x = 0$  plane in the lowest ( $m = 0$ ) modal analysis.

Figure 3 shows the longitudinal wake potentials computed by the analytical formulation given by Eq. (55) for cavities of  $Q = 1$  nC,  $p = 4$  mm, and  $x_b/p = 10$  (i.e.,  $x_b = 4$  cm),  $\sigma = 8$  mm, and  $y_b/x_b = 0.9, 0.5, 0.3$  as the eccentricity parameter. From the curves, we find that the dominant wavelength increases as  $y_b/x_b$  increases, that is, the effective radius given by  $R_0 = \sqrt{x_b y_b}$  increases. We also find that the amplitude of the longitudinal wake potential does not become maximum as  $y_b/x_b \rightarrow 1$ , indicating that an elliptical cross section has a larger acceleration gradient than the circular cross section. The acceleration gradient can be greater than 100 MeV/m for a cavity having total driving charge of  $1 \mu\text{C}$ , pill-box gap of 4 mm, and an elliptical cross section of  $x_b = 10$  cm and  $y_b = 5$  cm.

Figure 4 shows the transverse wake potentials for the same cavities as in Fig. 3. From the curves, we find that we can make the undulating electric field in the transverse direction whose amplitude and wavelength are greater than 100 MeV/m and on the order of 10 cm, respectively, with a cavity having total driving charge of  $1 \mu\text{C}$ , pill-box gap of 4 mm, and an elliptical cross section of  $x_b = 10$  cm and  $y_b = 5$  cm.

## VI. CONCLUSION AND DISCUSSIONS

The potential of the wake-field produced by a bunch of relativistic charged particles passing through a pill-box cavity is expressed as a Fourier series based on the vector eigenmode-functions of the unit pill box. The Fourier coefficients are uniquely determined by Floquet's theorem, and an obvious requirement that the energy gain over all acceleration cavity of many pill boxes must be proportional to the number of pill boxes. The eigenmode functions must satisfy the elliptic-type partial differential equations derived from Maxwell's equations. The complete boundary conditions on the

## LONGITUDINAL WAKE-POTENTIAL

ELLIPTICAL CAVITY

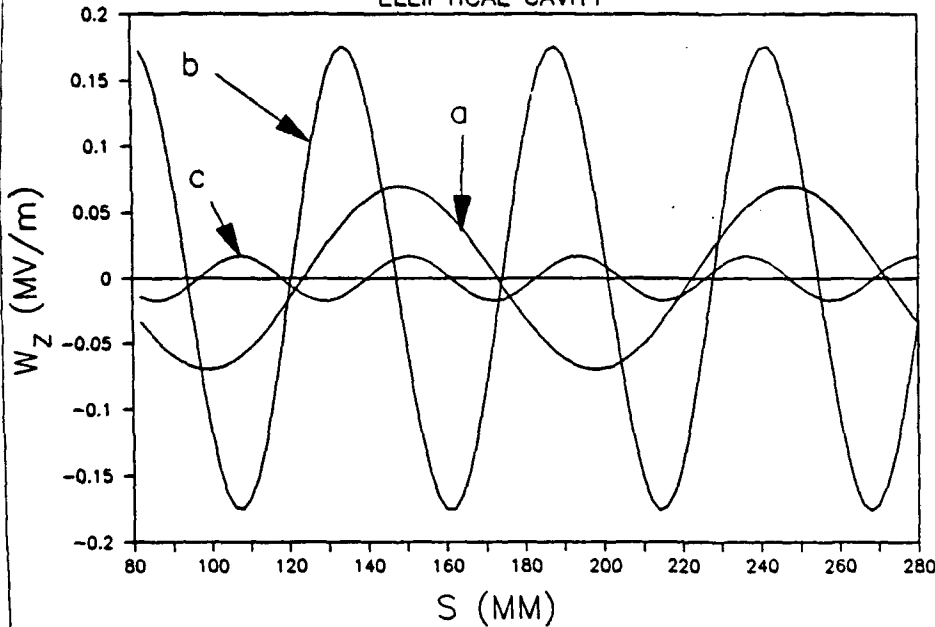


FIG. 3. Longitudinal wake potentials for three values of  $y_b/x_b$  in an elliptical cavity having  $Q = 1 \text{ nC}$ ,  $p = 4 \text{ n.m.}$ , and  $x_b/p = 10$  (i.e.,  $x_b = 4 \text{ cm}$ ),  $c = 8 \text{ mm}$ . (a)  $y_b/x_b = 0.9$ . (b)  $y_b/x_b = 0.5$ . (c)  $y_b/x_b = 0.3$ .

whole surface of the unit pill box, which are needed to determine uniquely the eigenmode functions, are assigned by taking into account the symmetry of the equation and boundary conditions, the continuity on the aperture, and the zero divergence of the eigenmode function, and the infinite conductivity on the conducting surface.

From the above formulation, we derive the wake field in a similar form of the Coulomb law. In particular, the wake potential of the circular cavity in the limit of vanishing aperture derived by our formulation is identical with that derived by the usual method using the synchronism between particle

and wave mode. It is found that the wake field consists of three classes of modes: the longitudinal modes which are independent of the aperture and the pill-box gap, the even hybrid modes which are independent of the aperture, but dependent of the pill-box gap, and the odd hybrid modes which are dependent on both the aperture and pill-box gap. The contributions from both the hybrid modes can be neglected compared to those from the longitudinal modes. We have found that the wake potential in most practical cavities is predominated by the contribution from the fundamental longitudinal mode whose wavelength is 2.6 times of the di-

## TRANSVERSE WAKE-POTENTIAL

ELLIPTICAL CAVITY

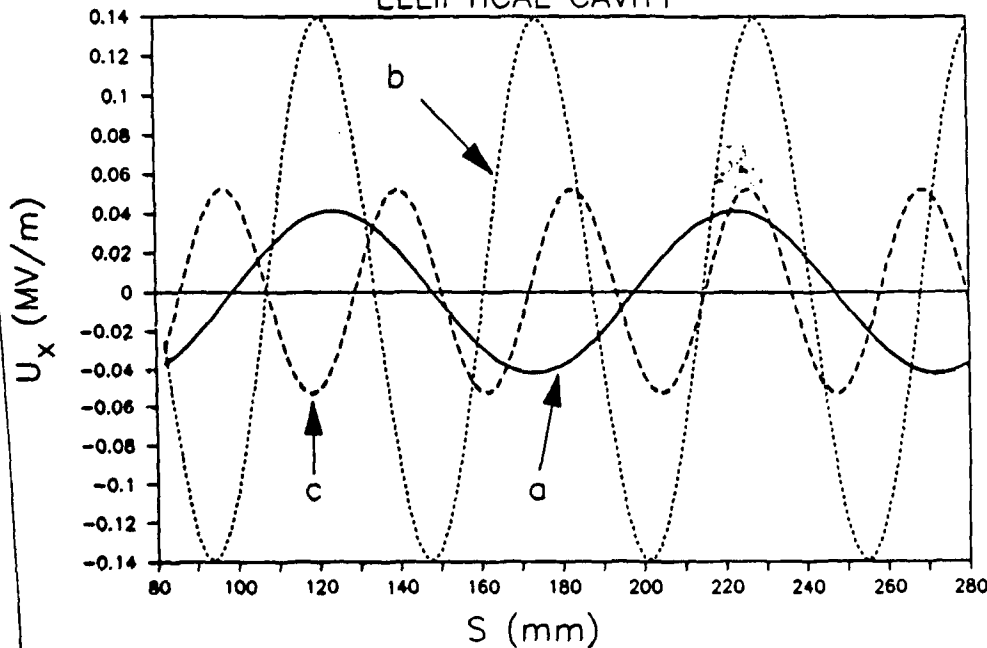


FIG. 4. Transverse wake potentials for three values of  $y_b/x_b$  in the same cavity as in Fig. 3. (a)  $y_b/x_b = 0.9$ . (b)  $y_b/x_b = 0.5$ . (c)  $y_b/x_b = 0.3$ .

1700wcl

ameter of the pill box, and is inversely proportional to the cross sectional area of the cavity. The result of this modal analysis is in excellent agreement with an experiment except that the length of the driving charge differs by a factor 2. We can attribute the difference to the aperture effect, which cannot be taken into account properly by the modal analysis when the aperture is large as in the experiment.

Unlike the circular cavity, we can generate the transverse wake field in the elliptical cavity. Both these fields can serve as a catalyzing field for stimulated bremsstrahlung, and thus are important in the application for a free electron laser. Both the wake fields from the longitudinal modes have been analytically obtained <sup>in terms of</sup> by the use of the Mathieu functions. The analytical result shows that we can generate both longitudinal and transverse wake fields having amplitude greater than 100 MV/m and wavelength on the order of 10 cm if we can produce a driving charge bunch of the order of 1  $\mu$ C in an elliptical cavity. *oe of*

#### ACKNOWLEDGMENT

This work was supported in part by the Air Force Office of Scientific Research under Grant No. 87-0280.

→ K. Nakajima

- <sup>1</sup>G. A. Voss and T. Weiland, DESY M82-10 (1982) and 82-074 (1982).
- <sup>2</sup>S. H. Kim, J. Plasma Phys. 36, 195 (1986); 41, 577 (1989); Phys. Lett. 135 A 39 (1989); in *Free-Electron Lasers and Applications*, ed. D. Prosnitz (SPIE, Bellingham, 1990), Vol. 1227, p. 66.
- <sup>3</sup>H. Figueroa, W. Gai, K. Konecny, J. Norem, A. Ruggiero, P. Schoessow, and J. Simpson, Phys. Rev. Lett. 60, 2144 (1988).
- <sup>4</sup>J. B. Rosenzweig, D. B. Cline, B. Cole, H. Figueroa, W. Gai, R. Konecny, J. Norem, P. Schoessow, and J. Simpson, Phys. Rev. Lett. 61, 98 (1989).
- <sup>5</sup>K. Nakajima, A. Eno, H. Kobayashi, H. Nakanishi, Y. Nishida, A. Ogata, S. Ohsawa, T. Oogoe, T. Shoji, and T. Urago, *Jpn. Phys. Soc.* (to be published). *Nucl. Instr. Methods A* 292, 12 (1990)
- <sup>6</sup>W. Gai, P. Schoessow, B. Cole, R. Konecny, J. Norem, J. Rozenzweig, and J. Simpson, Phys. Rev. Lett. 61, 2756 (1988).
- <sup>7</sup>K. L. F. Bane, P. B. Wilson, and T. Weiland, AIP Conf. Proc. 127, 876 (1983).
- <sup>8</sup>T. Weiland and B. Zotter, Particle Accelerators 2, 143 (1981).
- <sup>9</sup>Y. Chin, KEK-Report, 83-19 (1983).
- <sup>10</sup>For various numerical and analytical methods, see P. B. Wilson, AIP Conf. Proc. 184, 525 (1989).
- <sup>11</sup>M. Baranger and B. Mozer, Phys. Rev. 123, 25 (1961).
- <sup>12</sup>S. H. Kim and H. Y. Chung, J. Appl. Phys. 49, 5081 (1978).
- <sup>13</sup>S. J. Smith and E. M. Purcell, Phys. Rev. 92, 1069 (1953).
- <sup>14</sup>N. W. McLachlan, *Theory and Application of Mathieu Functions* (Dover, New York, 1964).
- <sup>15</sup>S. H. Kim, CAST-88-10-31 (1988).

Nuclear Instruments and Methods  
in Physics Research A 292, 12  
(1990)

WAKE-FIELD ACCELERATION OF CHARGED PARTICLES  
WITH AN ELLIPTICAL CAVITY

The members of the committee approve the doctoral dissertation of Jin-Seok Yang

K. Wendell Chen  
Supervising Professor



B. P. Wang



Albert Y. Tong



S. Nomura



C. Corduneanu



Dean of the Graduate School



Copyright © by Jin-Seok Yang 1990

All Rights Reserved

WAKE-FIELD ACCELERATION OF CHARGED PARTICLES  
WITH AN ELLIPTICAL CAVITY

by  
JIN-SEOK YANG

Presented to the Faculty of the Graduate School of  
The University of Texas at Arlington in Partial Fulfillment  
of the Requirements  
for the Degree of

DOCTOR OF PHILOSOPHY

THE UNIVERSITY OF TEXAS AT ARLINGTON

August 1990

## ACKNOWLEDGEMENTS

I would like to express my sincere thanks to my supervising professor, Dr. K. Wendell Chen, for sharing much of his time to help and guide me throughout this study. His guidance, help and interest in my work as well as his helpful financial support are very much appreciated. My thanks are also due to Dr. S. H. Kim for his valuable suggestions and discussions.

I would like to extend my appreciation to each member of my supervising committee, Dr. Albert Y. Tong, Dr. Bo P. Wang, Dr. S. Nomura and Dr. C. Corduneanu, for their instructions and help during my graduate study. The experience and willingness to help of Mr. Ngon H. Nguyen and Mr. T. Pham are gratefully acknowledged.

Finally, I wish to express my deepest thanks to my dear parents for their devotion and endless support in many ways and to my wife, whose patience and support helped in the completion of this work

This work was supported in part by the Air Force Office of Scientific Research under Contract AFOSR-87-0280.

July 17, 1990

## ABSTRACT

### WAKE-FIELD ACCELERATION OF CHARGED PARTICLES WITH AN ELLIPTICAL CAVITY

Publication No. \_\_\_\_\_

Jin-Seok Yang, Ph.D.

The University of Texas at Arlington, 1990

Supervising professor : K. Wendell Chen

Acceleration of charged particles by the wake fields excited in the elliptical cavity by an intense, short electron bunch is investigated. Two cavities are considered as a wake-field device: disk-loaded metallic cavity and dielectric-loaded cavity. The analytical methods are developed to evaluate the wake fields and wake potentials in these cavities. Using modal analysis method, it is shown that the longitudinal and transverse wake potentials in the disk-loaded elliptical cavity can be expressed analytically in terms of the Mathieu functions. The aperture effects are not considered in this calculation. The longitudinal wake potential in a circular cavity are derived from that in an elliptical cavity, and it is shown to be exactly the same formula that was derived earlier. These analytical results are compared with numerical ones, and excellent agreements in both frequencies and amplitudes are observed between these two methods. Also, the wake fields in the dielectric-loaded structures are derived analytically using the Fourier transform method. It is shown that the dielectric-loaded structure can support strong accelera-

tion field, and has a useful property that the transverse wake fields can be made quite small for the ultra-relativistic driving beam. It is demonstrated that acceleration gradient greater than a few hundred MeV/m/ $\mu$ C can be achieved in the disk-loaded elliptical cavity or in the dielectric-loaded elliptical cavity.

## TABLE OF CONTENTS

ACKNOWLEDGEMENTS . . . . .	iv
ABSTRACT . . . . .	v
LIST OF FIGURES . . . . .	ix
Chapter	
I. INTRODUCTION . . . . .	1
II. NORMAL MODE EXPANSION OF THE WAKE POTENTIALS . . . . .	12
2.1. Introduction . . . . .	12
2.2. Method of Calculation . . . . .	16
2.3. Normal Mode Analysis of the Wake Fields . . . . .	17
2.4. Wake Potentials in a Cavity . . . . .	20
2.4.1. Longitudinal Wake Potential . . . . .	20
2.4.2. Transverse Wake Potential . . . . .	23
III. WAKE POTENTIALS IN AN ELLIPTICAL CAVITY . . . . .	25
3.1. Eigenmodes in an Elliptical Pill-Box Cavity . . . . .	25
3.2. Wake Potentials in an Elliptical Pill-Box Cavity . . . . .	34
3.2.1. Longitudinal Wake Potential . . . . .	34
3.2.2. Transverse Wake Potential . . . . .	43
3.3. Numerical Examples . . . . .	45
IV. WAKE POTENTIAL IN A DIELECTRIC-LOADED ELLIPTICAL WAVEGUIDE . . . . .	59
4.1. Introduction . . . . .	59
4.2. Formulation of Solution . . . . .	60
4.3. Wake Fields Calculation . . . . .	65
4.3.1. Solution to the Boundary Value Problem . . . . .	65

4.3.2. Longitudinal and Transverse Wake Fields . . . . .	.68
4.3.3. Transition to the Dielectric-Loaded Circular Waveguide . . .	.74
4.4. Numerical Example and Discussion . . . . .	.76
V. SUMMARY AND CONCLUSIONS . . . . .	.80
APPENDIX A . . . . .	.83
REFERENCES . . . . .	.90
GLOSSARY . . . . .	.93

## LIST OF FIGURES

Figure 1.1.	Sketch of an annular wake-field cavity. . . . .	5
Figure 1.2.	Multi-stage wake-field accelerator using elliptical cavities. . . . .	7
Figure 1.3.	Elliptical cavity as an electric FEL wiggler. . . . .	9
Figure 2.1.	Electromagnetic fields farried by a point charge in free space. . . . .	13
Figure 2.2.	Fields in a perfectly conducting smooth pipe (a) and in a structure with perturbing walls (b). . . . .	14
Figure 2.3.	The driving beam and accelerated beam in a cavity. . . . .	21
Figure 3.1.	Confocal elliptical coordinate system. . . . .	26
Figure 3.2.	Elliptical pill-box cavity. . . . .	31
Figure 3.3.	Plot of $q_{01}$ as a function of eccentricity $e_c$ . . . . .	32
Figure 3.4.	Plot of the wavelength of the fundamental mode as a function of eccentricity $e_c$ . . . . .	33
Figure 3.5.	Configuration of resonant modes $a_{z_{omp}}$ in an elliptical cavity ( $m=0, n=1, p=0$ ). . . . .	35
Figure 3.6.	Configuration of resonant modes $a_{z_{omp}}$ in an elliptical cavity ( $m=1, n=1, p=0$ ). . . . .	36
Figure 3.7.	Configuration of resonant modes $a_{z_{omp}}$ in an elliptical cavity ( $m=2, n=1, p=0$ ). . . . .	37
Figure 3.8.	Configuration of resonant modes $a_{z_{omp}}$ in an elliptical cavity ( $m=3, n=1, p=0$ ). . . . .	38
Figure 3.9.	Cavity dimensions for example calculation. . . . .	48
Figure 3.10.	Longitudinal wake potential on the accelerated beam path ( $Q = 1\mu\text{C}, \sigma = 5 \text{ mm}$ , 5 modes are included). . . . .	49
Figure 3.11.	Longitudinal wake potential on the accelerated beam path ( $Q = 1\mu\text{C}, \sigma = 5 \text{ mm}$ , solid line for 24 modes and broken line for 12 modes). . . . .	50
Figure 3.12.	Longitudinal wake potential on the driving beam path ( $Q = 1\mu\text{C}, \sigma = 5 \text{ mm}$ , solid line for 24 modes and broken line for 12 modes). . . . .	51
Figure 3.13.	Normalized wake potentials on the accelerated beam path Solid line : longitudinal wake potential/(3.40 MeV/ $\mu\text{C}$ ) Broken line : transverse wake potential/(1.29 MeV/ $\mu\text{C}$ ) . . . . .	52

Figure 3.14.	Normalized wake potentials on the driving beam path. Solid line : longitudinal wake potential/(2.77 MeV/ $\mu$ C) Broken line : transverse wake potential/(1.68 MeV/ $\mu$ C) . . .	.53
Figure 3.15.	Longitudinal wake potential on the driving beam path ( $Q = 1\mu$ C, $\sigma = 5$ mm, major axis = 10 cm, minor axis = 4 cm, $\sigma = 5$ mm, gap distance = 2 cm). . . . .	.54
Figure 3.16.	Longitudinal wake potential on the driving beam path ( $Q = 1\mu$ C, $\sigma = 5$ mm, major axis = 10 cm, minor axis = 7 cm, $\sigma = 5$ mm, gap distance = 2 cm). . . . .	.55
Figure 3.17.	Longitudinal wake potential on the driving beam path ( $Q = 1\mu$ C, $\sigma = 5$ mm, major axis = 10 cm, minor axis = 8 cm, $\sigma = 5$ mm, gap distance = 2 cm). . . . .	.56
Figure 3.18.	Normalized wake potentials on the accelerated beam path (from ref. 22, $Q = 1\mu$ C, $\sigma = 5$ mm, major axis = 10 cm, minor axis = 6 cm, $\sigma = 5$ mm, gap distance = 2 cm) . . .	.57
Figure 3.19.	Normalized wake potentials on the driving beam path (from ref. 22, $Q = 1\mu$ C, $\sigma = 5$ mm, major axis = 10 cm, minor axis = 6 cm, $\sigma = 5$ mm, gap distance = 2 cm). . .	.58
Figure 4.1.	Cross section of the elliptical waveguide partially filled with dielectric. . . . .	.61
Figure 4.2.	Transition to the dielectric-loaded circular waveguide. . . . .	.77
Figure 4.3.	Dielectric-loaded elliptical waveguide dimensions. . . . .	.78
Figure 4.4.	Longitudinal wake potential in a dielectric-loaded elliptical waveguide ( $\epsilon = 2$ , major axis = 10 cm, minor axis = 6 cm). . . . .	.79
Figure A.1.	Plots of Mathieu functions of the first kinds of even integral order. . . . .	.88
Figure A.2.	Plots of Mathieu functions of the first kinds of odd integral order. . . . .	.89

## CHAPTER I

### INTRODUCTION

The invention and continued development of particle accelerators and the associated technologies have had a profound impact on many fields of pure and applied science and on variety of branches of modern technology. In the fields of high energy and nuclear physics, a marvelous complement of accelerator facilities exists around the world. In other area of science, synchrotron light sources and accelerator-driven pulsed neutron sources have opened up revolutionary new research opportunities in materials, chemistry, and biological research. In industry and medicine there are literally thousands of accelerators in use in health care treatment, radiation sterilization, radiation processing, ion implantation, microchip production, etc.

During the past few decades, accelerator energies have been increasing from KeV to TeV at the rate of an order of magnitude in about every seven years due mainly to imaginative advances in accelerator technology and design. As the demand of higher accelerator energy is increased, it becomes more important to produce higher acceleration gradient to decrease the size, cost and complexity of accelerators, especially for the future linear colliders. This has motivated the development of new ideas for charged particle acceleration, which are expected to produce acceleration gradient much higher than that conventional accelerators can produce. Typical acceleration gradient of conventional accelerators is about 20 MeV/m. The new acceleration schemes under active theoretical and experimental research are: (1) Laser-Plasma Acceleration,<sup>1-5</sup> (2) Plasma Wake-field Acceleration,<sup>6-9</sup> (3) Wake-

field Acceleration,<sup>10-16</sup> etc.

Over the last few years, substantial progress both theoretically and experimentally has been made on these new acceleration schemes. The plasma-based acceleration schemes utilize the extremely large high acceleration gradient associated with plasma waves excited by a number of ways, for example, by using high power laser beam<sup>1,2</sup> (Laser Wake-field Acceleration), beating of two relatively lower power laser beams<sup>3</sup> (Plasma Beat Wave Acceleration), or using relativistic electron beams<sup>6</sup> (Plasma Wake-field Acceleration). For those schemes involving plasmas, acceleration gradients of the order of 1 GeV/m are theoretically possible. But plasma devices are very complicated and their practical applications have a number of unresolved issues which have not been fully explored. These are: fine tuning of plasma density and laser frequency, production of driving beam with a slow rise time and very rapid fall time, laser-plasma instability, focusing of laser beam, etc. The plasma accelerators really exhibit advantages over other concepts only at frequencies greater than about 100 GHz, and the problem of producing a suitable driver beam which is capable of propagating a sufficiently long distance within the plasma becomes more difficult as the frequency is increased.

In the moderate acceleration gradients (several hundred MeV/m), a class of wake-field acceleration schemes based on metallic cavity<sup>10-14</sup> or dielectric-loaded structure<sup>15,16</sup> (or combination of both) are promising new concepts in view of their structural simplicity and ease of phase matching. In these wake-field schemes, an intense, low-energy beam excites the electromagnetic fields (so called "wake fields") in a metallic cavity or in a medium, which are then used to accelerate a second, less intense beam to

high energies. The periodic structure plays the necessary role to produce the wake fields and to keep constant phase between an accelerated beam and the wake fields in a metallic cavity, while in the dielectric-loaded structure a driving beam excites the slow electromagnetic waves through the Cerenkov radiation mechanism.

Let us briefly discuss some features of early works on these wake-field acceleration schemes. Recently, proof-of-principle tests for the wake-field acceleration schemes<sup>14,16</sup> have been demonstrated at the Argonne National Laboratory (ANL). It was shown that a few hundred MeV/m acceleration gradient can be achieved in the disk-loaded metallic cavity and in the dielectric-loaded cavity provided the driving beam is sufficiently intense (of the order of 1 micro-Coulomb). Wake-field cavities tested have a common geometry, i.e., both the driving and accelerated bunches pass through the same path (so called "co-linear geometry"). For the co-linear structures, there is a fundamental theorem that the transformer ratio, defined as the ratio of the maximum energy gain per particle of the accelerated bunch to the maximum energy loss per particle of the driving bunch, can not exceed two when the driving bunch has a symmetric charge distribution. This theorem complicates the practical applications of wake-field acceleration schemes, especially for high energy linear colliders.

However, we can overcome this problem by either increasing the transformer ratio or staging the cavities. The transformer ratio can be increased by a number of ways, for example, by mixing,<sup>17</sup> injecting an asymmetrical driver bunch,<sup>18</sup> injecting multiple bunches,<sup>13</sup> non-linear effects in dielectric, using cavity of annular geometry,<sup>10</sup> etc. But practical realization of such methods meets with some difficulties and limitations, and has not been

developed yet. Other method to overcome the low transformer ratio is to use multi-stage scheme, i.e., acceleration in short distance. For accelerators of low transformer ratio, it is inevitable to replenish the energy of the driving bunch or to replace used driving bunch by a new one frequently. For the co-linear cavities, re-acceleration of the decelerated driver or replacement of the driving charge appears difficult and technically unattractive, as it requires disposing of the spent driver beam and introducing new one without disturbing the accelerated beam. Multi-staging can be readily realized with non-concentric cavities which have separate paths for the driving and accelerated beams.

Among the co-linear wake-field devices, the cavity of an annular geometry had been once rigorously investigated.<sup>10</sup> Here, we briefly discuss the features of this well-known geometry. The largest transformer (impedance transformation) ratio is expected in a concentric arrangement as shown in figure 1.1. In this scheme, high current ring-shaped driver bunch is used to accelerate a low current beam following the central axis. For a symmetric driving bunch, transformer ratio in excess of 20 can be realized. Utilizing asymmetrical shaping of the driving beam, it has been shown numerically that an optimal transformer ratio as high as 100 is possible in this annular wake-field device. However, the practical realization of this device or the asymmetrical shaping of the driver beam meets with rather stringent experimental limitations. While the production of short, intense annular electron ring beam is already difficult, but feasible (e.g. workers at DESY, West Germany, once tried such an experiment), the additional requirement that the electron ring beams must possess no rotational movement while traversing the series of annular slots is exceedingly difficult because the

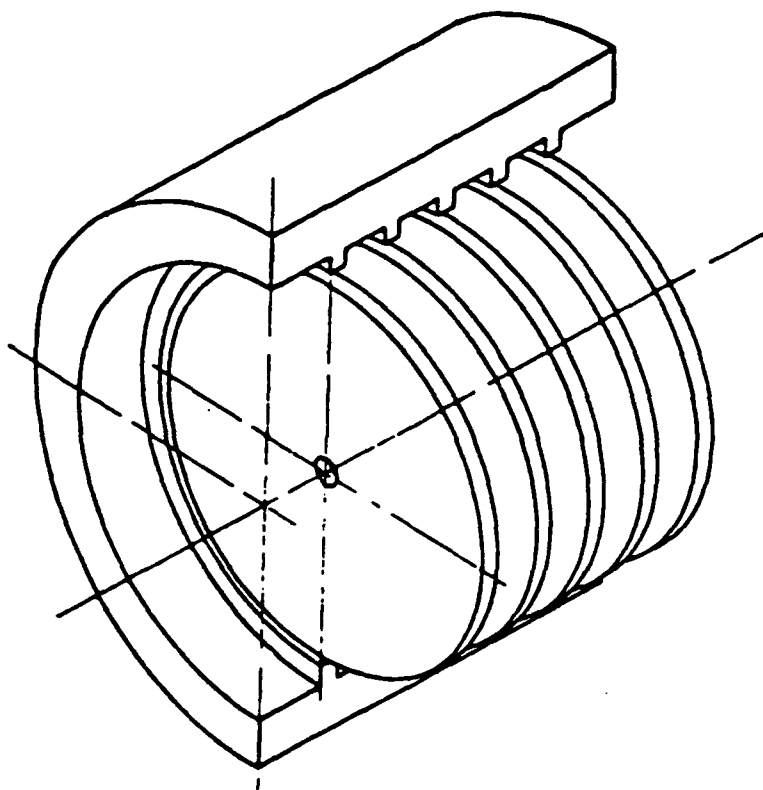


Figure 1.1. Sketch of an annular wake-field cavity

inner disks must be supported in place with wires or rods. The ring beam will be lost if rotation is present. In addition, even if the driver beam does not rotate appreciably, the supports destroy the apparent rotational symmetry by creating holes in the ring, thus make the ring beam much vulnerable to possible transverse beam instabilities.

The past experimental program at DESY is not adversely affected by these difficulties because of its very short accelerating structures of 40 cm. For a long accelerator structure, say even for a 1 GeV machine, these problems could become quite troublesome. Staging could help, but not so attractive due to its concentric geometry. Replacing the annular beam by cylindrical beamlets symmetrically located around the annular ring has been discussed. Here again the possible transverse instability inherent in this arrangement is difficult to eliminate and also required phase synchronism is difficult to achieve.

A different approach was employed in the UTA Wake-field and FEL program. Multi-stage acceleration scheme was adapted to overcome the low transformer ratio and still provide high acceleration gradient. For the staging purpose, we choose an elliptical geometry because of its inherent staging capability. Unlike the co-linear geometries, replenishing the energy-depleted driver beams is practical for the elliptical structures since two beam apertures of unequal size around the foci of an ellipse provide two separate paths for the driving and accelerated bunches. Although the transformer ratio is not as high, adequate acceleration gradients in such a structure are possible when the driving beam passes through a high-impedance aperture but is replenished periodically as shown schematically in figure 1.2. Since the driving beam is to deliver energy in a single stage, it is possible to

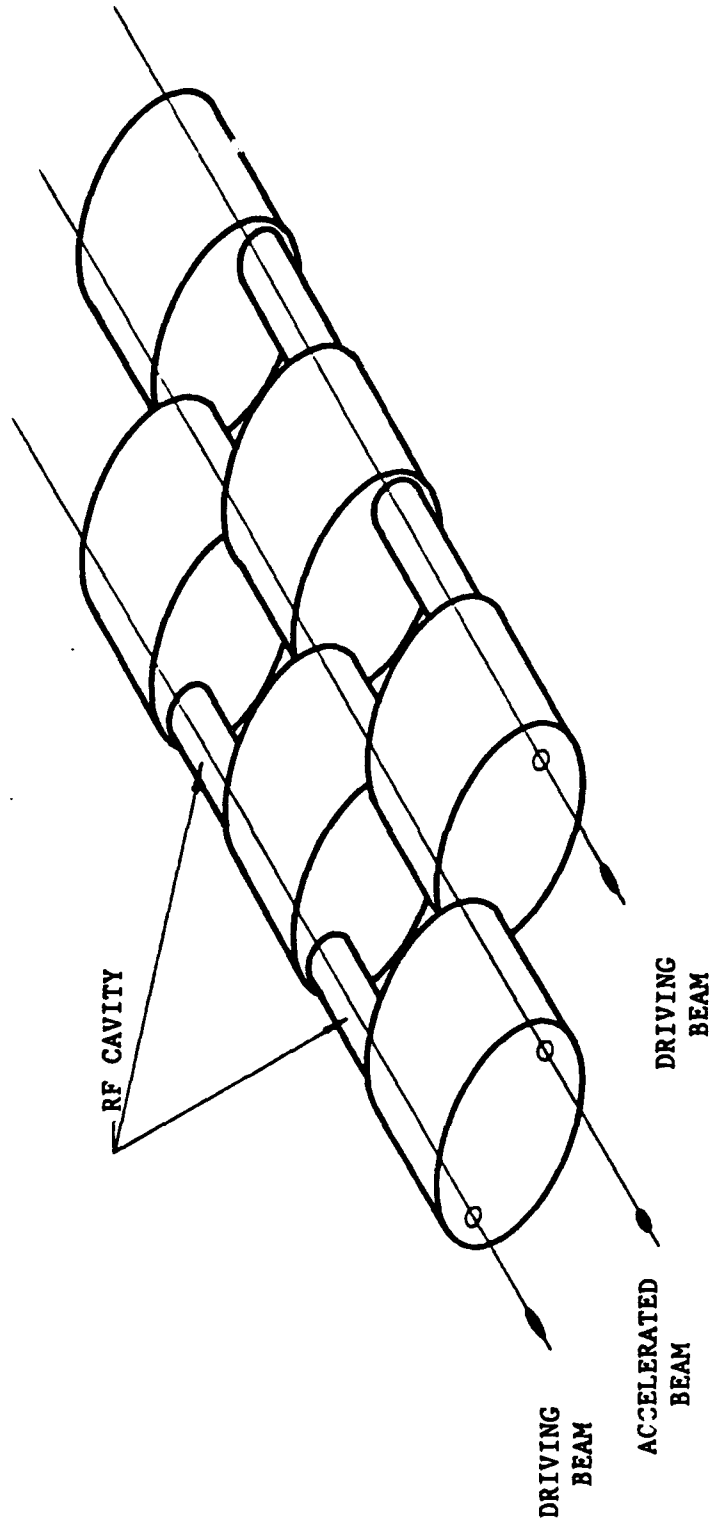


Figure 1.2. Multi-stage wake-field accelerator using elliptical cavities

do so at a high rate. Because of the staging capability, it is now possible to obtain the correct synchronism to overcome the usual "phase slippage" between the faster accelerated beam and the slower driver beam. Another unique application of the elliptical wake-field cavity which cannot be realized with the co-linear geometry is that it can be used as an electric wiggler in a Free Electron Laser<sup>19</sup> (FEL), as shown schematically in figure 1.3. Two separate paths along the focus axis of the elliptical cavity allow the lasing electron beam to be injected in the opposite direction of the driving bunches. The lasing electron bunches wiggle in the rippled wake electric fields produced by the driving bunches, analogous to the case of the magnetic wigglers in conventional FELs. This new lasing scheme promises sufficient gains in the soft x-ray region so that it might be feasible to operate it as a soft x-ray laser without requiring reflecting mirrors.

Based on these ideas, investigations of wake-field acceleration and its applications with the emphasis on the elliptical geometry have been going on<sup>13,19-21,23</sup> at the Center for Accelerator Science and Technology (CAST), UTA, in the last few years, part of which is the subject of this dissertation.

The purpose of this dissertation is to set up appropriate theoretical means to analyze the wake fields excited in the elliptical cavity which is loaded with metallic disks or a medium. The wake fields and wake potentials in the disk-loaded cavity can be evaluated by either modal analysis method or numerically solving the Maxwell equations directly in the time domain. Because analytical calculations are only known for closed cylindrical cavities, the wake fields in an elliptical cavity have been roughly estimated from those in the equivalent circular cavity. Furthermore, no method has been developed to calculate wake fields in a dielectric-loaded elliptical

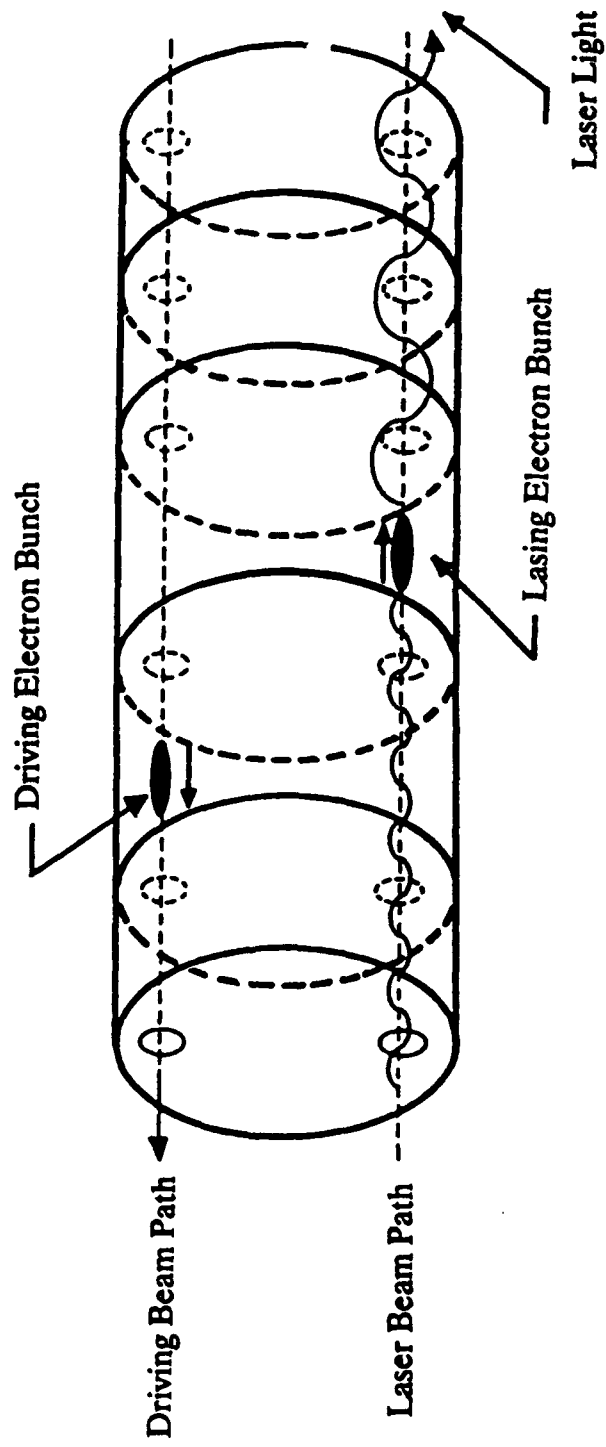


Figure 1.3. Elliptical cavity as an electric FEL wiggler

cavity. The numerical code WELL,<sup>22</sup> which directly solves the Maxwell equations in the time domain, has been recently developed to study the wake-field effects in the elliptical pill-box cavity. This particular code calculates the wake fields and wake potentials in an elliptical pill-box cavity by using the finite difference method, and the beam aperture effects are considered in the calculations.

In this investigation, new methods are developed to calculate the wake fields in the elliptical structure analytically in the limit of vanishing aperture. We do not take into account the aperture effects based on the recent experimental work,<sup>14</sup> which showed that the wake fields are predominated by a few lower-order longitudinal modes even when the ratio of the aperture radius to the cavity radius is considerably large. At lower frequencies, it was known that the impedance of a cavity with finite aperture and that of a closed cavity are practically same.<sup>37</sup> Therefore, the wake fields of bunches which is long compared to the aperture, or the long range wake fields of short bunches are almost the same for the two different structures. Since wake-field acceleration schemes require very short, intense bunches to excite strong accelerating field, and the distance between the driving bunch and accelerated bunch is usually large compared to the driving bunch length, the wake fields in the limit of vanishing aperture is a good approximation for the most practical cavities as long as apertures are not too large. Even though it is a limiting case for the cavities with finite apertures, it is of particular interest since the analytical solution exist, which will be formulated in this investigation. Therefore, we can readily estimate maximum energy gain of the accelerated particles and the parametric dependence of the wake potentials on the geometry and beam parameters. Furthermore, it becomes

possible to include the effects of dielectric material inside the cavity with this analytical approach.

A short review of the concepts of the wake fields, the wake potential, and detailed modal analysis method are presented in Chapter 2. We present analytical formulations of the wake fields and wake potentials in an elliptical pill-box cavity in Chapter 3. The wake-field effects in the dielectric-loaded elliptical cavity are described in Chapter 4, while in Chapter 5 discussions and conclusions are drawn.

## CHAPTER II

### NORMAL MODE EXPANSION OF THE WAKE POTENTIALS

#### 2. 1. Introduction

The wake fields are the electromagnetic fields induced by a bunch of relativistic charged particles passing through the structure of varying shape, and their concepts are important not only for the applications to future high current compact electron accelerators, but also for the calculation of energy loss and beam stability in the high energy particle accelerators. We begin with brief introduction of the concepts of the wake fields and wake potentials.

Consider a point charge  $Q$  in free space. When a charge is not moving, the electric field lines are directed outward in all radial directions as shown in figure 2.1(a). But the electromagnetic fields carried by a relativistic point charge  $Q$  in free space<sup>24</sup> is Lorentz contracted into a thin disk as shown in figure 2.1(c) with angular spread of the order of  $1/\gamma$ , where  $\gamma$  being the relativistic factor. The disk actually shrink into a delta function thickness in the ultra-relativistic limit of the particle velocity  $v = c$ , as shown in figure 2.1(d). In case the charge moves along the axis of a cylindrically symmetric pipe with perfectly conducting wall, the fields in the pipe are identical to the free space fields, because the sole function of the pipe wall is to truncate the field lines by terminating them onto the image charges on the wall as shown in figure 2.2(a). If the charge moves off-axis, or if the cross section of the pipe is not a circle, the fields

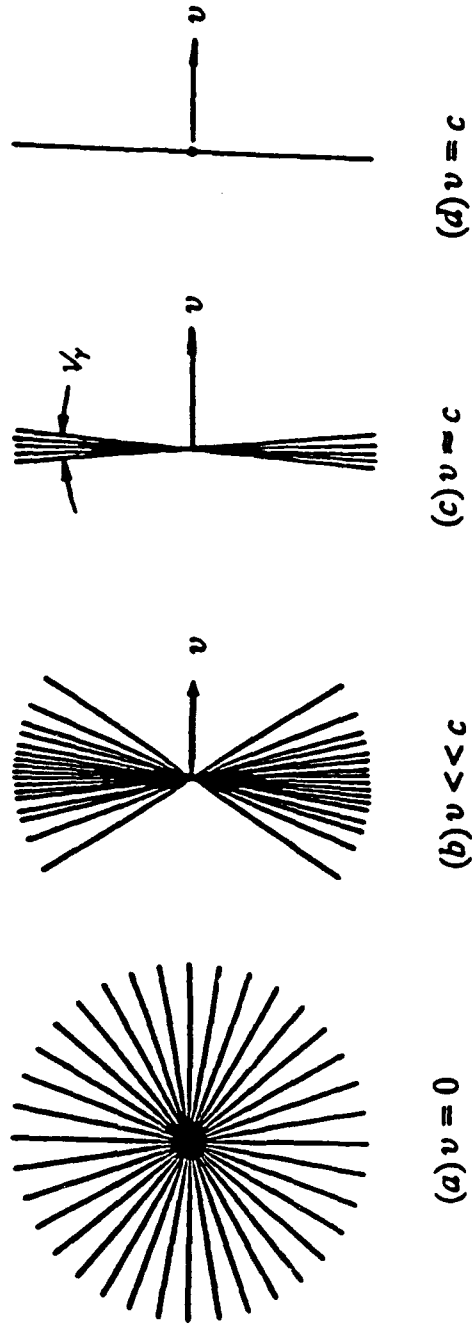


Figure 2.1. Electromagnetic fields carried by a point charge in free space  
(electric field lines are shown)

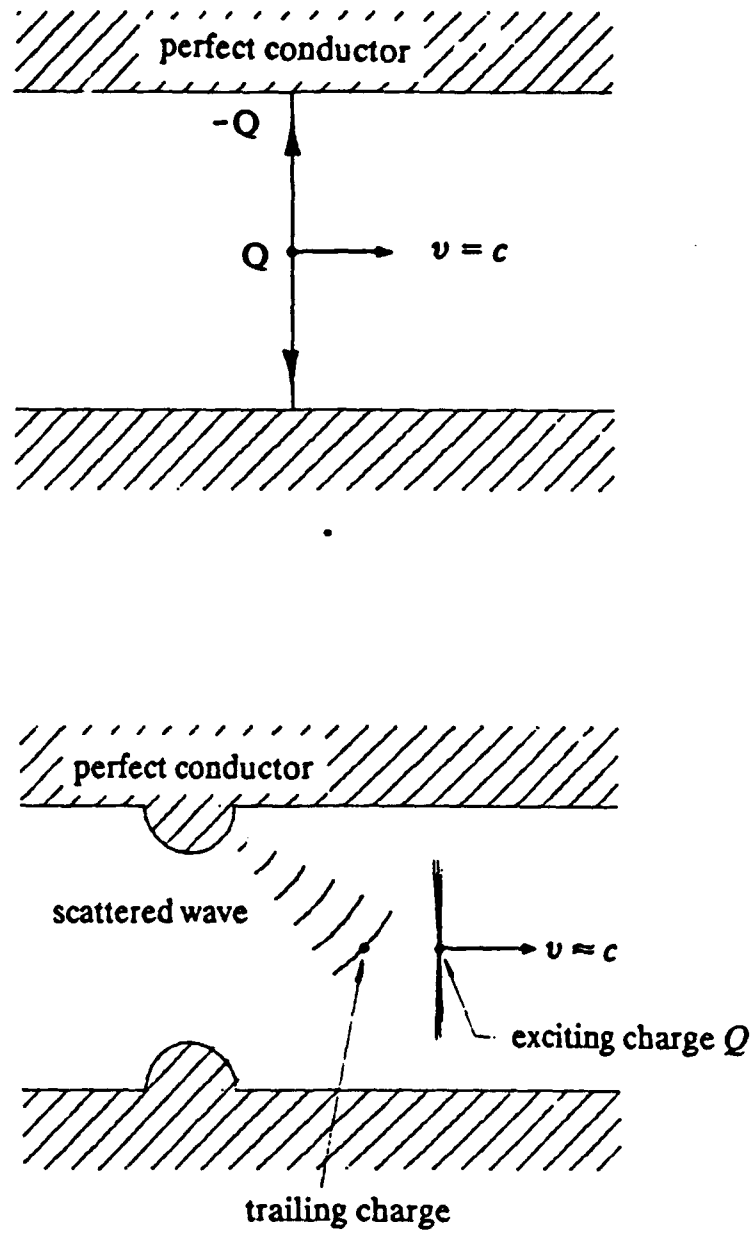


Figure 2.2. Fields in a perfectly conducting smooth pipe (a) and in a structure with perturbing walls (b)

in the pipe are perturbed from their free space values. But, no fields are left behind the moving charge since the fields are Lorentz contracted into a delta function in its longitudinal distribution.

Therefore, in free space or in a perfectly conducting smooth pipe, a particle does not see the fields carried by other particle unless the two particles move side by side with exactly same longitudinal position, in which case they see each other's fields but do not experience any force because the electric force and the magnetic force cancel exactly in the limit of particle velocity  $v = c$ .

When there are irregularities or discontinuities in the structure, the trailing charge still will not see the direct fields in the wavefront moving with the driving charge. However, this wavefront are scattered from the boundary discontinuities, and this scattered radiation can reach the trailing charge and exert forces parallel and perpendicular to its direction of motion. These scattered waves are called the wake fields, and the force integrated over the total passage time is usually called the wake potential (more precisely delta function wake potential).

If the wall is smooth but not perfectly conducting,<sup>25,26</sup> a charge will generate behind it the wake fields due to the small longitudinal electric field  $E_z$  at the wall, which is related to the dissipation in the wall. However, the effects of resistive wall are much smaller than other factors. Most of the wake fields come from effects associated with discontinuities and obstacles in the structures. Therefore, in the following section and thereafter, finite conductivity effects will not considered in the wake fields calculations. It is also assumed in this chapter that the driving charge and the test charge move with velocity of light  $c$ , and their paths through a cavity or

structure are not significantly changed from what would have been in the absence of the induced wake fields.

## 2. 2. Method of Calculation

The wake fields and wake potentials in a cavity can be evaluated by either modal analysis method or numerically solving the Maxwell equations in the time domain. In the modal analysis method, the eigenmodes of an empty cavity are used to calculate the time development of the fields. Analytical calculations of the eigenmodes are only known for cavities with simple geometries, usually for closed cylidrically symmetric cavities. For this reason, early studies on the wake-field cavities were mainly concentrated on the circular geometry. For non-axisymmetrical structures, one has to use numerical methods.

The straightforward way to calculate wake fields and wake potentials in the structure is to solve the Maxwell equations numerically. The numerical code TBCI<sup>27,28</sup> has been extensively used for the cylidrically symmetric structures, and MAFIA<sup>29</sup> code T3, a three dimensional version of the code TBCI, was recently developed. Previously, the particular code WELL,<sup>22</sup> the finite difference solution of the Maxwell equations in the time domain, has been developed for the calculation of the wake fields in an elliptical cavity. In this code, the aperture or beam hole effects are included in the calculation. However, we need not take into account the aperture effects seriously for the most practical cavities whose apertures are usually very small compare to the cross sectional area. This is clearly supported by the experiment,<sup>14</sup> which showed that the wake fields are predominated by a few lower-order longitudinal modes even when the ratio of the aperture radius to the cavity radius is considerably large ( $\approx 1/3$  for the cavity 1 in that ex-

periment). Since the impedance of a cavity with finite aperture and that of a closed cavity are practically same at lower frequencies, the wake fields of a bunch whose length is long compared to the aperture or the long range wake fields of a short bunch are almost the same for the two different structures. Since we are more interested in evaluating the long range wake fields induced by a short driving bunch, a closed pill-box cavity is a good approximation. Even though the final result is the limiting case for the cavity with beam holes, it is of particular interest since we can formulate an analytical solution under the assumption of zero aperture. The longitudinal and transverse wake potentials can be calculated to any degree of precision since we can express these fields analytically in closed series form. Also, we can readily estimate the maximum energy gain of the trailing particles, frequency contents, and the dependence on the cavity geometry and beam parameters.

### 2.3. Normal Mode Analysis of the Wake Fields

Consider a closed, empty cavity with perfectly conducting walls. The electric fields and the magnetic fields induced by a bunch of charged particles traversing the cavity can be derived from a scalar potential  $\varphi(\mathbf{x}, t)$  and a vector potential  $\mathbf{A}(\mathbf{x}, t)$  together with proper boundary conditions. First, let us start from the Maxwell equations (in MKS units)

$$\nabla \times \mathbf{E} = -\frac{\partial \mathbf{B}}{\partial t}, \quad (2.1)$$

$$\nabla \times \mathbf{B} = \mu_0 \mathbf{J} + \frac{1}{c^2} \frac{\partial \mathbf{E}}{\partial t}, \quad (2.2)$$

$$\nabla \cdot \mathbf{E} = \frac{\rho}{\epsilon_0}, \quad (2.3)$$

$$\nabla \cdot \mathbf{B} = 0, \quad (2.4)$$

where  $\epsilon_0$  and  $\mu_0$  are respectively the permittivity and permeability of vacuum. By introducing a vector potential  $\mathbf{A}(\mathbf{x}, t)$  and a scalar potential  $\varphi(\mathbf{x}, t)$  which are given by the relations

$$\mathbf{B} = \nabla \times \mathbf{A}, \quad (2.5)$$

$$\mathbf{E} = -\frac{\partial \mathbf{A}}{\partial t} - \nabla \varphi, \quad (2.6)$$

the inhomogeneous Maxwell eqs. (2.2) and (2.3) become

$$\nabla^2 \mathbf{A} - \frac{1}{c^2} \frac{\partial^2 \mathbf{A}}{\partial t^2} - \frac{1}{c^2} \frac{\partial \nabla \varphi}{\partial t} = -\mu_0 \mathbf{J}, \quad (2.7)$$

$$\nabla^2 \varphi = -\frac{\rho}{\epsilon_0}, \quad (2.8)$$

where the Coulomb gage,  $\nabla \cdot \mathbf{A} = 0$ , is used in deriving eqs. (2.7) and (2.8). The vector potential  $\mathbf{A}(\mathbf{x}, t)$  and a scalar potential  $\varphi(\mathbf{x}, t)$  due to current and charge sources can be expanded in terms of the orthogonal eigenfunctions  $\mathbf{a}_\lambda(\mathbf{x})$  and  $\phi_\lambda(\mathbf{x})$  as

$$\mathbf{A}(\mathbf{x}, t) = \sum_{\lambda} q_\lambda(t) \mathbf{a}_\lambda(\mathbf{x}), \quad (2.9)$$

$$\varphi(\mathbf{x}, t) = \sum_{\lambda} r_\lambda(t) \phi_\lambda(\mathbf{x}), \quad (2.10)$$

where  $\mathbf{a}_\lambda$  and  $\phi_\lambda$  are the sets of vector and scalar eigenfunctions of an empty cavity respectively, which satisfy the following homogeneous Helmholtz equations and boundary conditions:

$$\nabla^2 \mathbf{a}_\lambda + \left(\frac{\omega_\lambda}{c}\right)^2 \mathbf{a}_\lambda = 0, \quad (2.11)$$

$$\nabla \cdot \mathbf{a}_\lambda = 0 \text{ in } V, \quad (2.12)$$

$$\mathbf{n} \times \mathbf{a}_\lambda = 0 \text{ on the boundary}, \quad (2.13)$$

and

$$\nabla^2 \phi_\lambda + \left(\frac{\Omega_\lambda}{c}\right)^2 \phi_\lambda = 0, \quad (2.14)$$

$$\phi_\lambda = 0 \text{ on the boundary,} \quad (2.15)$$

where  $\mathbf{n}$  is the unit vector normal to the wall. In general,  $\omega_\lambda \neq \Omega_\lambda$ . Substituting eqs. (2.9) and (2.10) into (2.7), dotting this result with  $\mathbf{a}_\lambda$ , and integrating over the cavity volume  $V$  gives

$$(\ddot{q}_\lambda + \omega_\lambda^2 q_\lambda) \int \mathbf{a}_\lambda \cdot \mathbf{a}_\lambda \cdot dV = \mu_0 c^2 \int \mathbf{J} \cdot \mathbf{a}_\lambda dV. \quad (2.16)$$

If the eigenfunctions  $\mathbf{a}_\lambda$  are normalized by

$$\frac{\epsilon_0}{2} \int \mathbf{a}_\lambda \cdot \mathbf{a}_\lambda \cdot dV = u_\lambda \delta_{\lambda\lambda'}, \quad (2.17)$$

where  $u_\lambda$  is the normalizing factor and  $\delta_{\lambda\lambda'}$  is the Kronecker delta, then eq. (2.16) becomes simply

$$\ddot{q}_\lambda + \omega_\lambda^2 q_\lambda = \frac{1}{2u_\lambda} \int \mathbf{J} \cdot \mathbf{a}_\lambda dV. \quad (2.18)$$

Similarly, beginning with the Poisson's equation given in (2.8), we can get the expansion coefficients for the scalar potential, which is given by

$$r_\lambda(t) = \frac{1}{2T_\lambda} \int \rho \phi_\lambda dV, \quad (2.19)$$

where  $\phi_\lambda$  are normalized by

$$\frac{\epsilon_0}{2} \int \nabla \phi_\lambda \cdot \nabla \phi_{\lambda'} dV = T_\lambda \delta_{\lambda\lambda'}. \quad (2.20)$$

The expansion coefficients  $q_\lambda(t)$  and  $r_\lambda(t)$  can be determined from eqs. (2.18) and (2.19) provided the source terms  $\mathbf{J}$ ,  $\rho$  and the eigenfunctions  $\mathbf{a}_\lambda$  and  $\phi_\lambda$ , which will be derived in the following chapter, are known. Ac-

cordingly, we can rewrite the electric field  $\mathbf{E}$  and the magnetic induction  $\mathbf{B}$  in terms of these quantities as

$$\mathbf{E}(\mathbf{x}, t) = - \sum_{\lambda} \left( \dot{q}_{\lambda}(t) \mathbf{a}_{\lambda}(\mathbf{x}) + r_{\lambda}(t) \nabla \phi_{\lambda}(\mathbf{x}) \right), \quad (2.21)$$

$$\mathbf{B}(\mathbf{x}, t) = \sum_{\lambda} q_{\lambda}(t) \nabla \times \mathbf{a}_{\lambda}(\mathbf{x}). \quad (2.22)$$

These are the wake fields left by the sources. In order to solve eq. (2.18) and (2.19), we have to know the source terms.

## 2. 4. Wake Potentials in a Cavity

### 2. 4. 1. Longitudinal Wake Potential

Consider the cavity shown in figure 2.3, where a driving charge  $Q$  is assumed to enter the cavity at  $z = 0$ ,  $t = 0$  and to exit at  $z = L$ . The driving charge  $Q$  is passing through the cavity with velocity  $v = c$ , followed by a test charge by a fixed distance  $z_0$  in the  $z$ -direction. Let  $r$  and  $r_0$  be respectively the transverse coordinate of the test charge and that of the driving charge. The delta function longitudinal wake potential  $W_z$  is defined as the energy gained by the unit negative point charge following at a distance  $z_0$  behind the driving charge, divided by  $Q$ , or

$$W_z(\mathbf{r}, z_0) = \frac{-1}{Q} \int_0^L dz E_z(\mathbf{r}, z, t)_{t=(z+z_0)/c}. \quad (2.23)$$

The source terms due to the exciting charge are

$$\rho(\mathbf{x}, t) = Q \delta(\mathbf{r} - \mathbf{r}_0) \delta(z - vt), \quad (2.24)$$

$$\mathbf{J}(\mathbf{x}, t) = z\rho v = z\rho c(\mathbf{x}, t), \quad (2.25)$$

where  $\mathbf{z}$  is the unit vector in the  $z$ -direction and particle velocity of  $v = c$  is assumed. After substituting eq. (2.25) into (2.18), equation for  $q_{\lambda}$

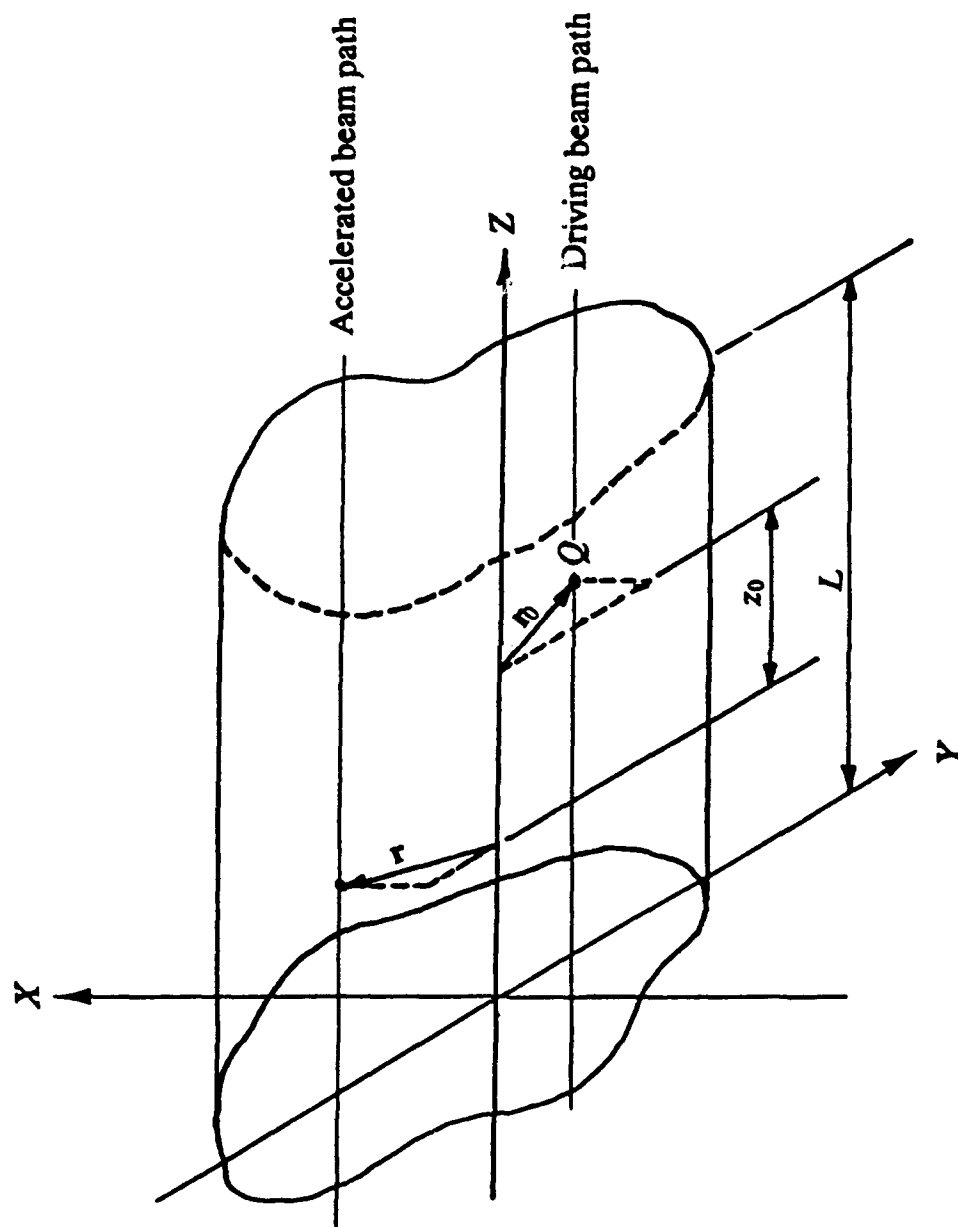


Figure 2.3. The driving and accelerated beams in a cavity

becomes

$$\ddot{q}_\lambda + \omega_\lambda^2 q_\lambda = \frac{Qc}{2u_\lambda} \begin{cases} 0, & t < 0 \\ a_{\lambda z}(r_0, ct), & 0 < t < L/c \\ 0, & t > L/c \end{cases} \quad (2.26)$$

where  $a_{\lambda z}$  is the z-component of the vector eigenfunction  $a_\lambda$ .

With the initial conditions  $q_\lambda(0) = \dot{q}_\lambda(0) = 0$ , i.e., no field exists before the driving charge  $Q$  enters the cavity, the solution for  $q_\lambda$  is

$$q_\lambda(t) = \frac{Qc}{2u_\lambda} \int_0^{\min(t, L/c)} dt' \sin \omega_\lambda(t - t') a_{\lambda z}(r_0, ct) \quad \text{for } t > 0. \quad (2.27)$$

Similarly, substituting source term, eq. (2.24), into (2.19) gives

$$r_\lambda(t) = \frac{Q}{2T_\lambda} \begin{cases} 0, & t < 0 \\ \phi_\lambda(r_0, ct), & 0 < t < L/c \\ 0, & t > L/c \end{cases} \quad (2.28)$$

Substituting these expressions of the expansion coefficients into eqs. (2.21) and (2.22), we can get the electric field  $E$  and the magnetic induction  $B$  at any position in a cavity, which are then used to calculate the longitudinal and transverse wake potentials by way of eqs. (2.23) and (2.32). By using the electric field  $E_z$  and imposing causality, i.e., no wake field will be produced ahead of the driving charge, Bane et al.<sup>12</sup> obtained the following equation for the delta function longitudinal wake potential:

$$\begin{aligned} W_z(r, r_0, z_0) &= \frac{1}{Q} \sum_\lambda \int_0^L dz \left( \dot{q}_\lambda \left( \frac{z+z_0}{c} \right) a_{\lambda z}(r, z) + r_\lambda \left( \frac{z+z_0}{c} \right) \frac{\partial \phi_\lambda(r, z)}{\partial z} \right) \\ &= \sum_\lambda \frac{V_\lambda^*(r_0) V_\lambda(r)}{2u_\lambda} \cos\left(\frac{\omega_\lambda}{c} z_0\right), \end{aligned} \quad (2.29)$$

where  $V_\lambda^*$  is a complex conjugate of  $V_\lambda$ . Notice that the longitudinal wake potential is solely expressed in terms of the z-component of the vector

eigenfunction, and is, in general, functions of the transverse positions of the driving charge and a test charge. In eq. (2.29),  $V_\lambda$  is defined as

$$V_\lambda(\mathbf{r}) = \int_0^L dz \exp\left(\frac{i\omega\lambda z}{c}\right) a_{\lambda_2}(\mathbf{r}, z). \quad (2.30)$$

Once the delta function wake potential given in eq. (2.29) has been calculated, it can be used as a Green's function to calculate the bunch wake potential  $U_z$  in and behind an arbitrary charge distribution  $\lambda(z)$ . The longitudinal potential for the distributed charge becomes

$$U_z(z_0) = \int_{-\infty}^{z_0} \lambda(z - z_0) W_z(z) dz. \quad (2.31)$$

#### 2. 4. 2. Transverse Wake Potential

Consider again the driving charge  $Q$  and a test charge in a cavity as shown in figure 2.3. The delta function transverse wake potential  $W_\perp(z_0)$  is defined as the transverse momentum kick experienced by a test charge following at a distance  $z_0$  behind a driving charge, divided by  $Q$ , or

$$\begin{aligned} W_\perp(z_0) &= \frac{1}{Q} \int_0^L dz \left( \mathbf{E}_\perp + c(\mathbf{z} \times \mathbf{B})_\perp \right)_{t=(z+z_0)/c} \\ &= \frac{1}{Q} \int_0^L dz \left( c\nabla_\perp A_z - \nabla_\perp \varphi \right)_{t=(z+z_0)/c} \end{aligned} \quad (2.32)$$

where the transverse gradient operator,  $\nabla_\perp$ , is defined as

$$\nabla_\perp = \nabla - \mathbf{z} \frac{\partial}{\partial z}. \quad (2.33)$$

Analogously to the longitudinal case, the transverse wake potential  $W_\perp(z_0)$  can be calculated by substituting the vector and scalar potentials which are expanded in terms of the eigenfunctions into eq. (2.32). But, we may use a rather simple formula known as the Panofsky-Wenzel theorem<sup>30</sup>

$$\frac{\partial}{\partial z_0} W_{\perp}(z_0) = \nabla_{\perp} W_z(z_0) \quad (2.34)$$

to derive the transverse wake potential from the knowledge of the longitudinal wake potential. Eq. (2.34) is valid for the selected cavity geometries,<sup>37</sup> e.g., for cylindrically symmetric structures for any value of  $z_0$ , for closed cavities of arbitrary shape for  $z_0 > L$ , and for structures with end plates normal to the path of particles for any value of  $z_0$ . Thus, we are going to use the Panofsky-Wenzel theorem in the next chapter to derive the transverse wake potential in an elliptical pill-box cavity. Combining eqs. (2.29) and (2.34), the delta function transverse wake potential becomes

$$W_{\perp}(z_0) = \sum_{\lambda} \frac{c V_{\lambda}^{\prime}(\mathbf{r}_0) \nabla_{\perp} V_{\lambda}(\mathbf{r})}{2u_{\lambda} \omega_{\lambda}} \sin\left(\frac{\omega_{\lambda}}{c} z_0\right), \quad (2.35)$$

and the transverse wake potential for an arbitrary charge distribution  $\lambda(z)$  can be obtained from

$$U_{\perp}(z_0) = \int_{-\infty}^{z_0} \lambda(z - z_0) W_{\perp}(z) dz. \quad (2.36)$$

## CHAPTER III

### WAKE POTENTIALS IN AN ELLIPTICAL CAVITY

#### 3. 1. Eigenmodes in an Elliptical Pill-Box Cavity

In chapter 2, we have derived the longitudinal and transverse wake potentials solely in terms of the  $z$ -component of the vector eigenfunctions, which is the solution of the homogeneous Helmholtz equation in a source free cavity with appropriate boundary conditions. The eigenfunctions in an elliptical pill-box cavity are derived in this section, and the wake potentials are formulated in the following sections.

Consider an elliptical pill-box cavity with the major axis  $2x_b$  and the minor axis  $2y_b$  as shown in figure 3.1. For a cavity of elliptical cross section, the eigenfunctions can be found in terms of known functions by transforming the Cartesian coordinates to the confocal elliptical coordinates as shown in figure 3.1. In these coordinates, the boundary conditions on the elliptical cavity walls are easily satisfied.

The confocal elliptical coordinates  $(\xi, \eta, z)$  are related to the Cartesian coordinates  $(x, y, z)$  by the following equations:

$$\begin{aligned}x &= h \cosh\xi \cos\eta, \\y &= h \sinh\xi \sin\eta,\end{aligned}\tag{3.1}$$

where  $h$  is the semi-interfocal distance of the confocal ellipses. The Helmholtz equation is then transformed to



$$\nabla^2 \psi + k^2 \psi = \frac{1}{h^2(\sinh^2 \xi + \sin^2 \eta)} \left( \frac{\partial^2 \psi}{\partial \xi^2} + \frac{\partial^2 \psi}{\partial \eta^2} \right) + \frac{\partial^2 \psi}{\partial z^2} + k^2 \psi = 0, \quad (3.2)$$

where  $k$  is the free space wave number.

Following the method of separation of variables, we seek to find solutions of the form

$$\psi = f(\xi) g(\eta) w(z). \quad (3.3)$$

Substituting eq. (3.3) into (3.2) and dividing by  $\psi$ , the Helmholtz equation is split into three ordinary differential equations:

$$\frac{d^2 f(\xi)}{d\xi^2} - (a - 2q \cosh 2\xi) f(\xi) = 0, \quad (3.4)$$

$$\frac{d^2 g(\eta)}{d\eta^2} + (a - 2q \cos 2\eta) g(\eta) = 0, \quad (3.5)$$

$$\frac{d^2 w(z)}{dz^2} + k_z^2 w(z) = 0, \quad (3.6)$$

where  $a$  is an arbitrary separation constant. The parameter  $q$  is defined as

$$2q = \frac{k_c^2 h^2}{2}, \quad (3.7)$$

and  $k_z$  and  $k_c$  are arbitrary constants, but are related to the free space wave number  $k$  by

$$k_c^2 = k^2 - k_z^2. \quad (3.8)$$

The above equations (3.4) and (3.5) are called the Mathieu equations.<sup>31,32</sup> Solutions to these equations are the Mathieu functions, details of which are given in Appendix A.

With the  $z$ -dependence of  $\exp(ik_z z)$  in eq. (3.6), we are interested in

the solution of the two dimensional Helmholtz equation

$$\nabla_{\perp}^2 \psi + k_c^2 \psi = 0 \quad (3.9)$$

in an elliptical pill-box cavity. Here, the transverse Laplacian operator  $\nabla_{\perp}^2$  is defined by

$$\nabla_{\perp}^2 = \nabla^2 - \frac{\partial^2}{\partial z^2}. \quad (3.10)$$

The particular modes that we are considering are the modes which have longitudinal acceleration fields. Therefore, only Transverse Magnetic (TM) modes will be considered for the calculation of the wake potentials. For modes TM to  $z$ , we may express the fields in terms of the vector potential  $A$ , or equivalently in terms of the vector eigenfunction  $a_{\lambda}$ , having only  $z$ -component. Hence  $\psi = a_{\lambda}$  in eq. (3.9). Any combinations of the Mathieu functions in the form of  $\psi = f(\xi)g(\eta)$  are solutions of eq. (3.9). In addition to the boundary conditions which must be satisfied on the walls of the cavity, the following two conditions must be satisfied, i.e.,

(i) continuity of function  $\psi$  on the interfocal line:

$$\psi(0, \eta) = \psi(0, -\eta). \quad (3.11)$$

(ii) continuity of gradient of function  $\psi$  on the interfocal line:

$$\frac{\partial}{\partial \xi} (\psi(\xi, \eta))_{\xi \rightarrow 0} = - \frac{\partial}{\partial \xi} (\psi(\xi, -\eta))_{\xi \rightarrow 0}. \quad (3.12)$$

Among the possible combinations, the only permissible form of the solution which satisfies above two conditions are

$$\psi = \sum_{m=1}^{\infty} S_m s e_m(\xi, q) s e_m(\eta, q) + \sum_{m=0}^{\infty} C_m c e_m(\xi, q) c e_m(\eta, q), \quad (3.13)$$

with the  $z$ -dependent factor  $\exp(ik_z z)$  being omitted. Here,  $C_m$  and  $S_m$  are arbitrary constants. The function  $ce_m(\eta, q)$  and  $se_m(\eta, q)$  are, respectively, the even and odd type Mathieu functions of the first kinds of integral order, and  $Ce_m(\xi, q)$  and  $Se_m(\xi, q)$  are the modified Mathieu functions of the first kinds of integral order.

We first notice that symmetry of the function  $\psi$  is determined by  $ce_m(\eta, q)$  and  $se_m(\eta, q)$ . The terms in the first summation are odd and the terms in the second summation are even with respect to  $\eta$ . From Appendix A, we have

$$se_m(\eta, q) = -se_m(-\eta, q), \quad (3.14)$$

$$ce_m(\eta, q) = ce_m(-\eta, q). \quad (3.15)$$

Therefore, the first summation is always zero on the median plane ( $y = 0$  plane) where the wake potentials are to be evaluated, and as a result it does not contribute to the calculation of the longitudinal and transverse wake potentials. For this reason, we are now considering only the TM modes of even type solutions,  $\psi_m = Ce_m(\xi, q) ce_m(\eta, q)$ , for the wake potential calculation.

The boundary conditions are

$$\psi = 0 \quad (3.16)$$

at the elliptical boundary where  $\xi = \xi_a$ . There remains the condition that no tangential component of  $\mathbf{a}_\lambda$  exists at the end-plate walls at  $z = 0$  and  $d$ , which is satisfied if we choose

$$k_z = \frac{p\pi}{d}, \quad p = 0, 1, 2, \dots, \quad (3.17)$$

where  $d$  is the gap distance of the pill-box cavity as shown in figure 3.2. From eq. (3.16), we have

$$C e_m(\xi_a, q) = 0, \quad (3.18)$$

which are satisfied by particular values of  $q$ . Let  $q_{mn}$  be the  $n^{\text{th}}$  root of eq. (3.18) for a given mode  $m$ . Then, we can calculate resonant frequency from the root  $q_{mn}$ . From eqs. (3.7) and (3.8), the resonant frequency is

$$\frac{\omega_{mnp}}{c} = \left\{ \frac{4q_{mn}}{h^2} + \left( \frac{p\pi}{d} \right)^2 \right\}^{1/2}. \quad (3.19)$$

From this equation, we see that the wavelength of the dominant mode becomes

$$\lambda_{010} = \frac{\pi h}{\sqrt{q_{01}}} = \frac{\pi x_b e_c}{\sqrt{q_{01}}}, \quad (3.20)$$

where  $e_c$  is the eccentricity of the boundary ellipse,  $e_c = 1/\cosh \xi_a$ . Figure 3.3 is a plot of  $q_{01}$  as a function of the eccentricity  $e_c$ . The ratio  $\lambda_{010}/x_b$  is plotted against  $e_c$  in figure 3.4. In this figure we see that as  $e_c \rightarrow 0$ , i.e., as the ellipse tends to a circle, the ratio approaches 2.61, which is the ratio of the wavelength to the radius,  $\lambda/r_a = 2\pi/\chi_{01}$ , for the  $TM_{010}$  mode of a circular pill-box cavity, where  $\chi_{01}$  is the first zero of Bessel function  $J_0(x)$ .

The transverse components of the vector eigenfunction can be easily found from the  $z$ -component. These eigenmodes are

$$a_{z_{mnp}} = C e_m(\xi, q_{mn}) c e_m(\eta, q_{mn}) \cos \frac{p\pi z}{d}, \quad (3.21)$$

$$a_{\xi_{mnp}} = -\frac{p\pi}{D_{mn} d} C e_m'(\xi, q_{mn}) c e_m(\eta, q_{mn}) \sin \frac{p\pi z}{d}, \quad (3.22)$$

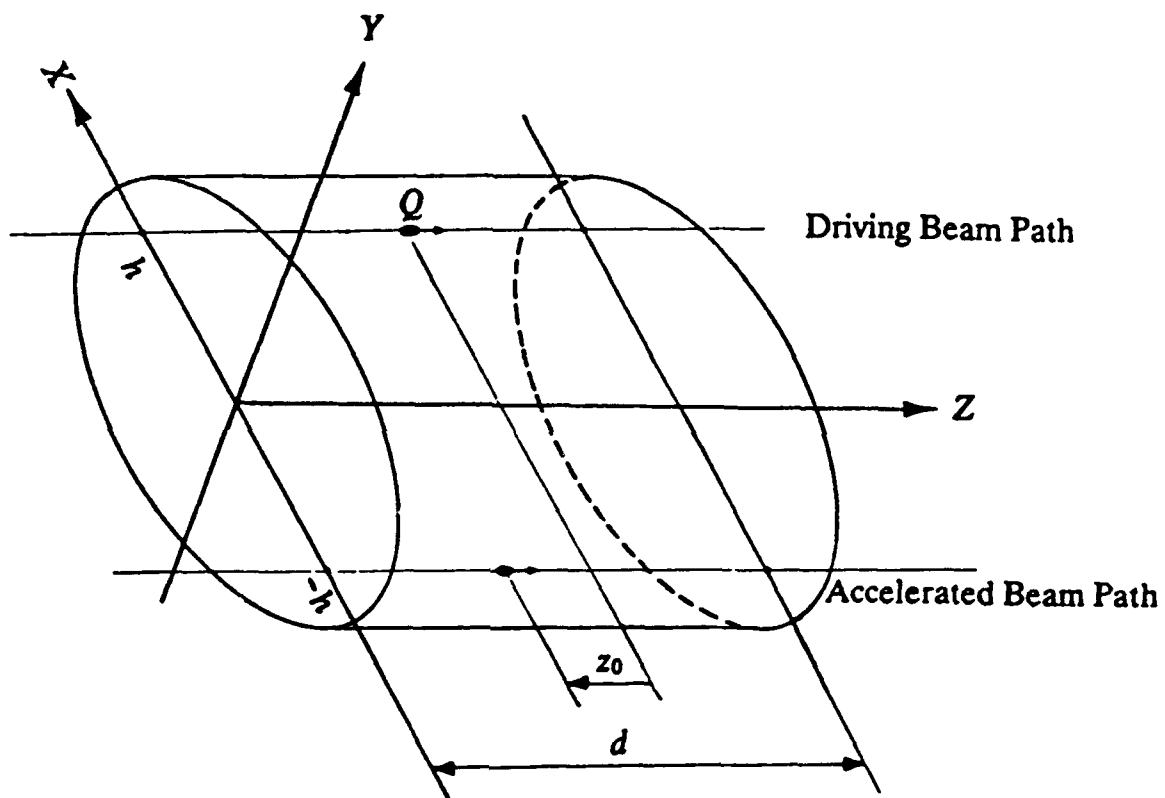


Figure 3.2. Elliptical pill-box cavity

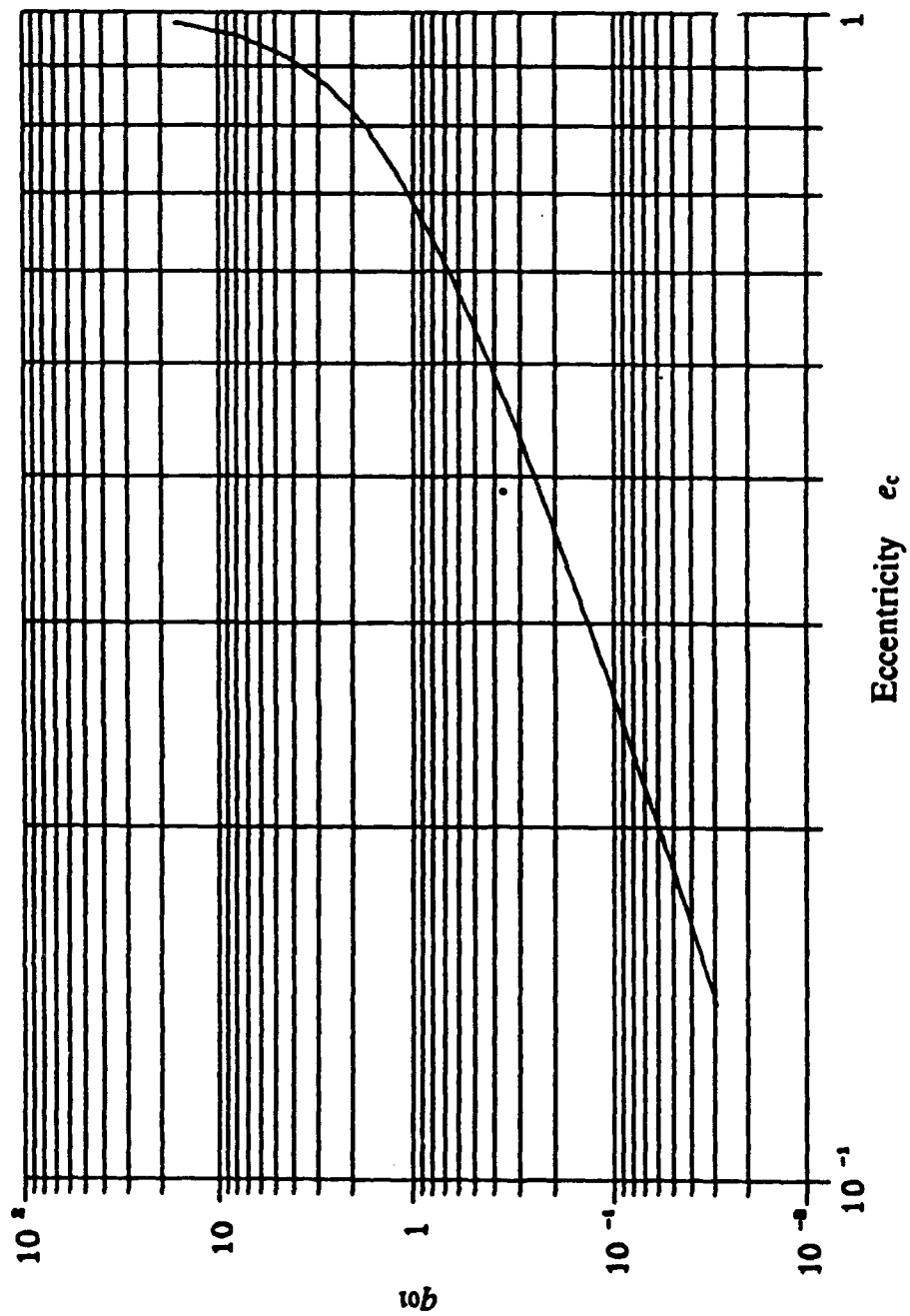


Figure 3.3. Plot of  $q_{01}$  as a function of eccentricity  $e_c$

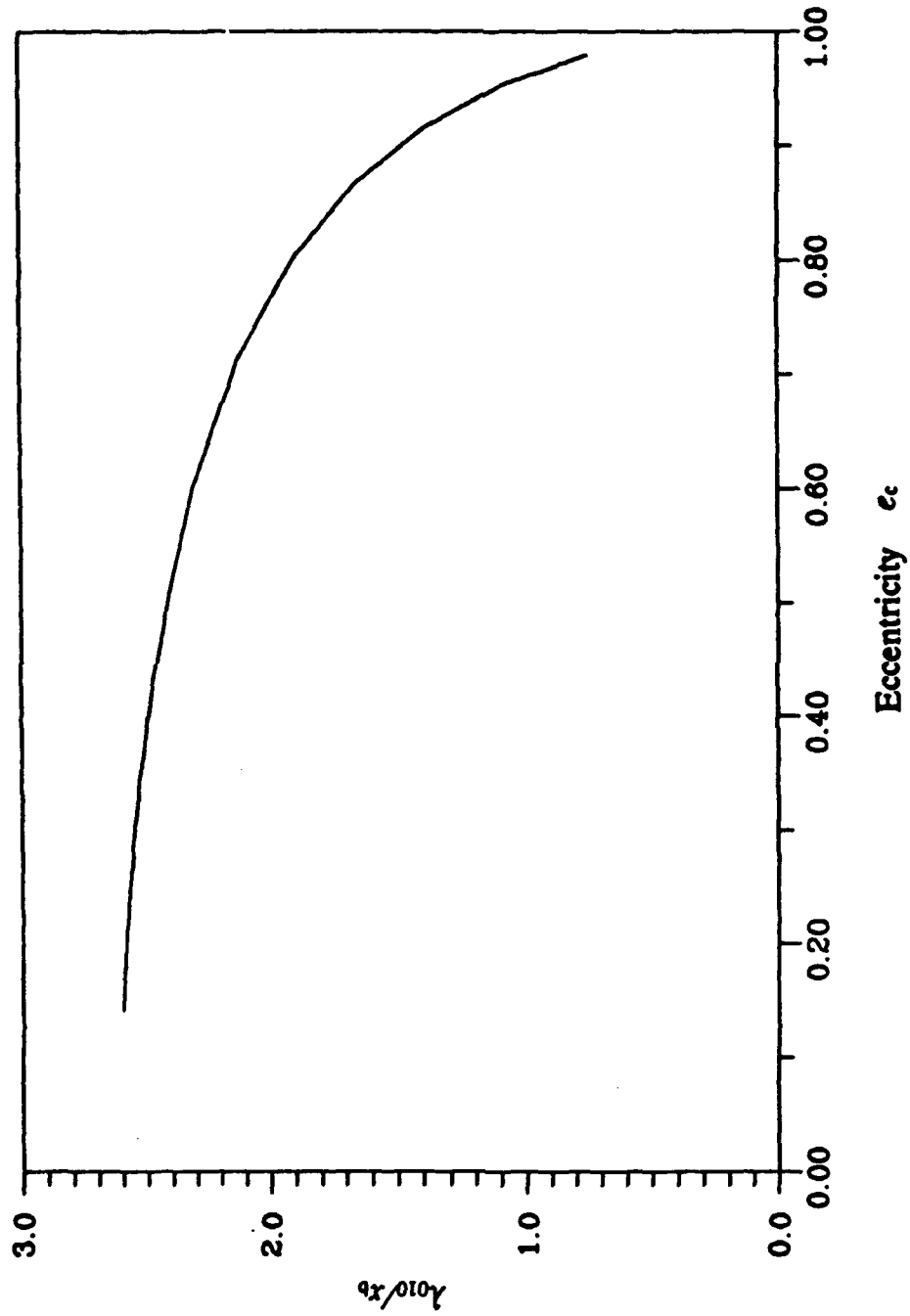


Figure 3.4. Plot of the wavelength of the fundamental mode as a function of eccentricity  $e_c$

$$a_{\eta_{\text{amp}}} = -\frac{D\pi}{D_{mn}d} C e_m(\xi, q_{mn}) c e_m'(\eta, q_{mn}) \sin \frac{D\pi z}{d}, \quad (3.23)$$

where

$$D_{mn} = \frac{4q_{mn}}{h} \left\{ \frac{\cosh 2\xi - \cos 2\eta}{2} \right\}^{1/2}. \quad (3.24)$$

The resonant mode patterns for some of the lower-order modes are shown in figures 3.5 - 3.8. Now, we proceed to calculate the wake potentials using eigenmodes given in eqs. (3.21) - (3.23).

### 3. 2. Wake Potentials in an Elliptical Pill-Box Cavity

#### 3. 2. 1. Longitudinal Wake Potential

The longitudinal and transverse wake potentials on the focus axis of an elliptical cavity are of particular interest since when the driving charge  $Q$  is passing through one of the foci of the cavity where  $\xi = \eta = 0$  (driving beam path), all the electromagnetic fields radiated will get focused again at the other foci where  $\xi = 0$  and  $\eta = \pi$  (accelerated beam path) in first order approximation, which are then used to accelerate a trailing charge.

Consider a test charge which is traveling through the cavity where  $\xi = 0$  and  $\eta = \pi$  (accelerated beam path) and trailing the driving charge  $Q$  by a fixed distance  $z_0$  in the  $z$ -direction. The delta function longitudinal wake potential  $W_z$ , or the energy gained by the unit negative test charge is given by eq. (2.29):

$$W_z(z_0) = \sum_{\lambda} \frac{V_{\lambda}^*(\mathbf{r}_0) V_{\lambda}(\mathbf{r})}{2u_{\lambda}} \cos\left(\frac{\omega_{\lambda} z_0}{c}\right) \text{ for } z_0 > 0, \quad (2.29)$$

where  $V_{\lambda}$  is the voltage induced by a point charge, and the normalizing

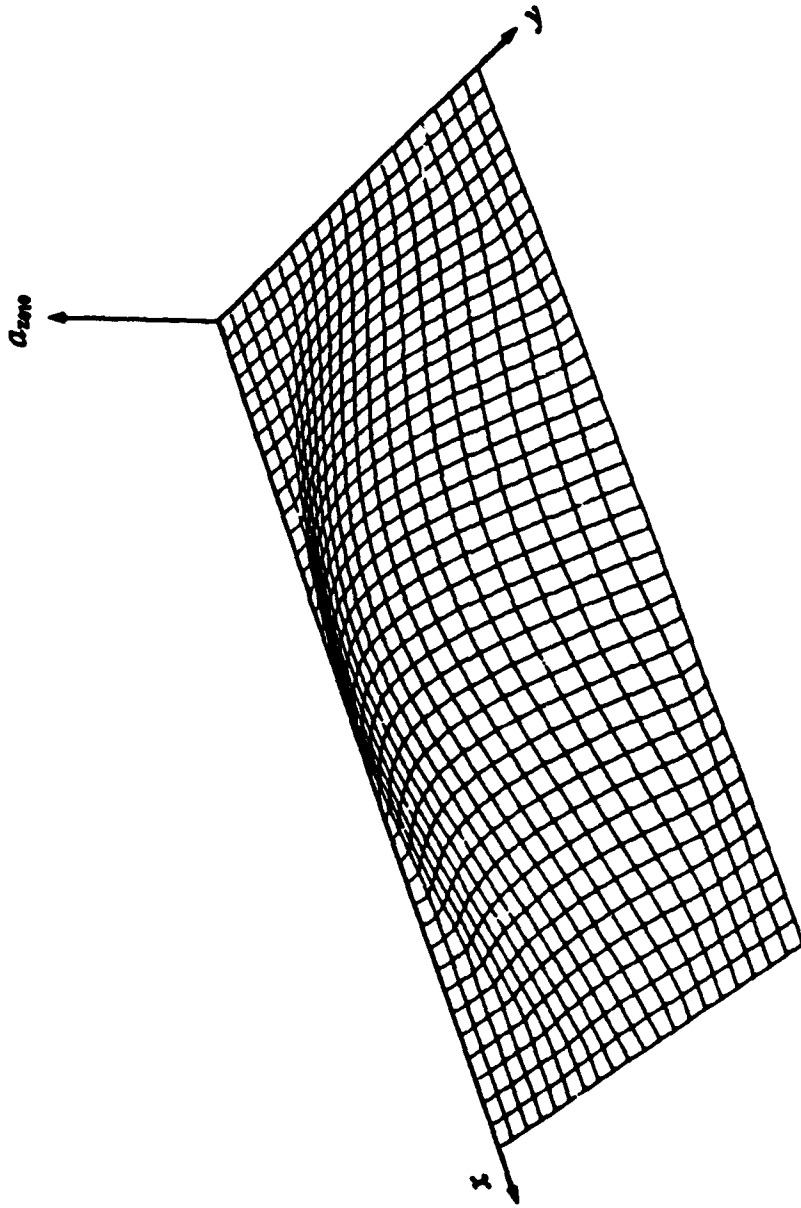


Figure 3.5. Configuration of the resonant mode  $a_{zmp}$  in an elliptical cavity ( $m=0, n=1, p=0$ )

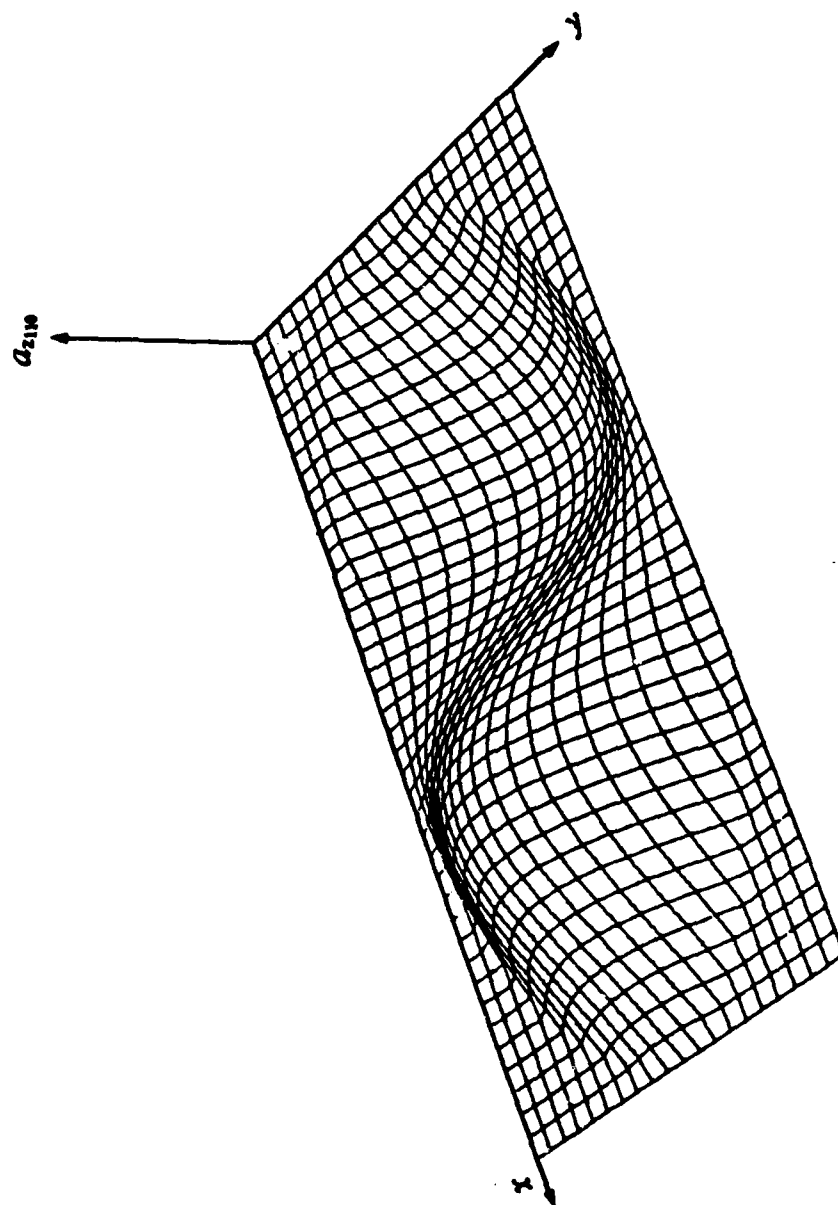


Figure 3.6. Configuration of the resonant mode  $a_{z,10}$  in an elliptical cavity ( $m = 1, n = 1, p = 0$ )

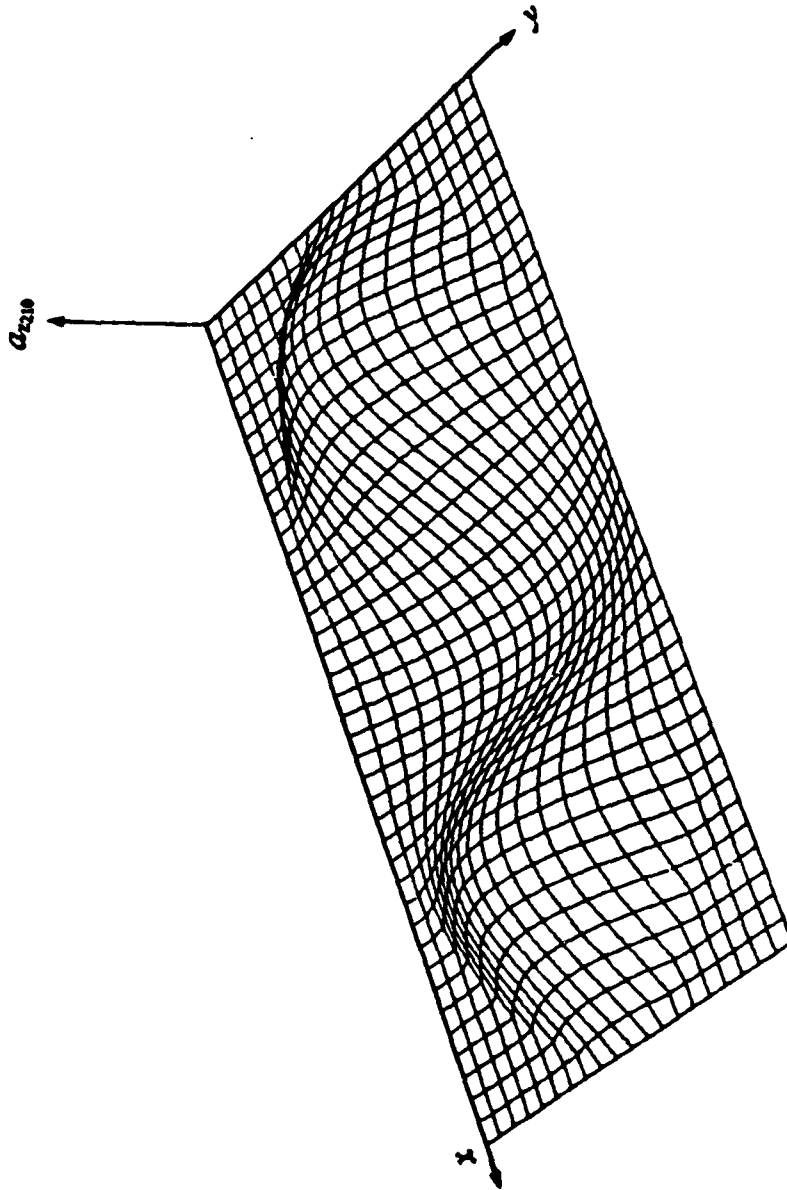


Figure 3.7. Configuration of the resonant mode  $a_{z_{amp}}$  in an elliptical cavity ( $m=2$ ,  $n=1$ ,  $p=0$ )

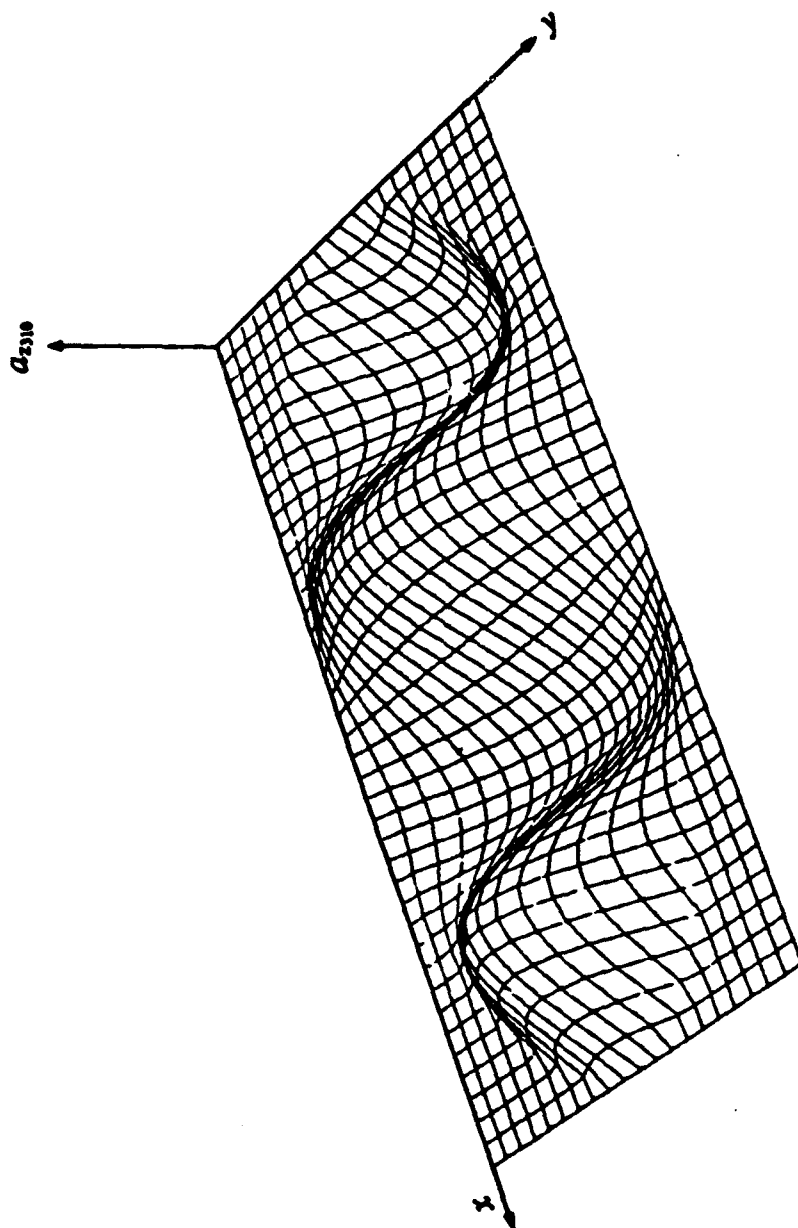


Figure 3.8. Configuration of the resonant mode  $a_{z_{amp}}$  in an elliptical cavity ( $m=3$ ,  $n=1$ ,  $p=0$ )

factor  $u_\lambda$ , which can be interpreted as the stored energy in the mode, is given by eq. (2.17):

$$\frac{\epsilon_0}{2} \int \mathbf{a}_\lambda \cdot \mathbf{a}_\lambda' dV = u_\lambda \delta_{\lambda\lambda'}. \quad (2.17)$$

After substituting the eigenfunction in eq. (3.21) into eq. (2.30), the voltage  $V_\lambda$  on the driving beam path and any position in a cavity become

$$\begin{aligned} V_\lambda(\mathbf{r}_0) &= \int_0^d dz \exp\left(\frac{i\omega z}{c}\right) a_{\lambda_i}(0, 0, z) \\ &= C_{em}(0, q_{mn}) c_{em}(0, q_{mn}) \int_0^d dz \exp\left(\frac{i\omega z}{c}\right) \cos\frac{p\pi}{d}z, \end{aligned} \quad (3.25)$$

$$\begin{aligned} V_\lambda(\mathbf{r}) &= \int_0^d dz \exp\left(\frac{i\omega z}{c}\right) a_{\lambda_i}(\xi, \eta, z) \\ &= C_{em}(\xi, q_{mn}) c_{em}(\eta, q_{mn}) \int_0^d dz \exp\left(\frac{i\omega z}{c}\right) \cos\frac{p\pi}{d}z, \end{aligned} \quad (3.26)$$

and further

$$V_\lambda^* V_\lambda = \frac{2C_{mn}\left(\frac{\omega}{c}\right)^2}{\left(\left(\frac{\omega}{c}\right)^2 - \left(\frac{p\pi}{d}\right)^2\right)^2} \left(1 - (-1)^p \cos\frac{\omega_{mnp}d}{c}\right), \quad (3.27)$$

where the coefficient  $C_{mn}$  is given by

$$C_{mn} = C_{em}(\xi, q_{mn}) C_{em}(0, q_{mn}) c_{em}(\eta, q_{mn}) c_{em}(0, q_{mn}). \quad (3.28)$$

The stored energy  $u_\lambda$  in the mode becomes

$$\begin{aligned} u_{mnp} &= \frac{\epsilon_0}{2} \int \mathbf{a}_\lambda \cdot \mathbf{a}_\lambda' dV \\ &= \frac{\epsilon_0}{2} \frac{\left(\frac{\omega_{mnp}}{c}\right)^2}{k_{c_{mn}}^2} \int C_{em}^2(\xi, q_{mn}) c_{em}^2(\eta, q_{mn}) \cos^2\left(\frac{p\pi}{d}z\right) dV. \end{aligned} \quad (3.29)$$

After integration of eq. (3.29) using  $dV = \frac{h^2}{2} (\cosh 2\xi - \cos 2\eta) d\xi d\eta dz$ , it is further reduced to

$$u_{mnp} = \frac{\epsilon_0 \pi h^2 d}{8} \frac{\left(\frac{\omega_{mnp}}{c}\right)^2}{k_{c_{mn}}^2} \int_0^{\xi_0} C e_m^2(\xi, q_{mn}) \times (\cosh 2\xi - \Theta_m) d\xi, \quad (3.30)$$

where

$$\begin{aligned} \Theta_m &= \frac{1}{\pi} \int_0^{2\pi} c e_m^2(\eta, q_{mn}) \cos 2\eta d\eta \\ &= \begin{cases} A_0^{(m)} A_2^{(m)} + \sum_{r=0}^{\infty} A_{2r}^{(m)} A_{2r+2}^{(m)}, & \text{for } m = 0, 2, 4, \dots, \\ \frac{1}{2} (A_1^{(m)})^2 + \sum_{r=0}^{\infty} A_{2r+1}^{(m)} A_{2r+3}^{(m)}, & \text{for } m = 1, 3, 5, \dots, \end{cases} \end{aligned} \quad (3.31)$$

and  $A_r^{(m)}$  in eq. (3.31) are the coefficients for the series representation of the Mathieu function  $c e_m(\eta, q)$ . Substituting eqs. (3.27) - (3.31) into (2.29) gives the delta function longitudinal wake potential  $W_z$ .

On the accelerated beam path ( $\xi = 0, \eta = \pi$ ), the delta function longitudinal wake potential becomes

$$W_z(z_0) = \frac{2}{\epsilon_0 \pi d} \sum_{m=0}^{\infty} \sum_{n=1}^{\infty} \sum_{p=0}^{\infty} \frac{\epsilon_p C_{mn} \left(1 - (-1)^p \cos \frac{\omega_{mnp} d}{c}\right)}{q_{mn} N_{mn}} \cos\left(\frac{\omega_{mnp} z_0}{c}\right), \quad (3.32)$$

where  $\epsilon_p = \nu_2$  for  $p = 0$  and 1 for  $p \neq 0$ , and  $N_{mn}$  is given by

$$N_{mn} = \int_0^{\xi_0} C e_m^2(\xi, q_{mn}) \times (\cosh 2\xi - \Theta_m) d\xi. \quad (3.33)$$

The coefficient  $C_{mn}$  can be expressed in terms of  $A_r^{(m)}$  as

$$C_{mn} = (C e_m(0, q_{mn}))^2 c e_m(0, q_{mn}) c e_m(\pi, q_{mn})$$

$$= \begin{cases} \left( \sum_{r=0}^{\infty} A_{2r}^{(m)} \right)^4 & \text{for } m = 0, 2, 4, \dots, \\ - \left( \sum_{r=0}^{\infty} A_{2r+1}^{(m)} \right)^4 & \text{for } m = 1, 3, 5, \dots, \end{cases} \quad (3.34)$$

When the boundary ellipse tends to a circle, the confocal hyperbolae in figure 3.1 become radii of the circle  $r$ , and the confocal ellipses become concentric circles of that radius. In this case, we get the longitudinal wake potential  $W_z$  for a circular pill-box cavity, which is expressed analytically<sup>11,12</sup> in the form

$$W_z(z_0) = \frac{4}{\epsilon_0 \tau d} \sum_{n=1}^{\infty} \sum_{p=0}^{\infty} \epsilon_p \frac{(1 - (-1)^p \cos \frac{\omega_{onp} d}{c})}{\chi_{on} J_1^2(\chi_{on})} \cos\left(\frac{\omega_{onp} z_0}{c}\right), \quad (3.35)$$

where  $\chi_{on}$  is the  $n^{\text{th}}$  zero of Bessel function  $J_0(x)$ . We can easily show that eq. (3.32) is exactly reduced to eq. (3.35) by using the limiting properties of the Mathieu functions. The functions  $ce_m(\eta, q)$  and  $Ce_m(\xi, q)$  degenerate into the following forms as the semi-interfocal distance  $h \rightarrow 0$  and  $\xi \rightarrow \infty$ , while keep the product  $h \cosh \xi \rightarrow r$ . From eq. (3.7), we see that  $q \rightarrow 0$  as  $h \rightarrow 0$ . Thus, as  $q \rightarrow 0$ , we have from Appendix A

$$ce_m(\eta, q) \rightarrow \begin{cases} \sqrt{V_2}, & \text{for } m = 0 \\ \cos m \phi, & \text{for } m \neq 0 \end{cases} \quad (3.36)$$

$$Ce_m(\xi, q) \rightarrow p_m J_m(kr) \quad (3.37)$$

$$A_r^{(m)} \rightarrow 0 \text{ (except } A_m^{(m)} \rightarrow 1 \text{ for } m \neq 0 \text{ and } A_0^{(0)} \rightarrow \sqrt{V_2}) \quad (3.38)$$

where  $p_m$  is a constant multiplier and  $J_m(x)$  is the Bessel function of the first kind of order  $m$ . Using above equations,  $C_{mn}$  in the numerator of eq. (3.32) becomes simply

$$\begin{aligned}
C_{mn} &= (C e_m(0, q_{mn}))^2 c e_m(0, q_{mn}) c e_m(\pi, q_{mn}) \\
&\rightarrow (p_m J_m(0) \cos m\phi)^2 = 0, \text{ for } m \neq 0 \\
&\rightarrow (p_0 J_0(0))^2 / 2 = p_0^2 / 2, \text{ for } m = 0.
\end{aligned} \tag{3.39}$$

It is apparent from eq. (3.39) that contributions from  $m \neq 0$  modes become zero as expected as an ellipse tends to a circle. The denominator in eq. (3.32) for  $m = 0$  becomes

$$\begin{aligned}
q_{on} \int_0^{\xi_a} C e_0^2(\xi, q_{on}) \cosh 2\xi d\xi &\rightarrow \frac{(p_0 k_c)^2}{2} \int_0^{r_a} J_0^2(k_c r) r dr \\
&\rightarrow \frac{p_0^2}{4} \chi_{on}^2 J_1^2(\chi_{on}),
\end{aligned} \tag{3.40}$$

where  $k_c = \chi_{on}/r_a$  for a circular pill-box cavity of radius  $r_a$ . By substituting eqs. (3.39) and (3.40) into (3.32), we can get exactly the same expression for the wake potential in a circular pill-box cavity as in references 11 and 12. No closed expression is known for the infinite sum in eqs. (3.32) and (3.35), which must be evaluated numerically.

The wake potential for the distributed charges can be calculated from eq. (2.31). For a Gaussian bunch with rms bunch length of  $\sigma$ ,

$$\lambda(z) = \frac{1}{\sqrt{2\pi} \sigma} \exp\left(-\frac{z^2}{2\sigma^2}\right), \tag{3.41}$$

the bunch wake potential is

$$\begin{aligned}
U_z(z_0) &= \int_{-\infty}^{z_0} \lambda(z) W_z(z_0 - z) dz \\
&= \frac{\sqrt{2/\pi}}{\epsilon_0 \pi d \sigma} \sum_{m=0}^{\infty} \sum_{n=1}^{\infty} \sum_{p=0}^{\infty} \frac{\epsilon_p C_{mn} (1 - (-1)^p \cos \frac{\omega_{mnp} d}{c})}{q_{mn} N_{mn}}
\end{aligned}$$

$$\times \int_{-\infty}^{z_0} \exp\left(\frac{-z^2}{2\sigma^2}\right) \cos\frac{\omega_{mnp}(z_0 - z)}{c} dz. \quad (3.42)$$

When  $z_0 \gg \sigma$ , the bunch wake potential becomes

$$U_z(z_0) \approx \frac{2}{\epsilon_0 \pi d} \sum_{m=0}^{\infty} \sum_{n=1}^{\infty} \sum_{p=0}^{\infty} \exp\left(-\left(\frac{\omega_{mnp}}{c}\right)^2 \sigma^2 / 2\right) \\ \times \frac{\epsilon_p C_{mn} (1 - (-1)^p \cos\frac{\omega_{mnp} d}{c})}{q_{mn} N_{mn}} \cos\frac{\omega_{mnp} z_0}{c}. \quad (3.43)$$

It is apparent from this equation that contributions from the modes whose resonant wavelengths are much shorter than the bunch length  $\sigma$  become negligible. For the dominant mode, eq. (3.43) can be written as

$$U_{z_{010}} = \frac{(1 - e_c^2)^{1/2} \lambda^2 C_{01}}{\epsilon_0 \pi^2 d e_c^2 S N_{01}} e^{-\frac{1}{2} \left(\frac{2\pi\sigma}{\lambda}\right)^2} \left(1 - \cos\frac{2\pi d}{\lambda}\right) \cos\frac{2\pi z_0}{\lambda}, \quad (3.44)$$

where  $S = \pi x_b y_b$  is the cross sectional area of the cavity,  $\lambda$  is the wavelength of the dominant mode,  $e_c$  is the eccentricity of the boundary ellipse. The coefficients  $C_{01}$  and  $N_{01}$  are found from eqs. (3.33) and (3.34). From this equation, we see that the wake potential scales as  $\omega_\lambda^{-2}$  and  $S^{-1}$ . When the boundary ellipse is very close to a circle, i.e.,  $e_c \ll 1$ , the wake potential scales as  $e_c^{-2}$ .

### 3. 2. 2. Transverse Wake Potential

As discussed in Chapter 2, we can derive the transverse wake potential in a pill-box cavity from the longitudinal wake potential by using the Panofsky-Wenzel theorem, eq. (2.35). That is

$$W_\perp(z_0) = \sum_\lambda c \frac{V_\lambda \nabla_\perp V_\lambda}{2u_\lambda \omega_\lambda} \sin\left(\frac{\omega_\lambda z_0}{c}\right). \quad (2.35)$$

On the accelerating beam path where  $\xi = 0$  and  $\eta = \pi$ , we have

$$V_{\lambda}^* \nabla_{\perp} V_{\lambda} = C e_m(0, \sigma) c e_m(0, q_{\lambda}) c e_m(\pi, q_{\lambda}) \nabla_{\perp} C e_m(0, q_{\lambda}) \\ \times \left( \int_0^d dz \exp\left(\frac{i\omega z}{c}\right) \cos\frac{p\pi}{d} z \right)^2. \quad (3.45)$$

Since the driving and test charges are assumed to move on each focus axis which are parallel to the z-axis and on the plane of symmetry ( $y = 0$  plane), only  $\xi$ -component of the transverse wake potential exists at the foci of the elliptical cavity. Hence,

$$\nabla_{\perp} C e_m(0, q_{\lambda}) = \xi \lim_{\xi \rightarrow 0} \frac{1}{h \sinh \xi} \frac{\partial}{\partial \xi} C e_m(\xi, q_{\lambda}) \\ = \xi \begin{cases} \frac{1}{h} \sum_{r=0}^{\infty} (2r)^2 A_{2r}^{(m)}, & \text{for } m = 0, 2, 4, \dots \\ \frac{1}{h} \sum_{r=0}^{\infty} (2r+1)^2 A_{2r+1}^{(m)}, & \text{for } m = 1, 3, 5, \dots \end{cases} \quad (3.46)$$

Therefore, the delta function transverse wake potential is written as

$$W_{\perp}(z_0) = \frac{2c}{\epsilon_0 \pi d} \sum_{\lambda} \frac{\epsilon_p \bar{C}_{\lambda} (1 - (-1)^p \cos\frac{\omega_{\lambda} d}{c})}{\omega_{\lambda} q_{\lambda} N_{\lambda}} \sin\left(\frac{\omega_{\lambda}}{c} z_0\right), \quad (3.47)$$

where

$$\bar{C}_{\lambda} = C e_m(0, q_{mn}) c e_m(0, q_{mn}) c e_m(\pi, q_{mn}) \nabla_{\perp} C e_m(0, q_{mn}) \\ = \begin{cases} \frac{1}{h} \left( \sum_{r=0}^{\infty} A_{2r}^{(m)} \right)^3 \left( \sum_{r=0}^{\infty} (2r)^2 A_{2r}^{(m)} \right), & \text{for } m = 0, 2, 4, \dots \\ \frac{-1}{h} \left( \sum_{r=0}^{\infty} A_{2r+1}^{(m)} \right)^3 \left( \sum_{r=0}^{\infty} (2r+1)^2 A_{2r+1}^{(m)} \right), & \text{for } m = 1, 3, 5, \dots \end{cases} \quad (3.48)$$

For the driving beam with a Gaussian charge distribution, the transverse bunch wake potential becomes

$$\begin{aligned}
U_{\perp}(z_0) &= \int_{-\infty}^{z_0} dz \lambda(z) W_{\perp}(z_0 - z) \\
&= \frac{c \sqrt{2/\pi}}{\epsilon_0 \pi d} \sum_{m=0}^{\infty} \sum_{n=1}^{\infty} \sum_{p=0}^{\infty} \frac{\epsilon_p \bar{C}_{mn} (1 - (-1)^p \cos \frac{\omega_{mnp} d}{c})}{\omega_{mnp} q_{mn} N_{mn}} \\
&\quad \times \int_{-\infty}^{z_0} \exp\left(\frac{-z^2}{2\sigma^2}\right) \sin \frac{\omega_{mnp}(z_0 - z)}{c} dz. \tag{3.49}
\end{aligned}$$

When  $z_0 \gg \sigma$ , the transverse bunch wake potential becomes

$$\begin{aligned}
U_{\perp}(z_0) &\approx \frac{2c}{\epsilon_0 \pi d} \sum_{m=0}^{\infty} \sum_{n=1}^{\infty} \sum_{p=0}^{\infty} \exp\left(-\left(\frac{\omega_{mnp}}{c}\right)^2 \sigma^2 / 2\right) \\
&\quad \times \frac{\epsilon_p \bar{C}_{mn} (1 - (-1)^p \cos \frac{\omega_{mnp} d}{c})}{\omega_{mnp} q_{mn} N_{mn}} \sin \frac{\omega_{mnp} z_0}{c}. \tag{3.50}
\end{aligned}$$

### 3. 3. Numerical Examples

The longitudinal and transverse wake potentials in an elliptical pill-box cavity are calculated by using eqs. (3.42) and (3.49). The results are plotted in figures 3.10 - 3.14. In these calculations, a driving beam with a Gaussian charge distribution of  $\sigma = 5$  mm is assumed. We choose the same cavity dimensions bunch length as in ref. 22 to compare the results of two methods. The cavity dimensions are shown in figure 3.9.

Figure 3.10 is the plot of the longitudinal wake potential on the accelerated beam path, in which only 5 modes are included in the calculation. The modes summation converges as the number of modes are increased. Figures 3.11 and 3.12 are the curves of the longitudinal wake potentials respectively on the accelerated beam path and on the driving beam path, in which different number of modes are included in the mode summation (solid lines for 24 modes and broken lines for 12 modes). From figures

3.10 - 3.12, we readily find very rapid convergence of the mode summation, indicating clearly that the wake potentials are predominated by a few lower-order modes. Even 5 modes summation (figure 3.10) gives a well-defined curve.

On the accelerated beam path, we obtain about 125 MeV/m/ $\mu$ C acceleration gradient, while about 110 MeV/m/ $\mu$ C was obtained by Y. Chin<sup>22</sup> (figures 3.17 and 3.18).

The path length for the fields radiated from one focus axis to reach the other after one reflection at the elliptical boundary is 10 cm for this cavity. The peak accelerating potential on the accelerated beam path (point A in figure 3.11) is the very fields radiated from the driving beam path (point B in figure 3.12) and focused again after one reflection at the elliptical wall. From figures 3.11 and 3.12, we can see that the delay distance between the point A and point B is about 10 cm.

The transverse wake potential on the accelerated beam path and that on the driving beam path are shown in figures 3.13 and 3.14 respectively by the broken lines. The corresponding longitudinal wake potentials are plotted together in order to see if we can find the positions, such as the point C in figure 3.13, at which the accelerating potential is large while the transverse potential is small. The charge to be accelerated should be positioned at such a point in order to avoid large transverse deflection during acceleration. However, we also found that at the point of peak accelerating potential, the transverse wake potential is not zero. The accelerated particles positioned at this peak will be deflected and efficiency of acceleration will drop gradually because of the displacement from the focus axis and proper phase.

The longitudinal wake potentials for different size cavities are plotted in figures 3.15 - 3.17. Figures 3.18 and 3.19 are the curves for the longitudinal and transverse wake potentials calculated by pure numerical method, the code WELL,<sup>22</sup> which include the effects of the beam apertures of 1cm diameter. Comparing figures 3.13 and 3.14 with 3.18 and 3.19, very good agreements in magnitudes and frequencies are observed.

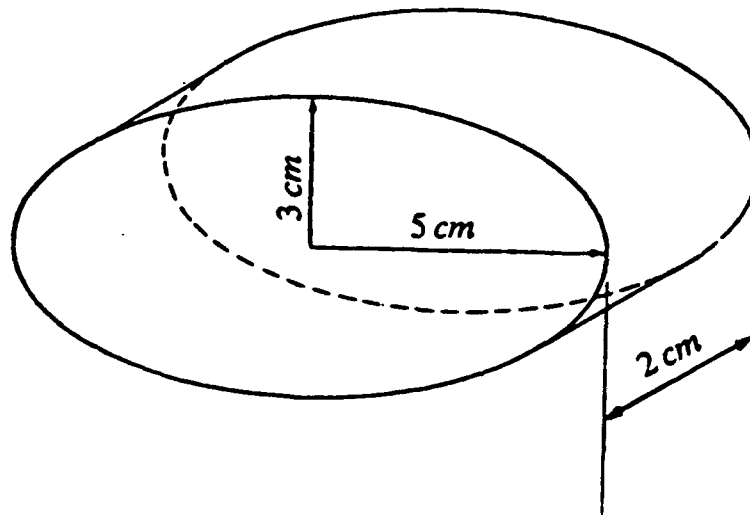


Figure 3.9. Cavity dimensions for example calculation

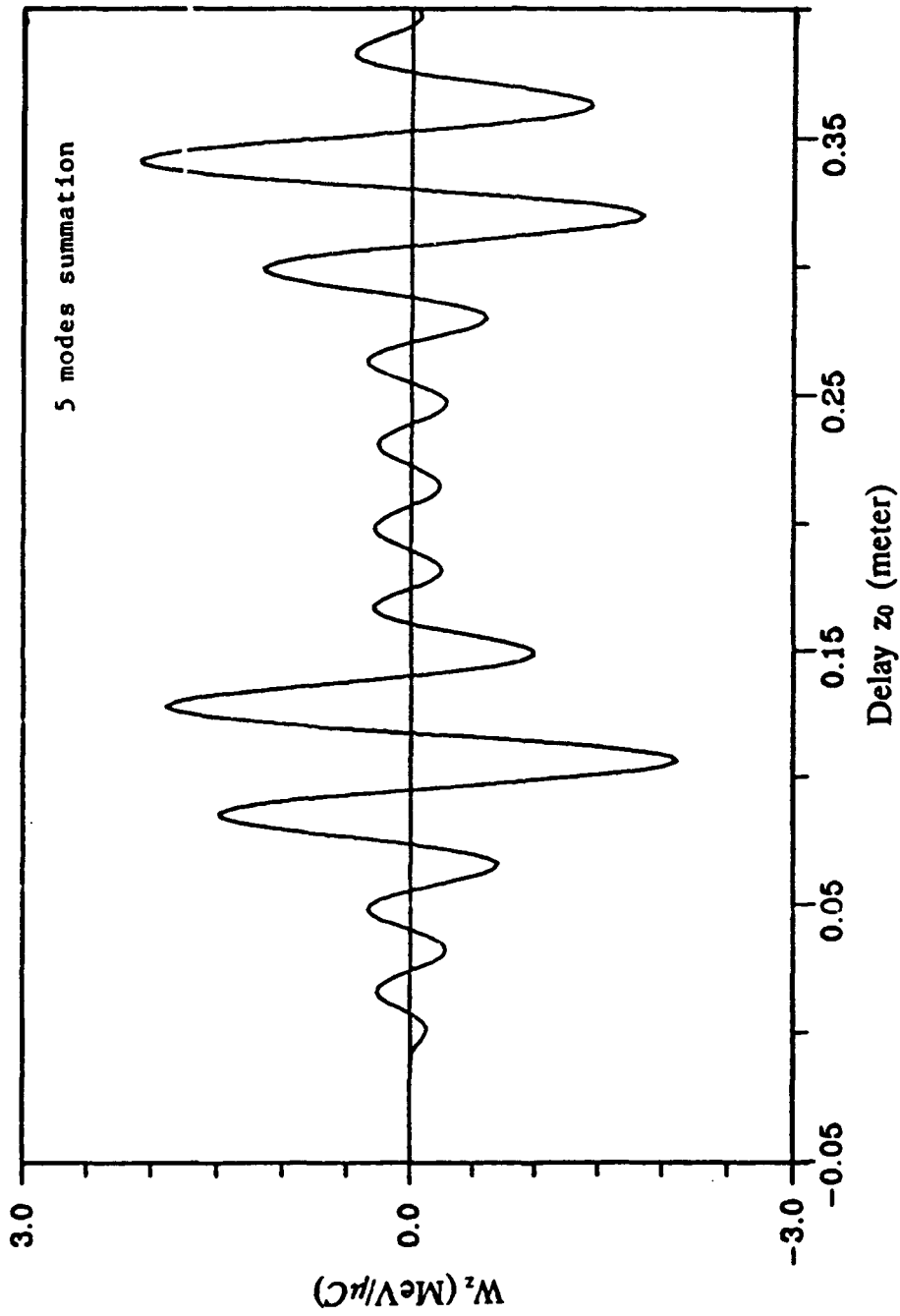


Figure 3.10. Longitudinal wake potential on the accelerated beam path  
 ( $Q = 1 \mu\text{C}$ ,  $\sigma = 5 \text{ mm}$ , 5 modes are included)

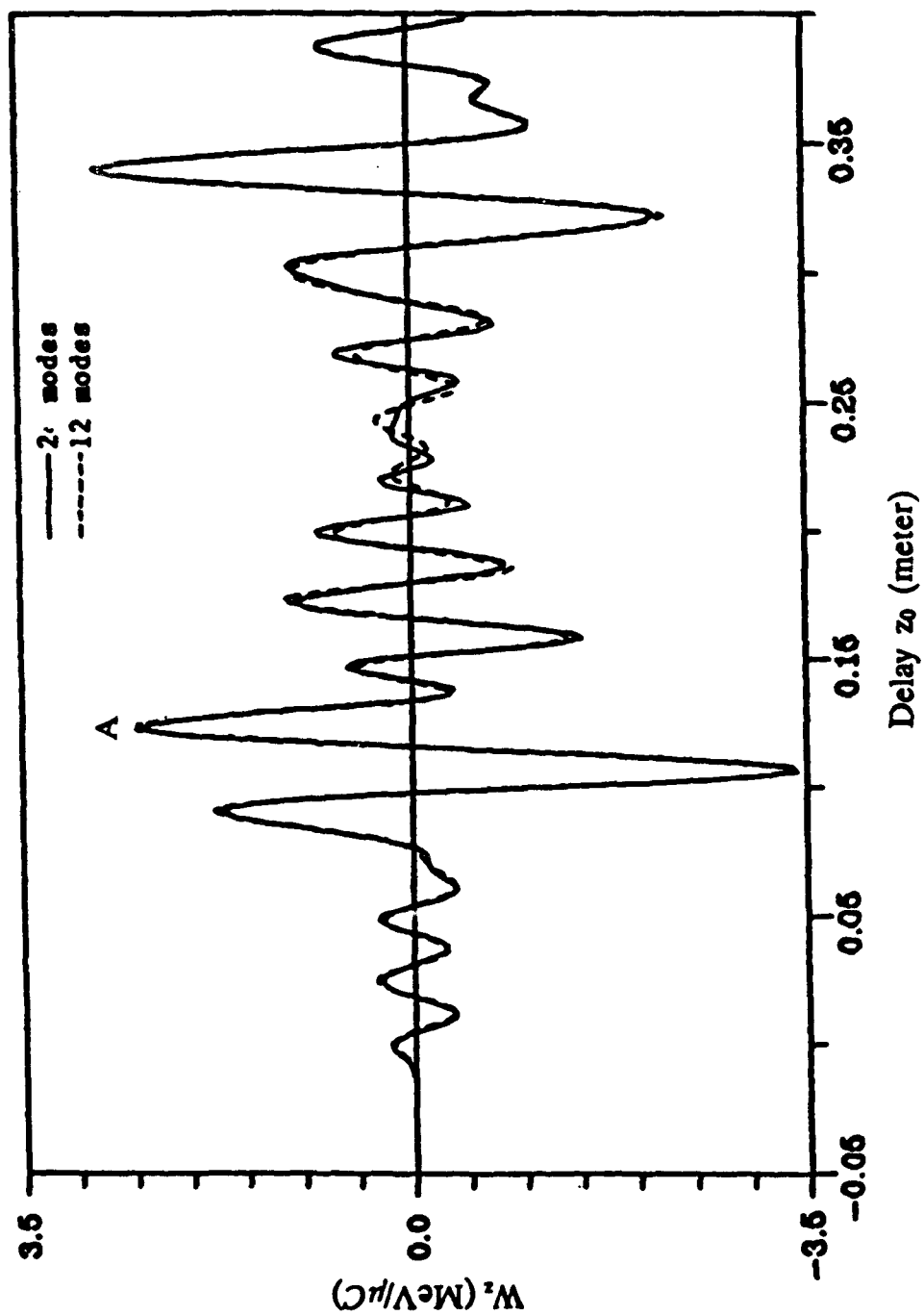


Figure 3.11. Longitudinal wake potential on the accelerated beam path  
 ( $Q = 1 \mu\text{C}$ ,  $\sigma = 5 \text{ mm}$ , solid line for 24 modes and broken line for 12 modes)

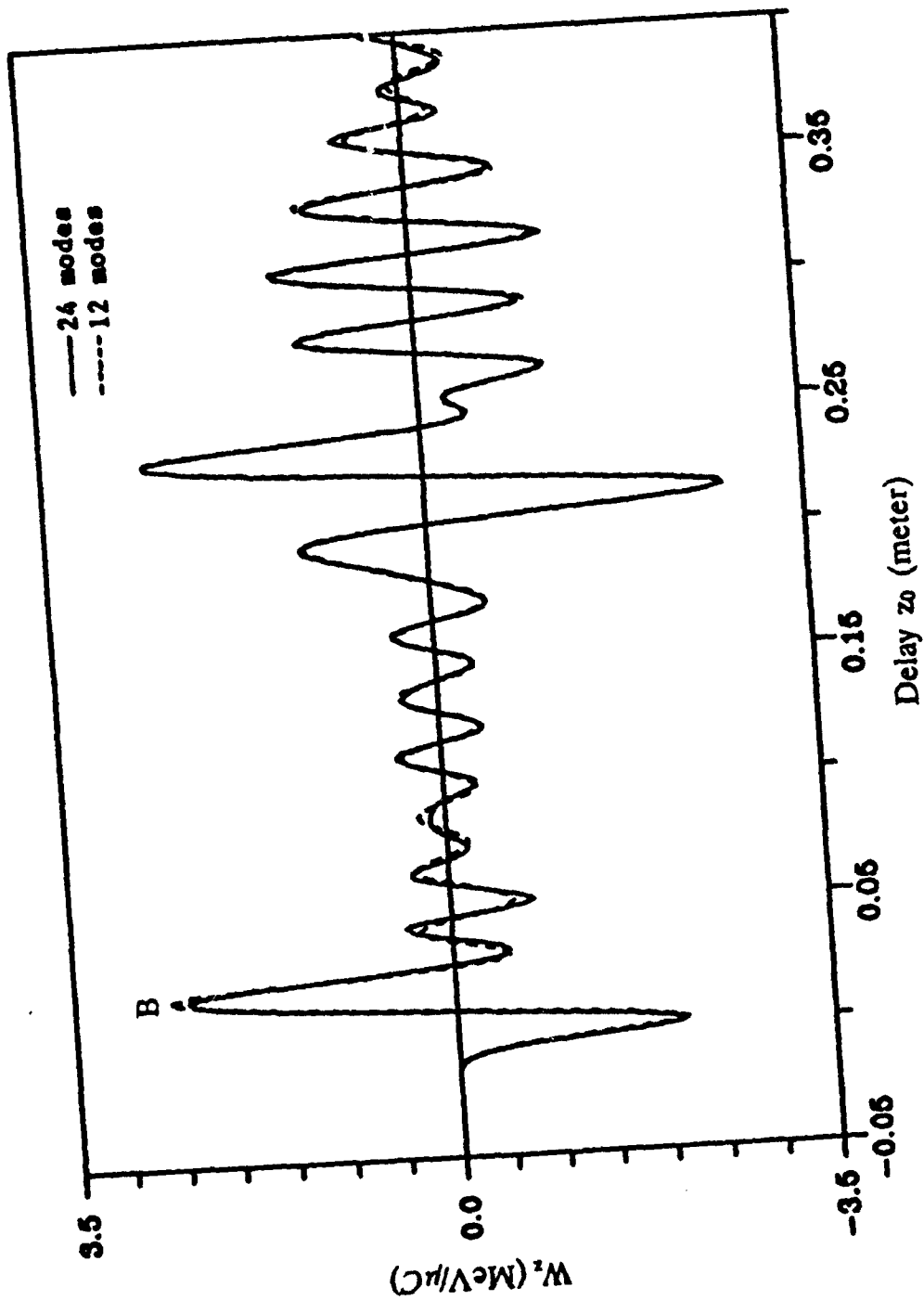


Figure 3.12. Longitudinal wake potential on the driving beam path  
( $Q = 1 \mu\text{C}$ ,  $\sigma = 5 \text{ mm}$ , solid line for 24 modes and broken line for 12 modes)

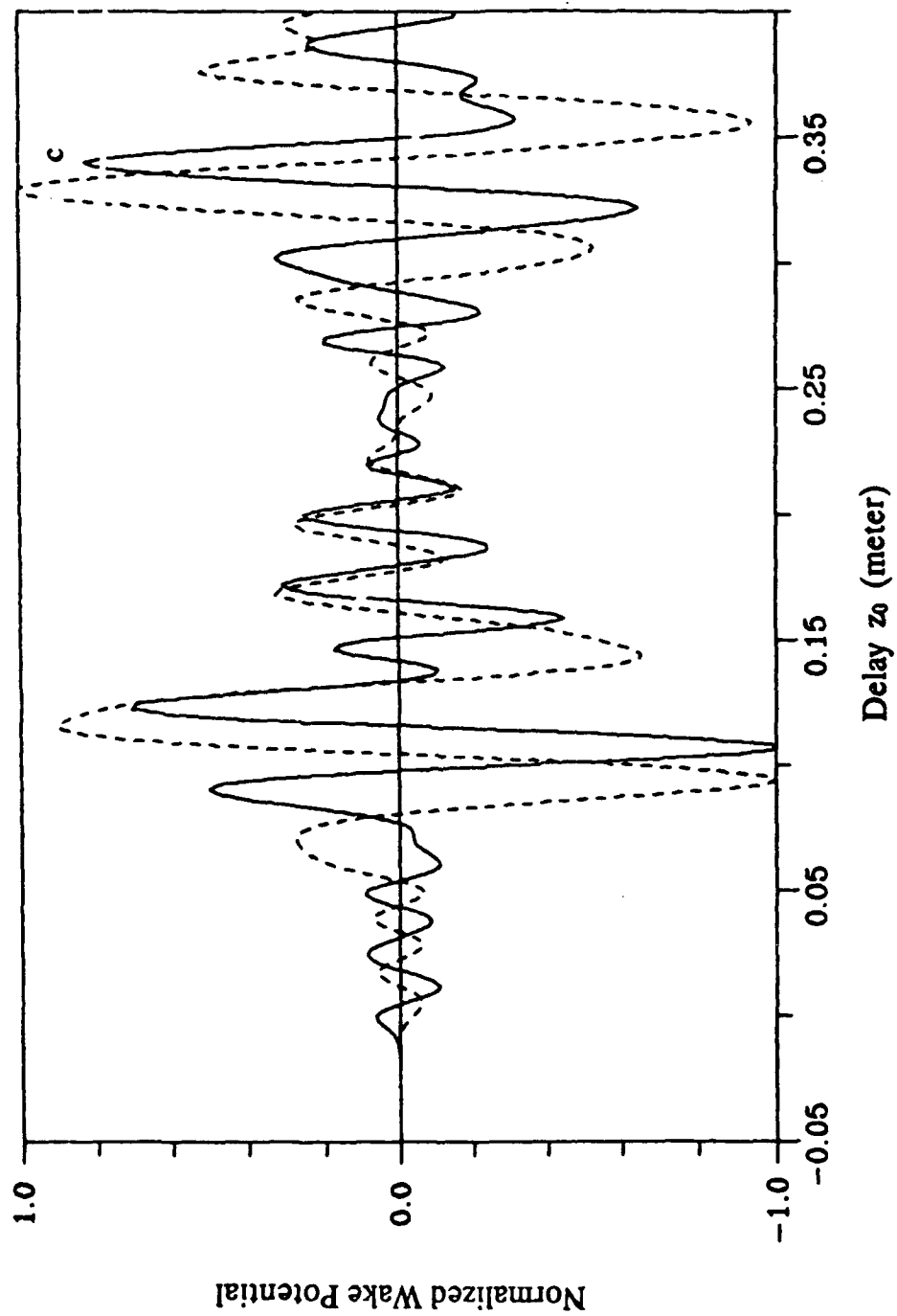


Figure 3.13. Normalized wake potential on the accelerated beam path  
Solid line : longitudinal wake potential/(3.40 MeV/ $\mu$ C)  
Broken line : transverse wake potential/(1.29 MeV/ $\mu$ C)

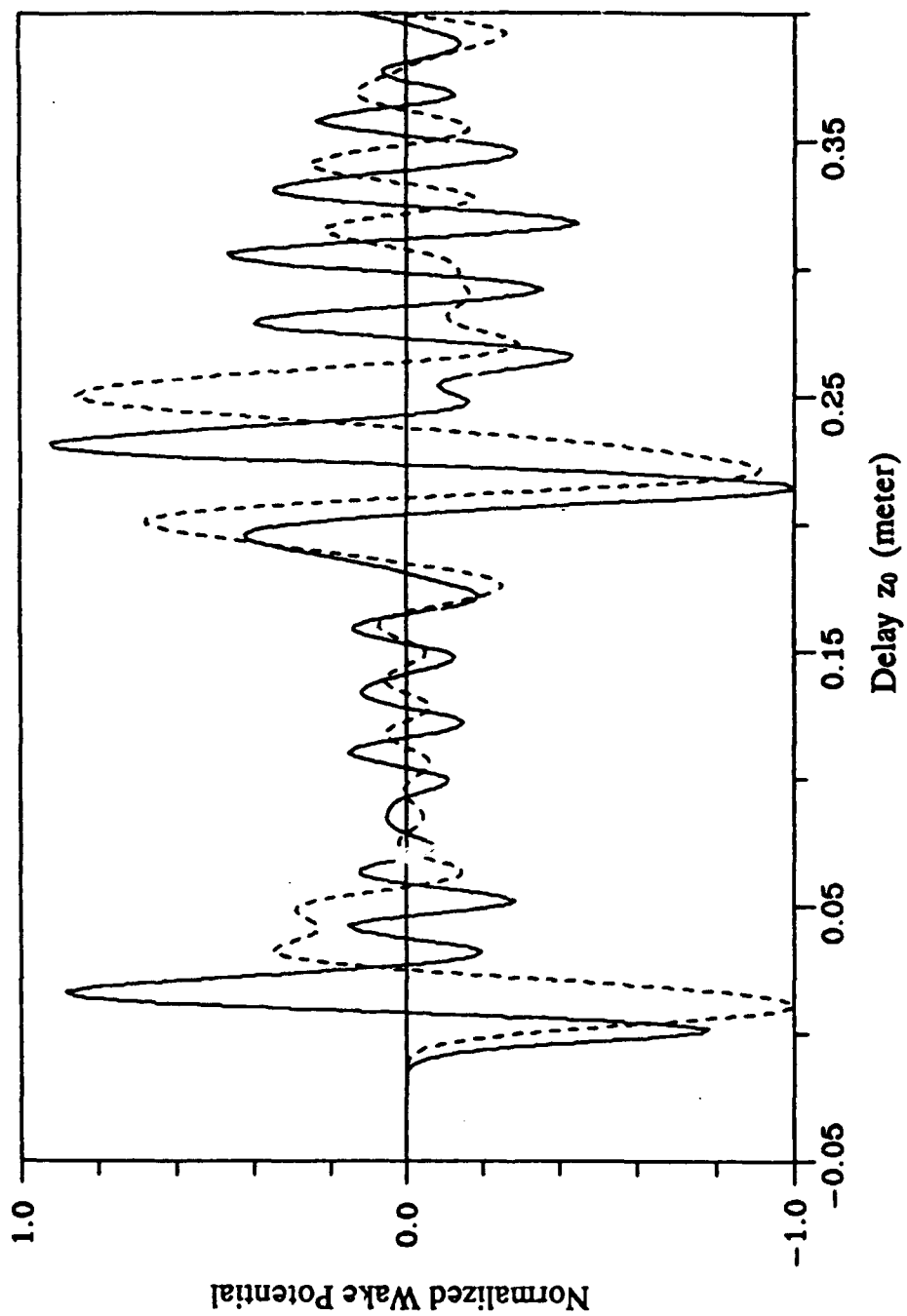


Figure 3.14. Normalized wake potential on the driving beam path  
Solid line : longitudinal wake potential/(2.77 MeV/ $\mu$ C)  
Broken line : transverse wake potential/(1.68 MeV/ $\mu$ C)

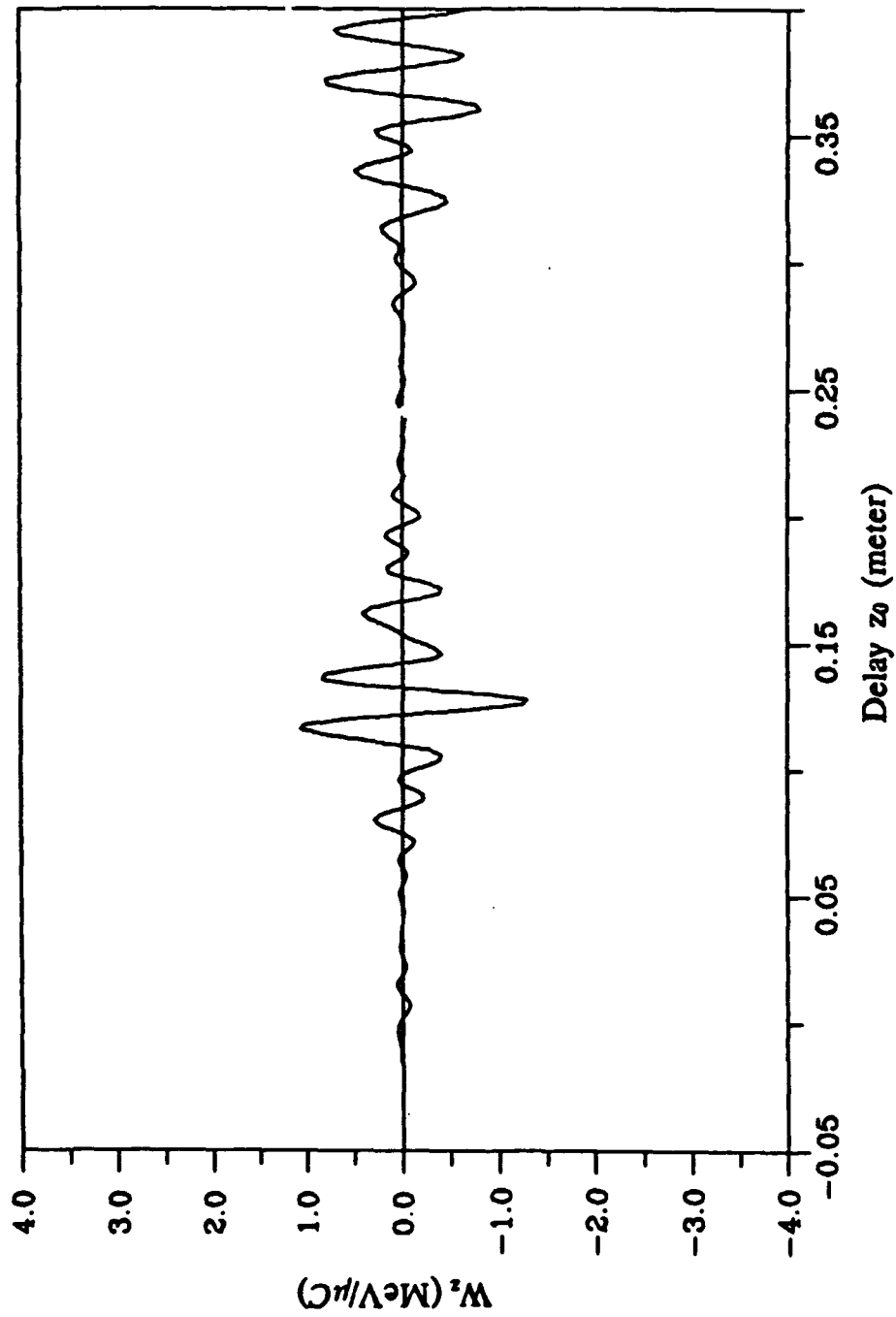


Figure 3.15. Longitudinal wake potential on the driving beam path  
 ( $Q = 1 \mu\text{C}$ ,  $\sigma = 5 \text{ mm}$ ,  $x_b = 5 \text{ cm}$ ,  $y_b = 2 \text{ cm}$ ,  $d = 2 \text{ cm}$ )

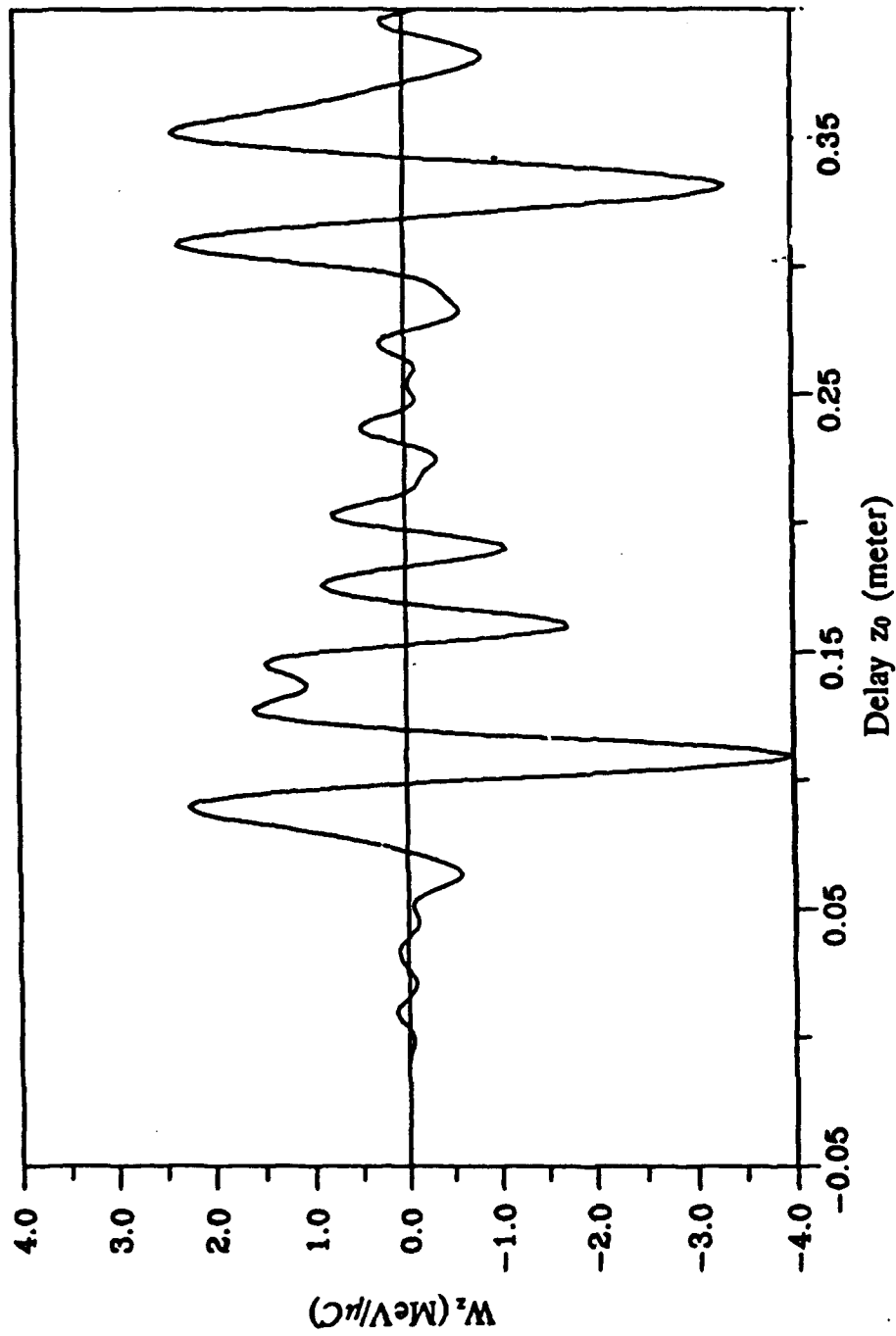


Figure 3.16. Longitudinal wake potential on the driving beam path  
 ( $Q = 1 \mu\text{C}$ ,  $\sigma = 5 \text{ mm}$ ,  $x_b = 5 \text{ cm}$ ,  $y_b = 3.5 \text{ cm}$ ,  $d = 2 \text{ cm}$ )

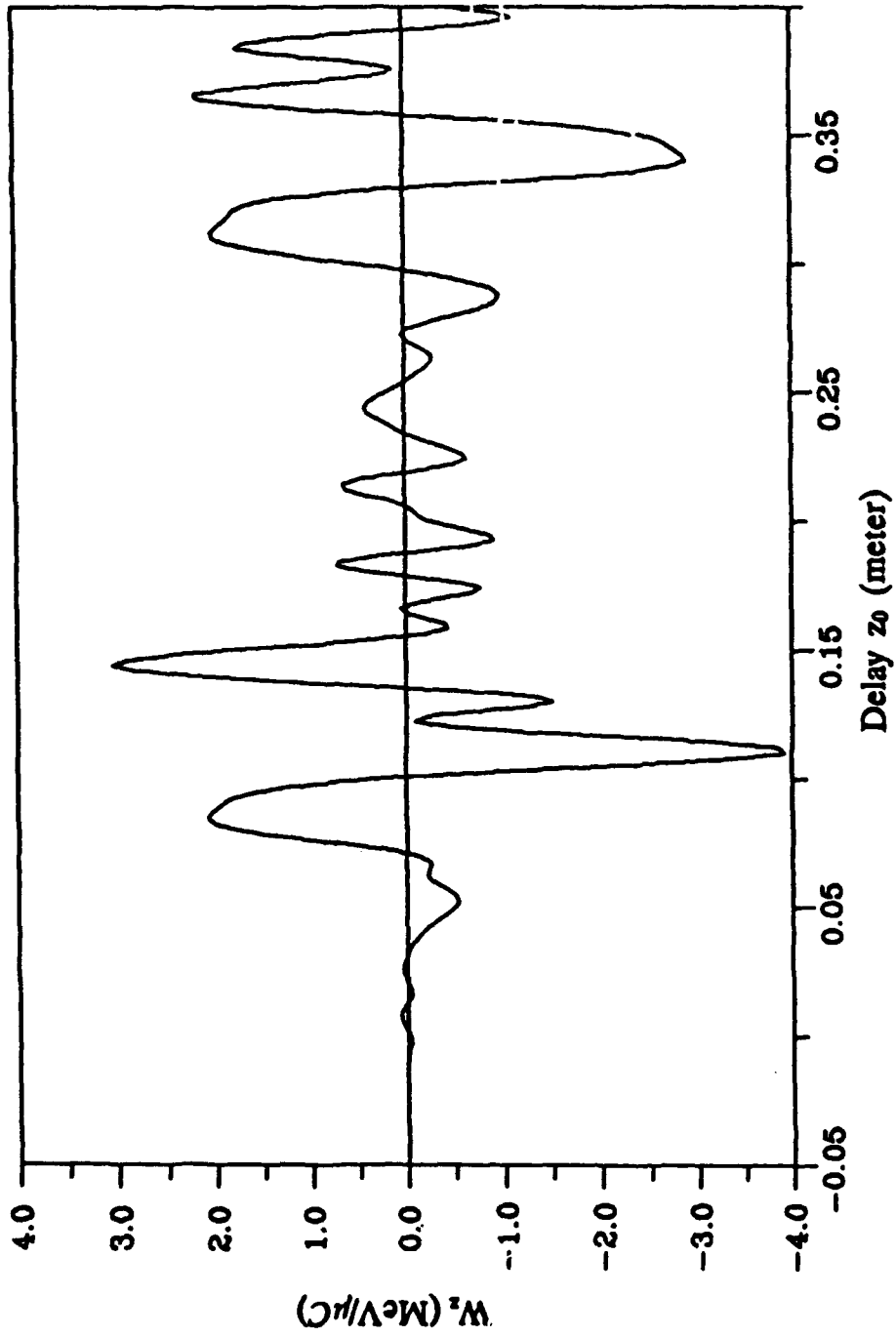


Figure 3.17. Longitudinal wake potential on the driving beam path  
 ( $Q = 1 \mu\text{C}$ ,  $\sigma = 5 \text{ mm}$ ,  $x_b = 5 \text{ cm}$ ,  $y_b = 4 \text{ cm}$ ,  $d = 2 \text{ cm}$ )

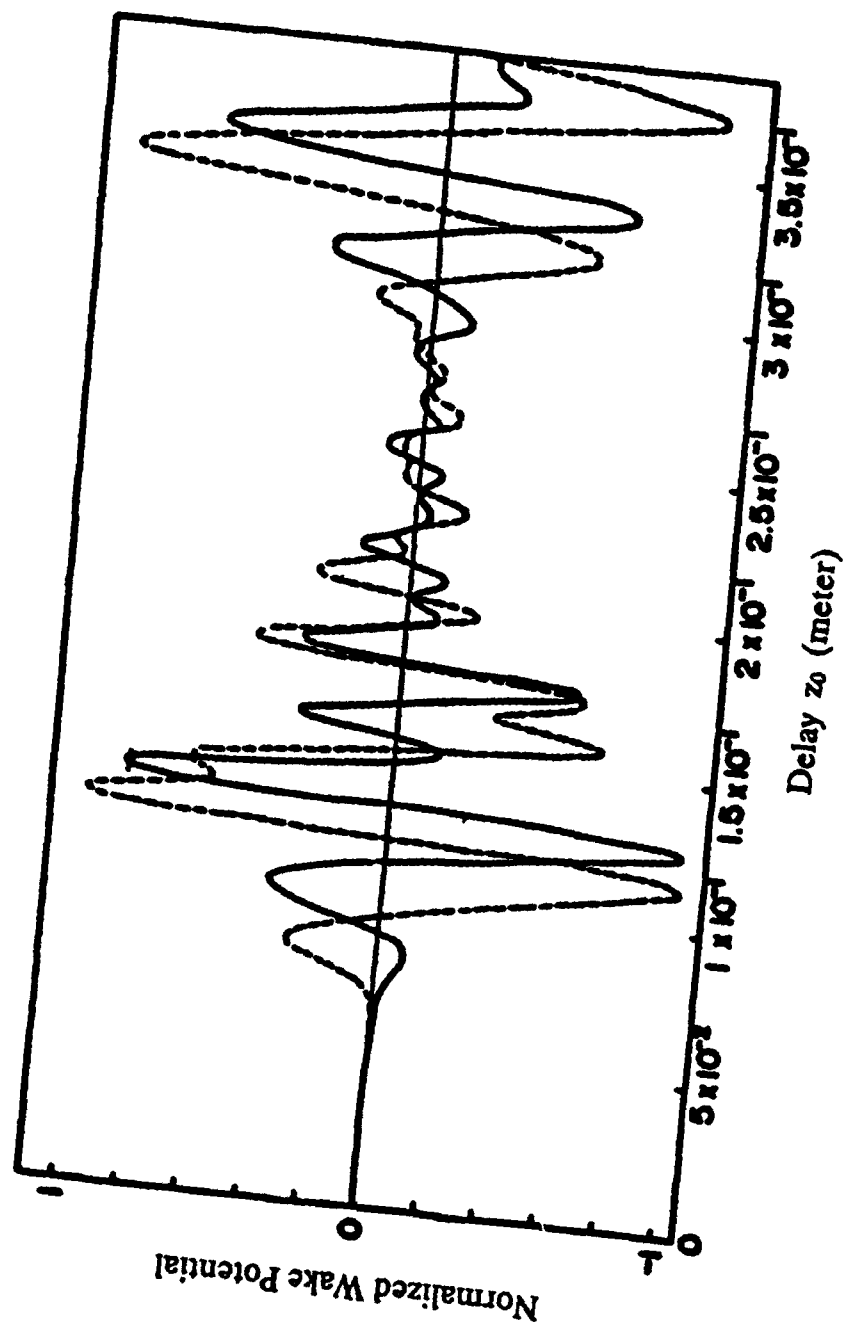


Figure 3.18. Normalized wake potential on the accelerated beam path (from ref. 22)  
 $(Q = 1 \mu\text{C}, \sigma = 5 \text{ mm}, x_b = 5 \text{ cm}, y_b = 3 \text{ cm}, d = 2 \text{ cm})$   
 Solid line : longitudinal wake potential/(2.54 MeV/ $\mu\text{C}$ )  
 Broken line : transverse wake potential/(1.11 MeV/ $\mu\text{C}$ )

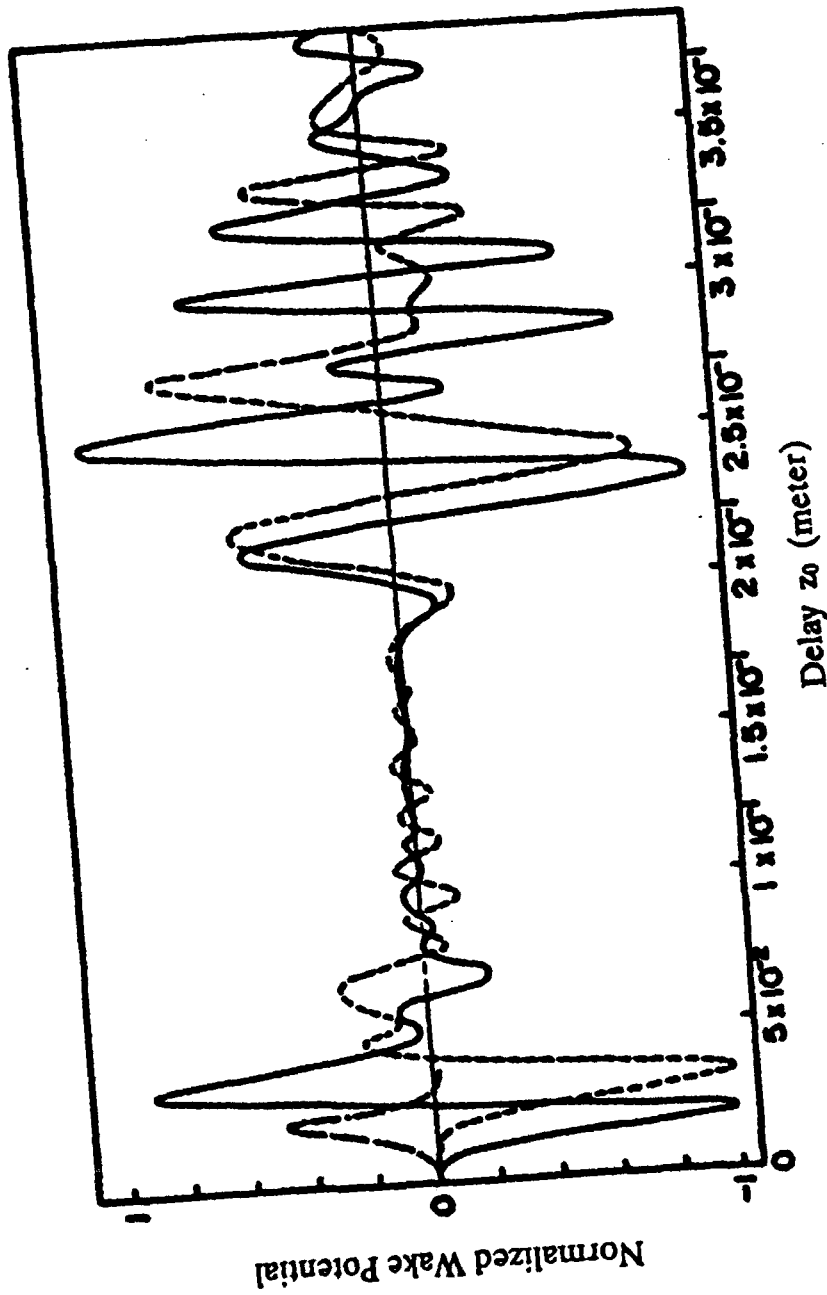


Figure 3.19. Normalized wake potential on the driving beam path (from ref. 22)  
 ( $Q = 1 \mu\text{C}$ ,  $\sigma = 5 \text{ mm}$ ,  $x_b = 5 \text{ cm}$ ,  $y_b = 3 \text{ cm}$ ,  $d = 2 \text{ cm}$ )  
 Solid line : longitudinal wake potential/(1.92 MeV/ $\mu\text{C}$ )  
 Broken line : transverse wake potential/(1.48 MeV/ $\mu\text{C}$ )

## CHAPTER IV

### WAKE POTENTIAL IN A DIELECTRIC-LOADED ELLIPTICAL WAVEGUIDE

#### 4. 1. Introduction

As discussed in Chapter 3, disk-loaded elliptical cavity is capable of producing an acceleration gradient greater than 100 MeV/m/ $\mu\text{C}$ . But one disadvantage of using this cavity as a wake-field acceleration device is its uncancellable transverse wake fields even when alternately rotated stages are used to minimize net transverse deflection. The transverse wake fields are useful as an electric wiggler fields for the FEL applications,<sup>19</sup> but are the source of beam instability and blow up for the acceleration application. One possible solution to this non-zero transverse wake fields is to use a waveguide, or a cavity, which are partially filled with dielectric (known alternatively as Dielectric Wakefields Acceleration scheme). In this scheme an intense driving charge excites the wake fields through the Cerenkov radiation mechanism. This radiation is then used to accelerate a second, less intense particles to higher energies.

This method has a particular advantage over other wake-field acceleration schemes that the transverse wake fields can be made quite small for the ultra-relativistic driving beam. Recent experimental<sup>16</sup> and theoretical<sup>17</sup> studies have shown that the transverse wake potential in a dielectric-loaded circular waveguide vanishes in the limit of the particle velocity  $v \rightarrow c$  even when the driving beam is off-center, and the longitudinal acceleration

gradient is of the same order of magnitude that can be obtained in the disk-loaded metallic cavity.

Being a co-linear geometry like the circular waveguide used in that experiment, staging is not quite attractive. Since we are primarily concerned with the geometry which can permit easy staging in this investigation, the wake fields excited in the dielectric-loaded waveguide of an elliptical cross section are of greater interest. In this chapter, we will investigate the wake fields excited in the dielectric-loaded elliptical waveguide. The property of vanishing transverse wake fields is investigated for a use as a wake-field acceleration device. We use the Fourier transform method to solve this problem for convenience in calculations, and consequently all quantities are treated in the frequency domain. It is also assumed that the waveguide wall is perfectly conducting and the waveguide is filled with isotropic dielectric.

#### 4. 2. Formulation of Solution

Consider the elliptical waveguide which is partially filled with medium of dielectric constant  $\epsilon$  and permeability  $\mu$  as shown in figure 4.1. Again the problem is solved in the confocal elliptical coordinates. The coordinate of the waveguide wall and that of the vacuum-dielectric interface are, respectively,  $\xi = \xi_a$  and  $\xi = \xi_b$ . A point charge  $Q$  is assumed to move in a vacuum with velocity  $v$  along the arbitrary line  $(\xi_0, \eta_0)$  which is parallel to the focus axis of an elliptical cavity. The electromagnetic fields produced by the motion of a charge in a structure is given again by the Maxwell equations. In this chapter, we use cgs units.

The Maxwell equations are

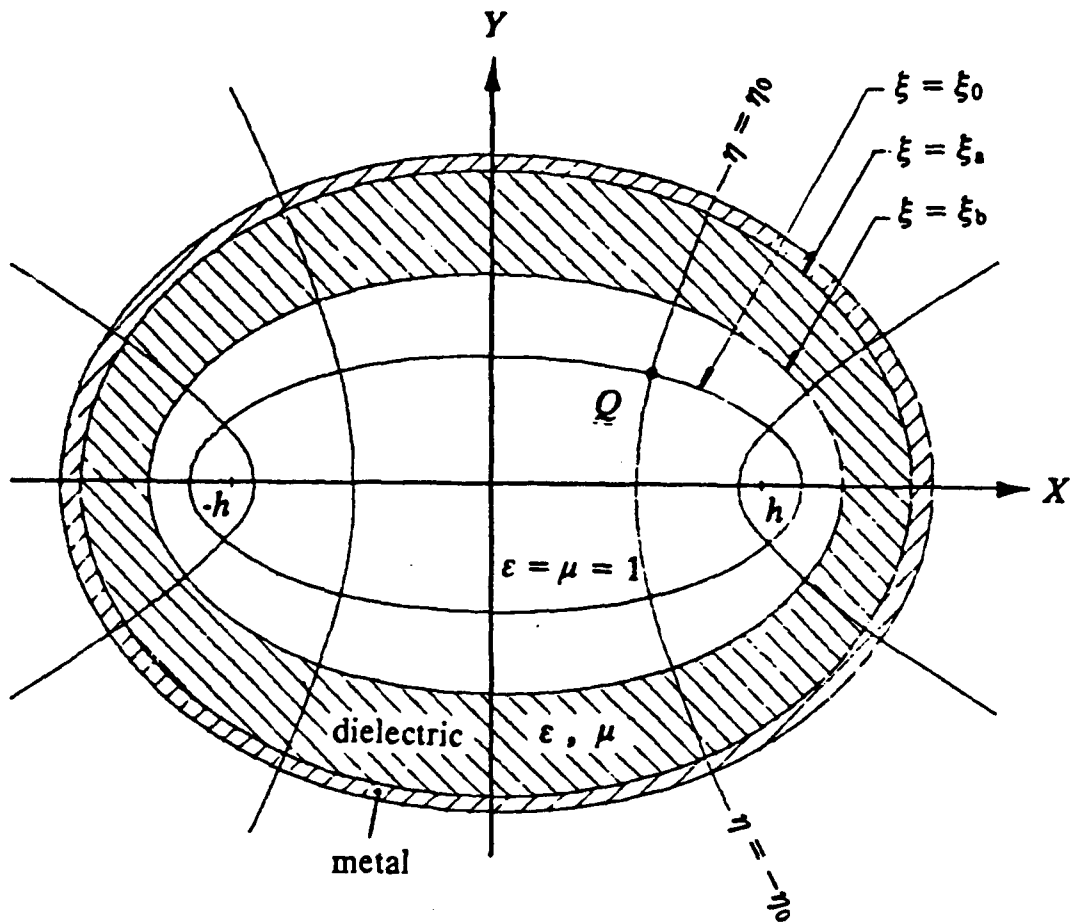


Figure 4.1. Cross section of the elliptical waveguide partially filled with dielectric

$$\nabla \times \mathbf{E} = -\frac{1}{c} \frac{\partial \mathbf{B}}{\partial t}, \quad (4.1)$$

$$\nabla \times \mathbf{H} = \frac{4\pi}{c} \mathbf{J} + \frac{1}{c} \frac{\partial \mathbf{D}}{\partial t}, \quad (4.2)$$

$$\nabla \cdot \mathbf{D} = 4\pi\rho, \quad (4.3)$$

$$\nabla \cdot \mathbf{B} = 0, \quad (4.4)$$

$$\mathbf{D} = \epsilon \mathbf{E}, \quad (4.5)$$

$$\mathbf{B} = \mu \mathbf{H}. \quad (4.6)$$

The electric field  $\mathbf{E}$  and the magnetic induction  $\mathbf{B}$  can be written in terms of a vector potential  $\mathbf{A}$  and a scalar potential  $\varphi$  as

$$\mathbf{E} = -\nabla\varphi - \frac{1}{c} \frac{\partial \mathbf{A}}{\partial t}, \quad (4.7)$$

$$\mathbf{B} = \nabla \times \mathbf{A}. \quad (4.8)$$

In the Lorentz gauge,  $\nabla \cdot \mathbf{A} + \frac{\epsilon\mu}{c} \frac{\partial \varphi}{\partial t} = 0$ , the Maxwell equations (4.2) and (4.3) are transformed to

$$\nabla^2 \mathbf{A} - \frac{\epsilon\mu}{c^2} \frac{\partial^2 \mathbf{A}}{\partial t^2} = -\frac{4\pi\mu}{c} \mathbf{J}, \quad (4.9)$$

$$\nabla^2 \varphi - \frac{\epsilon\mu}{c^2} \frac{\partial^2 \varphi}{\partial t^2} = -\frac{4\pi}{\epsilon} \rho. \quad (4.10)$$

The charge density in the elliptical coordinates  $(\xi, \eta, z)$  is given by

$$\begin{aligned} \rho &= Q \delta(\mathbf{r} - \mathbf{r}_0) \delta(z - vt) \\ &= \frac{Q}{\Delta} \delta(\xi - \xi_0) \delta(\eta - \eta_0) \delta(z - vt), \end{aligned} \quad (4.11)$$

where  $\mathbf{r}_0$  is the transverse coordinate of an exciting charge  $Q$ , and  $\Delta$  is the Jacobian relation given by

$$\Delta = \left| \frac{\partial(x, y)}{\partial(\xi, \eta)} \right| = \frac{h^2}{2} (\cosh 2\xi - \cos 2\eta), \quad (4.12)$$

where  $h$  is a semi-interfocal distance as shown in figure 4.1. Through the continuity equation, the current density becomes

$$\mathbf{J} = z\rho v, \quad (4.13)$$

where  $z$  is the unit vector in the  $z$ -direction. Since the current density of the particle has only  $z$ -component, and the metallic waveguide wall and dielectric surface are smooth, the vector potential  $\mathbf{A}$  has only  $z$ -component, i.e.,  $\mathbf{A} = zA_z$ . As a result, scalar and vector potentials are proportional to each other. In fact,

$$A_z = \frac{\epsilon\mu}{c} v\phi. \quad (4.14)$$

Therefore, we can construct a solution with the knowledge of a scalar potential  $\phi$  alone. We are going to Fourier transform the inhomogeneous wave equation (4.10) and solve in the frequency domain. In addition, the dependence on  $z$  and  $t$  are such that all quantities depend on the combined variable  $(z - vt)$ .

First, we expand the delta functions in eq. (4.11). The well-known Fourier expansion of  $\delta(z - vt)$  is<sup>34</sup>

$$\delta(z - vt) = \frac{1}{\pi v} \operatorname{Re} \int_0^\infty e^{i\frac{\omega}{v}(z - vt)} d\omega, \quad (4.15)$$

where  $\operatorname{Re}$  stands for the real part of the complex quantity. It is convenient to expand  $\delta(\eta - \eta_0)$  in terms of the orthogonal Mathieu functions of the first kind,  $ce_m(\eta, -q)$ , as

$$\delta(\eta - \eta_0) = \frac{1}{\pi} \sum_{m=0}^{\infty} ce_m(\eta, -q) ce_m(\eta_0, -q), \quad (4.16)$$

where  $q$  is given by the relation

$$2q = \frac{h^2}{2} \left(\frac{\omega}{v}\right)^2 (1 - \epsilon\mu\beta^2), \quad (4.17)$$

where  $\beta = v/c$ . Here, we use the orthogonality property of the Mathieu function  $ce_m(\eta, -q)$ ,

$$\frac{1}{\pi} \int_0^{2\pi} ce_m(\eta, -q) ce_n(\eta, -q) d\eta = \delta_{mn}, \quad (4.18)$$

to derive eq. (4.16), and  $\delta_{mn}$  is a Kronecker delta. Substituting eqs. (4.15) and (4.16) into (4.11), the charge density becomes

$$\rho = \frac{Q\delta(\xi - \xi_0)}{\pi^2 v \Delta} \sum_{m=0}^{\infty} ce_m(\eta, -q) ce_m(\eta_0, -q) \times \text{Re} \int_0^{\infty} e^{i\frac{\omega}{v}(z - vt)} d\omega. \quad (4.19)$$

Similarly, the scalar potential  $\varphi$  can be expanded in harmonics of the form

$$\begin{aligned} \varphi(\xi, \eta, z - vt) &= \frac{1}{\pi^2} \sum_{m=0}^{\infty} ce_m(\eta, -q) ce_m(\eta_0, -q) \\ &\times \text{Re} \int_0^{\infty} e^{i\frac{\omega}{v}(z - vt)} \Phi_m(\xi, \omega) d\omega. \end{aligned} \quad (4.20)$$

From the definition of  $\varphi$  given by eq. (4.20), the Laplacian operator  $\nabla^2$  in the elliptical coordinates  $(\xi, \eta, z)$  becomes

$$\nabla^2 = \frac{1}{\Delta} \left( \frac{\partial^2}{\partial \xi^2} + \frac{\partial^2}{\partial \eta^2} \right) + \frac{\partial^2}{\partial z^2} = \frac{1}{\Delta} \left( \frac{\partial^2}{\partial \xi^2} + \frac{\partial^2}{\partial \eta^2} \right) - \left(\frac{\omega}{v}\right)^2, \quad (4.21)$$

and the differential operators  $\frac{\partial^2}{\partial t^2}$  and  $\frac{\partial^2}{\partial z^2}$  become

$$\frac{\partial^2}{\partial t^2} = -\omega^2, \quad (4.22)$$

$$\frac{\partial^2}{\partial z^2} = -\left(\frac{\omega}{v}\right)^2. \quad (4.23)$$

Substituting eqs. (4.19) - (4.23) into (4.10), the equation for  $\Phi_m(\xi, \omega)$  is reduced to

$$\Phi_m'' + \frac{ce_m''(\eta, -q)}{ce_m(\eta, -q)} \Phi_m - \Delta \left(\frac{\omega}{v}\right)^2 (1 - \epsilon\mu\beta^2) \Phi_m = -\frac{4\pi Q}{\epsilon v} \delta(\xi - \xi_0). \quad (4.24)$$

Since, the Mathieu function  $ce_m(\eta, -q)$  is a solution of the Mathieu equation with negative  $q$ ,  $y'' + (a + 2q \cos 2\eta)y = 0$ , the second term in eq. (4.24) can be expressed in terms of parameters  $a$ ,  $q$ , and  $\eta$ . Finally, we obtain the following equation for  $\Phi_m(\xi, \omega)$ :

$$\Phi_m''(\xi, \omega) - (\alpha + 2q \cosh 2\xi) \Phi_m(\xi, \omega) = -\frac{4\pi Q}{\epsilon v} \delta(\xi - \xi_0). \quad (4.25)$$

Eq. (4.25) together with (4.7), (4.8), (4.14) and (4.20) completely determines the fields produced by the moving charge, from which we can determine the longitudinal and transverse wake potentials.

### 4. 3. Wake Fields Calculation

#### 4. 3. 1. Solution to the Boundary Value Problem

Two independent solutions of the corresponding homogeneous equation of (4.25) are the modified Mathieu functions of the first kind  $Ce_m(\xi, -q)$  and the second kind  $Fek_m(\xi, -q)$ , which are given in Appendix A. Here, we denote the vacuum region as region 1 and the dielectric medium as region 2. Let us first find the particular solution of inhomogeneous Mathieu equation (4.25) in the vacuum region where  $\xi < \xi_b$ .

In region 1, we have

$$\varepsilon = \mu = 1, \beta^2 \leq 1,$$

$$q = \frac{h^2}{4} \left(\frac{\omega}{v}\right)^2 (1 - \beta^2) \geq 0. \quad (4.26)$$

The particular solution of eq. (4.25) can be found by using the Green function technique, i.e.,  $\Phi_m$  is continuous while the derivative of  $\Phi_m$  has a jump at  $\xi = \xi_0$ . Furthermore, if we demand  $\Phi_m$  be finite at  $\xi = 0$  and vanish as  $\xi \rightarrow \infty$  for all values of  $q$ , then the solution is

$$\Phi_{m, \text{inhomo}} = -\frac{4\pi Q}{D_m v} C e_m(\xi_<, -q) F e k_m(\xi_>, -q), \quad (4.27)$$

where subscript  $<$  (or  $>$ ) is the smaller (or the bigger) of  $\xi$  and  $\xi_0$ , and  $D_m$  is a Wronskian, which is independent of  $\xi$  and is a function of  $q$  only. That is

$$\begin{aligned} D_m(q) &= C e_m(\xi_0, -q) F e k_m'(\xi_0, -q) - C e_m'(\xi_0, -q) F e k_m(\xi_0, -q) \\ &= C e_m(0, -q) F e k_m'(0, -q), \end{aligned} \quad (4.28)$$

where  $f' = df/d\xi$ , and  $C e_m'(0, -q) = 0$  is used.

In order to form a complete set of solutions which satisfy all the boundary conditions, we have to have a homogeneous solution of eq. (4.25), which is given by

$$\Phi_{m, \text{homo}} = C_m C e_m(\xi_0, -q) C e_m(\xi, -q), \quad (4.29)$$

where  $C_m$  is an arbitrary constant. The solution of the form  $F e k_m(\xi, -q)$  is not considered in eq. (4.29) for the same reasons discussed in chapter 3.1, i.e., the product  $C e_m(\eta, -q) F e k_m(\xi, -q)$  must satisfy two additional conditions given by eqs. (3.11) and (3.12). We see that it is continuous but its derivative with respect to  $\xi$  is not continuous on the interfocal line.

Combining eqs. (4.27) and (4.29),  $\Phi_m$  in region 1 can be written in the form

$$\begin{aligned} \Phi_{m,1} = \frac{-4\pi Q}{D_m \nu} [C e_m(\xi_<, -q) F e_{l:m}(\xi_>, -q) \\ + C_m C e_m(\xi_0, -q) C e_m(\xi, -q)]. \end{aligned} \quad (4.30)$$

In a dielectric medium ( $\xi_b < \xi < \xi_a$ ), we have

$$\begin{aligned} \mu = 1, \quad \epsilon \beta^2 > 1, \\ q = \frac{h^2}{4} \left(\frac{\omega}{\nu}\right)^2 (1 - \epsilon \beta^2) = -s < 0. \end{aligned} \quad (4.31)$$

The solution in region 2 is simply

$$\Phi_{m,2} = A_m F e y_m(\xi, s) + B_m C e_m(\xi, s), \quad (4.32)$$

where  $A_m$  and  $B_m$  are arbitrary constant. We use the parameter  $s$  instead of  $q$  in this region.  $F e y_m(\xi, s)$ , the Y-type modified Mathieu function of the second kind, is used as a second solution in (4.32) for convenience in calculations.

The coefficients  $C_m$ ,  $A_m$  and  $B_m$  are determined from the boundary conditions at the metallic wall ( $\xi = \xi_a$ ) and at the vacuum-dielectric interface ( $\xi = \xi_b$ ). The boundary conditions are:

- (i)  $E_z = 0$  at  $\xi = \xi_a$ .
- (ii)  $E_z$  is continuous at  $\xi = \xi_b$ .
- (iii)  $D_\xi$  is continuous at  $\xi = \xi_b$ .

From eqs. (4.7), (4.14) and (4.20), we see that  $E_z$  and  $D_\xi$  are proportional to

$$E_z \sim \frac{\omega}{v} (1 - \epsilon\mu\beta^2) \Phi_m, \quad (4.33)$$

$$D_\xi \sim \epsilon \frac{\partial \Phi_m}{\partial \xi}. \quad (4.34)$$

Therefore, the above boundary conditions can be written in terms of transformed potential  $\Phi_m$  as

$$A_m Fey_m(\xi_a, s) + B_m Ce_m(\xi_a, s) = 0, \quad (4.35)$$

$$(1 - \beta^2) \left[ \frac{-4\pi Q Ce_m(\xi_0, -q)}{D_m v} \right] [Fek_m(\xi_b, -q) + C_m Ce_m(\xi_b, -q)] \\ = (1 - \epsilon\beta^2) [A_m Fey_m(\xi_b, s) + B_m Ce_m(\xi_b, s)], \quad (4.36)$$

$$\frac{-4\pi Q Ce_m(\xi_0, -q)}{D_m v} [Fek_m'(\xi_b, -q) + C_m Ce_m'(\xi_b, -q)] \\ = \epsilon [A_m Fey_m'(\xi_b, s) + B_m Ce_m'(\xi_b, s)]. \quad (4.37)$$

We only need to know the coefficient  $C_m$  to calculate the fields in a vacuum region. It is found to be

$$C_m = - \frac{s Fek_m'(\xi_b, -q) \Psi_1^{(m)} + \epsilon q Fek_m(\xi_b, -q) \Psi_0^{(m)}}{s Ce_m'(\xi_b, -q) \Psi_1^{(m)} + \epsilon q Ce_m(\xi_b, -q) \Psi_0^{(m)}}, \quad (4.38)$$

where

$$\Psi_1^{(m)} = Ce_m(\xi_a, s) Fey_m(\xi_b, s) - Ce_m(\xi_b, s) Fey_m(\xi_a, s), \quad (4.39)$$

$$\Psi_0^{(m)} = Ce_m(\xi_a, s) Fey_m'(\xi_b, s) - Ce_m'(\xi_b, s) Fey_m(\xi_a, s). \quad (4.40)$$

#### 4. 3. 2. Longitudinal and Transverse Wake Fields

The longitudinal electric field can be calculated from the scalar potential directly. From eqs. (4.7), (4.14) and (4.20), the electric field in region 1 becomes

$$E_z(\xi, \eta, z - vt) = \frac{4Q}{\pi v^2} (1 - \beta^2) \sum_{m=0}^{\infty} ce_m(\eta - q) ce_m(\eta_0, -q) \operatorname{Re} \int_0^{\infty} d\omega i\omega \\ \times \frac{Ce_m(\xi_0, -q)}{D_m(q)} (Fek_m(\xi, -q) + C_m Ce_m(\xi, -q)) e^{i\frac{\omega}{v}(z - vt)}. \quad (4.41)$$

For a test charge at position  $t = (z + z_0)/c$ , or trailing the driving charge by  $z_0$ , the longitudinal electric field experienced by a test charge is given by

$$E_z(\xi, \eta, z_0) = \frac{4Q}{\pi v^2} (1 - \beta^2) \sum_{m=0}^{\infty} ce_m(\eta, -q) ce_m(\eta_0, -q) \operatorname{Re} \int_0^{\infty} d\omega i\omega \\ \times \frac{Ce_m(\xi_0, -q)}{D_m(q)} (Fek_m(\xi, -q) + C_m Ce_m(\xi, -q)) e^{i\frac{\omega}{v}z_0} \\ = \sum_{m=0}^{\infty} E_z^{(m)}. \quad (4.42)$$

This is the wake fields left by the source. The longitudinal wake potential  $W_z$ , defined as the energy change of a test charge per unit driving charge, becomes simply

$$W_z = \frac{-1}{Q} \int_0^L E_z dz, \quad (4.43)$$

where  $L$  is the structure length.

The wake fields excited by the ultra-relativistic particle are of particular interest. Consider the case when the particle velocity  $v \rightarrow c$ , or  $\beta \rightarrow 1$ . From eq. (4.26), we see that the parameter  $q$  becomes zero as  $\beta \rightarrow 1$ . In this case, we can use the following limiting properties of the Mathieu functions to simplify eq. (4.42). As  $q \rightarrow 0$ , we have

$$ce_m(\eta, -q) \rightarrow \begin{cases} \frac{1}{\sqrt{2}}, & \text{for } m = 0 \\ \cos m\eta, & \text{for } m \geq 1 \end{cases} \quad (4.44)$$

$$Ce_m(\xi, -q) \rightarrow \begin{cases} \frac{1}{\sqrt{2}}, & \text{for } m = 0 \\ \cosh m\xi, & \text{for } m \geq 1 \end{cases} \quad (4.45)$$

$$Fek_m(\xi, -q) \rightarrow$$

$$\begin{cases} \frac{-1}{\pi\sqrt{2}} ((\gamma - \ln 2 + \xi + \frac{1}{2} \ln q) (1 + \frac{1}{2} q \cosh 2\xi) - \frac{1}{2} q \sinh 2\xi), & \text{for } m = 0 \\ \frac{2^{2m-2} (m-1)! m!}{\pi q^m e^{m\xi}}, & \text{for } m \geq 1 \end{cases} \quad (4.46)$$

$$Fek'_m(\xi, -q) \rightarrow \begin{cases} \frac{-1}{\pi\sqrt{2}}, & \text{for } m = 0 \\ \frac{-2^{2m-2} m! m!}{\pi q^m e^{m\xi}}, & \text{for } m \geq 1 \end{cases} \quad (4.47)$$

$$D_m(q) \rightarrow \begin{cases} \frac{1}{\sqrt{2}} Fek'_0(0, -q), & \text{for } m = 0 \\ Fek'_m(0, -q), & \text{for } m \geq 1 \end{cases} \quad (4.48)$$

where  $\gamma$  in eq. (4.46) is the Euler constant.

First, let us concentrate on the monopole component, or  $m = 0$ , for the case of  $v \approx c$ . Substituting eqs. (4.44) - (4.48) into (4.38), the coefficient  $C_0$  for the monopole mode becomes

$$(1 - \beta^2) C_0 = \frac{\epsilon - 1}{\epsilon\pi} \left\{ \frac{\Psi_1^{(0)}}{\Psi_0^{(0)} + \frac{s \sinh 2\xi_b}{\epsilon} \Psi_1^{(0)}} \right\}, \quad (4.49)$$

where  $\Psi_0^{(0)}$  and  $\Psi_1^{(0)}$  are given in eqs. (4.39) and (4.40). Substituting eq. (4.49) into (4.42) then gives the longitudinal electric field as

$$E_z^{(0)}(\xi, \eta, z_0) = \frac{-2Q(\epsilon - 1)}{\epsilon\pi c^2} \operatorname{Re} \int_0^\infty d\omega i\omega \frac{\Psi_1^{(0)}}{\Psi_0^{(0)} + \frac{s \sinh 2\xi_b}{\epsilon} \Psi_1^{(0)}} e^{i\frac{\omega}{c}z_0}. \quad (4.50)$$

Here, the integral involving  $Fek_0$  can be neglected because the integrand involving  $Fek_0$  is real and has no poles when  $\beta^2 \rightarrow 1$ . Thus it does not make a contribution to the real part of the integral as  $\beta^2 \rightarrow 1$  and it is reduced to

$$(1 - \beta^2) \operatorname{Re} \int_0^\infty d\omega i\omega e^{i\frac{\omega}{v}z_0} \rightarrow 0. \quad (4.51)$$

The real part of the integral in eq. (4.50) comes from the contributions from the poles of the integrand. The integrand is purely imaginary and the real part can come only from the residues at the poles. From complex analysis, we know that

$$\int_{-\infty}^{\infty} \frac{f_1}{f_0} d\omega = 2\pi i \sum_l \left. \frac{f_1}{\frac{d}{d\omega} f_0} \right|_{\omega = \omega_l}. \quad (4.52)$$

From eq. (4.31), we have the relation

$$\frac{d}{d\omega} = \frac{ds}{d\omega} \frac{d}{ds} = \frac{2s}{\omega} \frac{d}{ds}, \quad (4.53)$$

then the longitudinal electric field of the monopole mode can be written as an infinite sum over all discrete harmonics as

$$E_z^{(0)} = \frac{4Q}{\epsilon h^2} \sum_l \left. \frac{\Psi_1^{(0)}}{\frac{d}{ds} (\Psi_0^{(0)} + \frac{s \sinh 2\xi_b}{\epsilon} \Psi_1^{(0)})} \right|_{s=s_l} \cos \frac{\omega_l}{c} z_0, \quad (4.54)$$

where  $s_l$  are the roots of

$$\Psi_0^{(0)} + \frac{s \sinh 2\xi_b}{\epsilon} \Psi_1^{(0)} = 0. \quad (4.55)$$

From eq. (4.31), the resonant frequencies  $\omega_\lambda$  are related to  $s_\lambda$  by

$$s_\lambda = \frac{h^2}{4} \left(\frac{\omega_\lambda}{c}\right)^2 (\epsilon - 1). \quad (4.56)$$

Notice that there is no  $\xi$  or  $\eta$  dependence of  $E_z^{(0)}$  in eq. (4.54). It is apparent from eq. (4.54) that there is no transverse wake fields associated with  $m = 0$  mode in the limit of  $v = c$ , since the transverse wake fields are related to the transverse gradient of  $E_z$  through the Panofsky-Wenzel theorem, eq. (2.34).

Similarly,  $E_z$  for  $m \geq 1$  can be found from eq. (4.42) as

$$\begin{aligned} E_z^{(m)} &= \frac{4Q}{\pi v^2} (1 - \beta^2) \sum_{m=0}^{\infty} c e_m(\eta, -q) c e_m(\eta_0, -q) \\ &\times \operatorname{Re} \int_0^{\infty} d\omega i\omega \frac{C e_m(\xi_0, -q)}{D_m(q)} (F e k_m(\xi, -q) + C_m C e_m(\xi, -q)) e^{i\frac{\omega}{v} z_0} \\ &\approx \frac{4Q}{\pi v^2} (1 - \beta^2) \sum_{m=0}^{\infty} c e_m(\eta, -q) c e_m(\eta_0, -q) \\ &\times \operatorname{Re} \int_0^{\infty} d\omega i\omega \frac{C_m}{D_m(q)} C e_m(\xi_0, -q) C e_m(\xi, -q) e^{i\frac{\omega}{v} z_0}. \end{aligned} \quad (4.57)$$

Again, by using the limiting values given in eqs. (4.44) - (4.48), we get

$$(1 - \beta^2) \frac{C_m}{D_m(q)} C e_m(\xi_0, -q) C e_m(\xi, -q) \approx -(1 - \beta^2) \frac{\cosh m \xi_0 \cosh m \xi}{m \sinh m \xi_b \exp(m \xi_b)} \quad (4.58)$$

and consequently the longitudinal electric field of the multipole mode becomes

$$\begin{aligned} E_z^{(m)} &\approx \frac{-4Q}{\pi v^2} \frac{\cos m \eta_0 \cosh m \xi_0}{m \sinh m \xi_b \exp(m \xi_b)} \cos m \eta \cosh m \xi \times (1 - \beta^2) \operatorname{Re} \int_0^{\infty} d\omega i\omega e^{i\frac{\omega}{v} z_0} \\ &\rightarrow 0, \text{ as } \beta \rightarrow 1. \end{aligned} \quad (4.59)$$

Here, we found that only monopole mode ( $m = 0$ ) is excited in a

dielectric loaded elliptical waveguide in the limit of the particle velocity  $v \rightarrow c$ . The contributions from multipole modes become negligible for the ultra-relativistic particles because  $E_z$  tends to zero as  $\gamma^{-2}$ .

The transverse wake fields can be calculated from the longitudinal wake field by using the Panofsky-Wenzel theorem, eq. (2.34):

$$\frac{\partial}{\partial z_0} \mathbf{W}_\perp = \nabla_\perp W_z = \nabla_\perp e E_z \quad (2.34)$$

where  $\nabla_\perp$  in the elliptical coordinates is given by

$$\nabla_\perp = \frac{1}{h \sqrt{\sinh^2 \xi + \sin^2 \eta}} \left( \hat{\xi} \frac{\partial}{\partial \xi} + \hat{\eta} \frac{\partial}{\partial \eta} \right). \quad (4.60)$$

As discussed earlier, there is no transverse wake fields associated with  $m = 0$  mode because  $E_z^{(0)}$  is independent of the transverse coordinates  $\xi$  and  $\eta$ . For  $m \neq 0$  modes, the transverse wake fields are found by substituting eq. (4.57) into (2.34). Again, using the limiting properties in eq. (4.64) - (4.68), we have

$$\begin{aligned} \frac{\partial}{\partial z_0} \mathbf{W}_\perp &= \nabla_\perp e E_z \\ &\rightarrow \text{constant} \times \nabla_\perp (\cos m \eta \cosh m \xi) \times (1 - \beta^2) \text{Re} \int_0^\infty d\omega i \omega e^{i \frac{\omega}{v} z_0} \\ &\rightarrow 0 \text{ as } \beta \rightarrow 1. \end{aligned} \quad (4.61)$$

We see again that in the vacuum region the transverse wake fields become negligible for the ultra-relativistic particles and tend to zero as  $\gamma^{-2}$ .

For the driving beam with an arbitrary charge distribution of  $\lambda(z)$ , the longitudinal electric field becomes

$$E_z^{(0)} = \frac{4Q}{\epsilon h^2} \sum_{\lambda} \frac{\Psi_1^{(0)}}{\frac{d}{ds} (\Psi_0^{(0)} + \frac{s \sinh 2\xi_b}{\epsilon} \Psi_1^{(0)})} \Big|_{s=s_{\lambda}} \int_{-\infty}^{z_0} \lambda(z) \cos \frac{\omega \lambda}{c} (z - z_0). \quad (4.62)$$

Let us consider the following two limiting cases. First, if the waveguide is completely filled with a medium ( $\xi_b = 0$ ), then eq. (4.54) is reduced to

$$E_z^{(0)} = \frac{4Q}{\epsilon h^2} \sum_{\lambda} \frac{C_{e0}(\xi_a, s) F_{ey0}(0, s) - C_{e0}(0, s) F_{ey0}(\xi_a, s)}{F_{ey0}'(0, s) \frac{dC_{e0}(\xi_a, s)}{ds}} \Big|_{s=s_{\lambda}} \cos \frac{\omega \lambda}{c} z_0, \quad (4.63)$$

where  $s_{\lambda}$  are roots of  $C_{e0}(\xi_a, s) = 0$ . Here,  $F_{ey0}'(0, s)$  has no pole since

$$F_{ey0}'(0, s) = \text{constant} \times c_{e0}\left(\frac{\pi}{2}, s\right) > 0 \quad (4.64)$$

for any  $s$ . When  $\xi_b \approx 0$  but finite, we see that the fields are little different from those in a completely filled waveguide because

$$\frac{dC_{e0}(\xi_b, s)}{d\xi} \approx 0 \quad (4.65)$$

for  $\xi_b \approx 0$ . The important fact is that a charge moving close to a medium radiates as if it were moving through a medium, and the fields in the vacuum is not very sensitive to the vacuum-dielectric boundary conditions.

When  $\xi_b \rightarrow \xi_a$ , we see that both  $\Psi_0^{(m)}$  and  $\Psi_1^{(m)}$  in eq. (4.54) become zero. Therefore, no wake fields are generated in the perfectly conducting smooth waveguide, as discussed previously in section 2.1.

#### 4. 3. 3. Transition to the Dielectric-Loaded Circular Waveguide

When the boundary ellipse degenerates into a circle, we get the equation for the wake fields excited in a dielectric-loaded circular waveguide. We can show this again by using the limiting properties of the Mathieu

functions given in Appendix A:

$$Ce_m(\xi, s) \rightarrow p_m J_m(kr), \quad (4.66)$$

$$Ce_m'(\xi, s) \rightarrow p_m kr J_m'(kr), \quad (4.67)$$

$$Fey_m(\xi, s) \rightarrow p_m N_m(kr), \quad (4.68)$$

$$Fey_m'(\xi, s) \rightarrow p_m kr N_m'(kr), \quad (4.69)$$

$$ce_m(\eta, -s) \rightarrow p_m \cos m\phi, \quad (4.70)$$

where  $p_m$  is a constant multiplier, and  $J_m$ ,  $N_m$  are respectively the Bessel functions of the first and second kinds. The relation between  $s$  and  $k$  is given by

$$2s = \frac{h^2}{2} \left(\frac{\omega}{v}\right)^2 (\epsilon\beta^2 - 1) = \frac{h^2 k^2}{2}. \quad (4.71)$$

From eq. (4.71), we have the relation

$$\frac{d}{ds} = \frac{2}{kh^2} \frac{d}{dk}. \quad (4.72)$$

If confocal ellipses with  $\xi = \xi_a$  and  $\xi = \xi_b$  become concentric circles of radius  $r = a$  and  $r = b$  respectively as shown in figure 4.2, then substituting eqs. (4.66) - (4.72) into (4.54) gives the longitudinal electric field  $E_z^{(0)}$  excited in the dielectric-loaded circular waveguide:

$$E_z^{(0)} = \frac{2Q}{\epsilon b} \sum_1 \frac{f_1^{(0)}}{\frac{d}{dk} (f_0^{(0)} + \frac{kb}{2\epsilon} f_1^{(0)})} \Big|_{k=k_1} \cos \frac{z_0}{v} \omega \lambda, \quad (4.73)$$

where

$$f_1^{(0)} = J_0(ka) N_0(kb) - J_0(kb) N_0(ka), \quad (4.74)$$

$$f_0^{(0)} = J_0(ka) N_0'(kb) - J_0'(kb) N_0(ka), \quad (4.75)$$

which is exactly the same equation as in ref. 18. Here,  $J_0$  and  $N_0$  are the zero order Bessel functions of the first kind and second kind respectively.

#### 4. 4. Numerical Example and Discussion

As an example, the longitudinal wake potential in the dielectric-loaded elliptical waveguide is calculated for the limiting case of  $v = c$ . The dimensions of the waveguide are shown in figure 4.3, and the driving beam with a Gaussian charge distribution of  $\sigma = 5$  mm is assumed. Figure 4.4 is a plot of the longitudinal wake potential in the vacuum when the dielectric constant is  $\epsilon = 2$  and vacuum hole is very narrow, i.e.,  $\xi_b \approx 0$ . Here, we obtain about 40 MeV/m acceleration gradient per 1 micro-Coulomb driving charge, while about 120 MeV/m was obtained in chapter 3 for the disk-loaded cavity which has the same cross sectional area. We found that in a dielectric-loaded elliptical waveguide only monopole mode ( $m = 0$ ) is excited and the transverse wake fields, which exist in the disk-loaded elliptical cavity, become zero as the particle velocity  $\beta \rightarrow 1$ . This result is very important when we consider using the dielectric-loaded waveguide as a wake-field acceleration device. It can support high accelerating gradient, but has no deflecting force which might lead to beam instabilities. The amplitude of the longitudinal electric field is a function of the transverse position of the driving beam. Since the longitudinal electric field is uniform within the vacuum region, we can inject the driving beam and accelerated beam at two different locations in the vacuum region so that staging becomes practical.

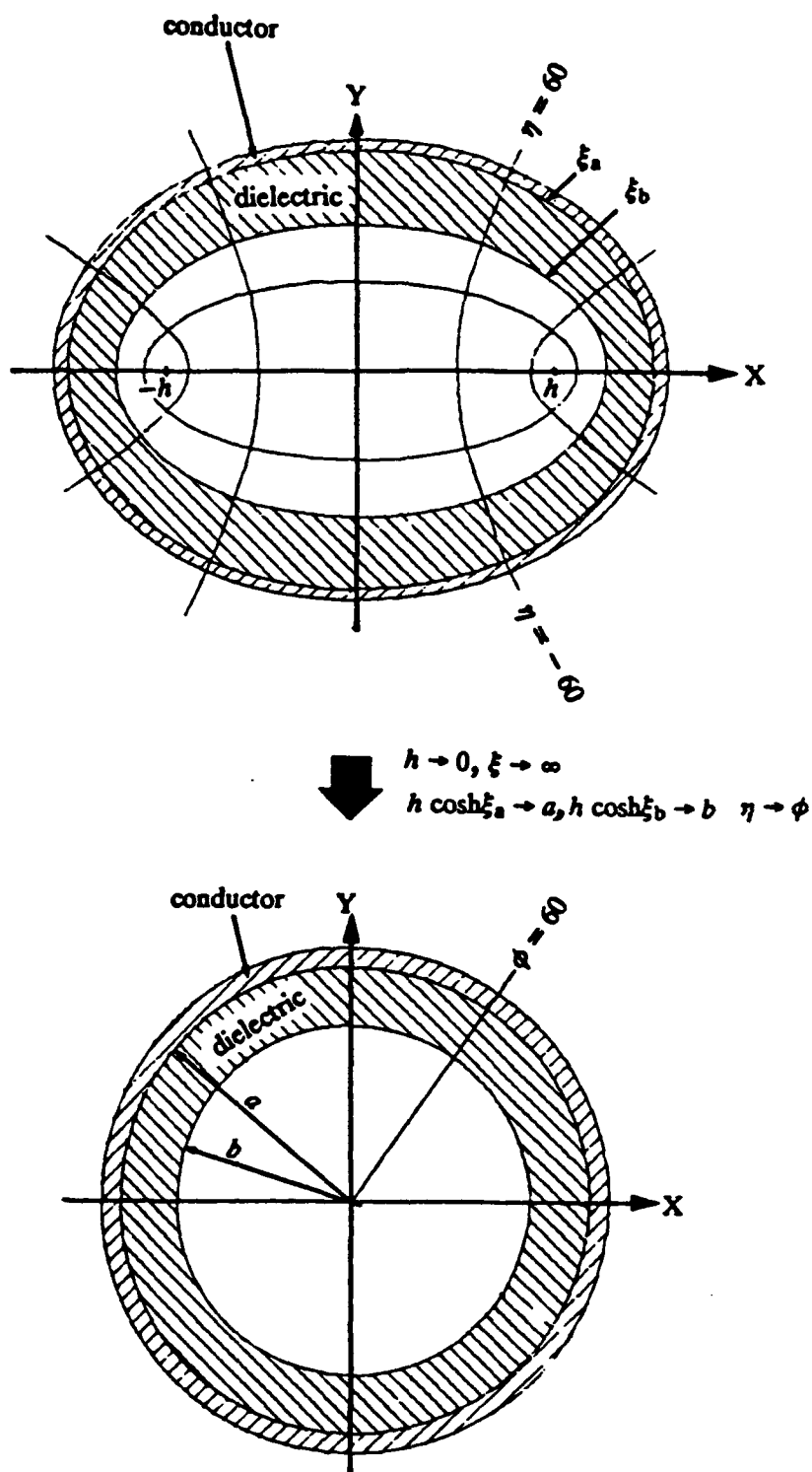


Figure 4.2. Transition to the dielectric-loaded circular waveguide

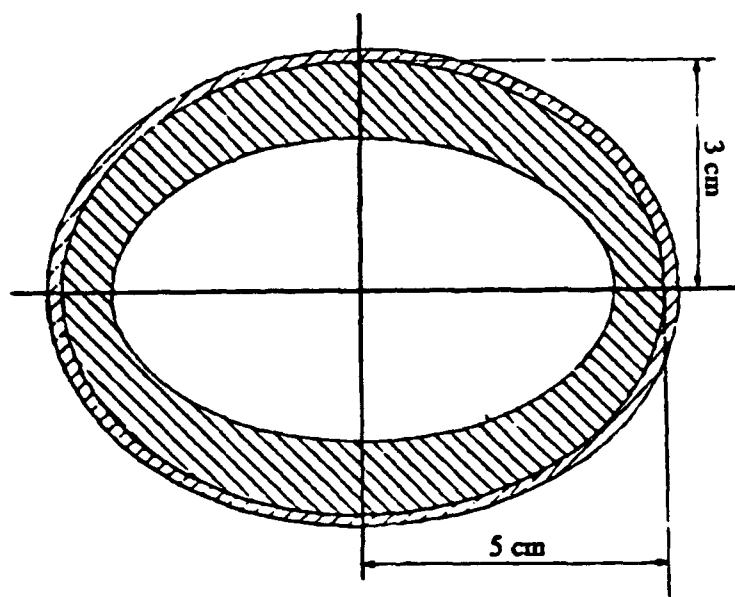


Figure 4.3. Dielectric-loaded elliptic waveguide dimensions

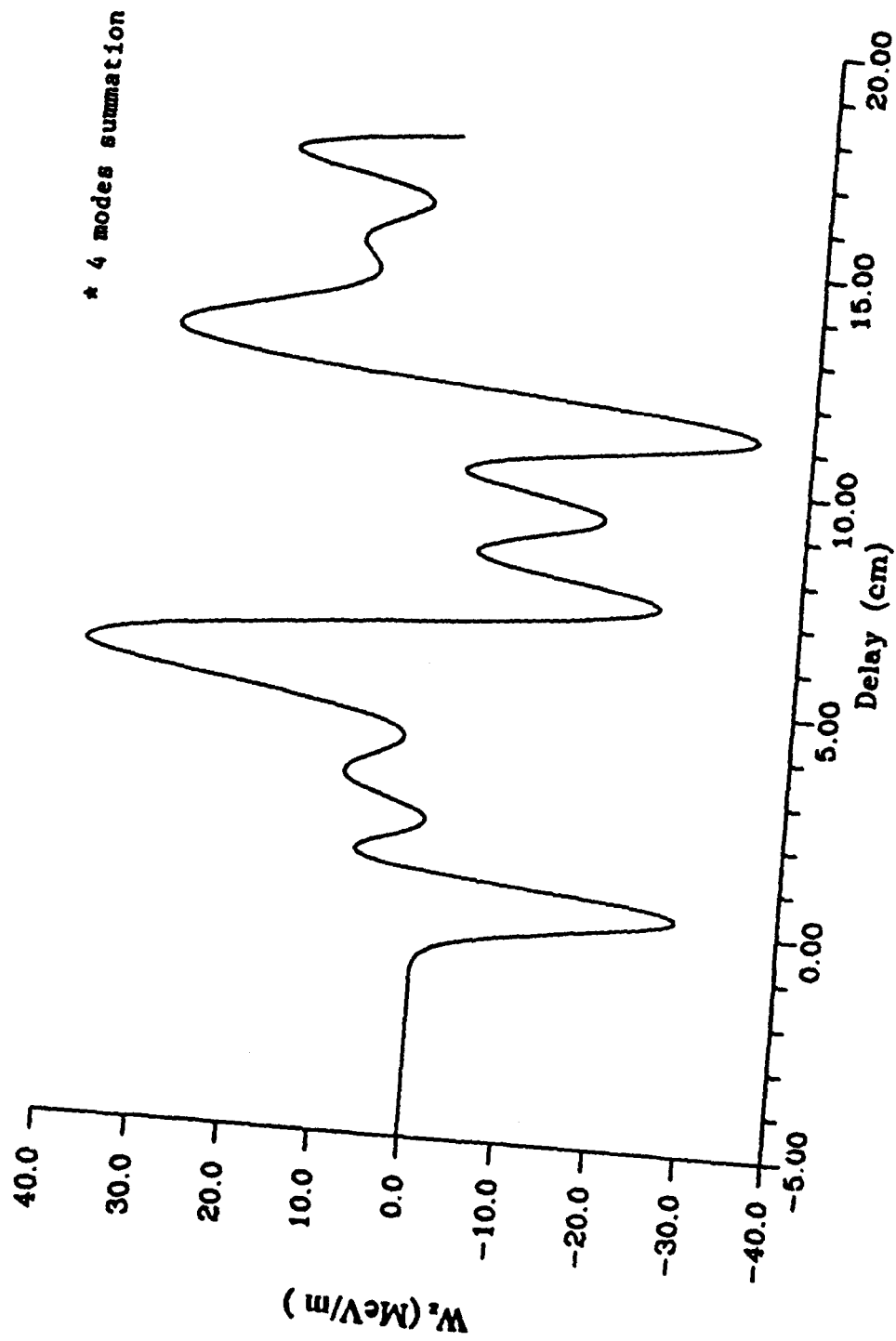


Figure 4.4. Longitudinal wake potential in a dielectric-loaded elliptical waveguide  
 ( $\epsilon = 2$ , major axis = 10 cm, minor axis = 6 cm)

## CHAPTER V

### SUMMARY AND CONCLUSIONS

Acceleration of charged particles by the wake fields produced by a bunch of relativistic charged particles passing through the elliptical wake-field cavities has been investigated. The expressions for the wake potentials have been derived analytically for the disk-loaded metallic cavity and dielectric-loaded waveguide. For the disk-loaded elliptical cavity, modal analysis method is used under the assumption of no aperture in a cavity, and the wake fields and wake potentials are derived in terms of the Mathieu functions. It is found that these analytical results agree well with the numerical analysis of Chin,<sup>22</sup> in which finite difference method is used to directly solve the Maxwell equations in the time domain. For a dielectric-loaded elliptical cavity, the longitudinal wake potential is derived analytically using Fourier transform method. It is shown that both disk-loaded and dielectric-loaded cavities can support an acceleration gradient in excess of a few hundred MeV/m. It is also found that strong transverse wake fields, which could be useful for the FEL application as an electric wiggler, are excited in the disk-loaded cavity, while no transverse wake fields are induced in a dielectric-loaded cavity for the ultra-relativistic driving beam.

The idea of wake-field acceleration by means of the elliptical cavity offers a promising way for reaching acceleration gradients of a few hundred MeV/m. The wake-field cavities discussed in the previous chapters do not represent the maximum acceleration gradient that can be achieved. The longitudinal wake potential or acceleration gradient is proportional to the num-

ber of particles in the driving beam, and inversely proportional to the cross sectional area of the cavity. Taking the parameters used in example calculations, an elliptical cavity with the major axis of 5 cm and the minor axis of 3 cm will yield 600 MeV/m/ $\mu\text{C}$ . Although the transformer ratio of this elliptical cavity is not as high, a wake-field accelerator not based on the impedance transformation principle can be achieved by using multi-stage scheme in which short stages are used with the driving beam which is replaced with new one or whose energy is replenished after each stage. For the elliptical cavity, we can simplify the replacement of decelerated driving beam considerably. The need for a fast kicker, or bending the driver beam can be eliminated. Furthermore, the fact that the wake-field devices are simply shaped metallic pill-boxes or waveguides partially filled with dielectric without any frequency tuning or phasing devices make this kind of accelerator unexpensive and reliable.

The limitations to achieving a high acceleration gradient should be pointed out. The principle limitation is due to breakdown and electrical discharges which may damage the metallic surface, dielectric breakdown, and change of dielectric properties. We do not concern ourselves with this problem about which little is known yet. However, breakdown limits are considered to be less severe than any other near-field accelerating devices since the high field strength exists only a limited area and only for a short period of time. Another difficulty is the production of very short, high current driving beam. A charge of 1  $\mu\text{C}$ , which corresponds to about  $6 \times 10^{12}$  electrons within the driving beam or a peak current of nearly 60 KA, could be achieved in the induction linac. The laser-driven photoinjector may allow a simpler solution to this problem.

As mentioned, we have made several simplifying assumptions in order to obtain the analytical solutions of the wake potentials in the elliptical cavity. Further investigations are needed on the following issues: (1) Beam aperture effects are not considered for the disk-loaded cavity. Although we have demonstrated that these analytical results are in good agreement with the results of the numerical code for the cavity with small apertures, large aperture will affect the calculation in both magnitudes and frequencies of the wake potentials. (2) The wake fields inside a driving beam can not be accurately calculated with this method due to the slow convergence of the modes summation, therefore we cannot calculate the energy loss of the driving beam accurately. (3) Beam dynamics calculation and instability study due to the transverse deflecting modes in the elliptical pill-box cavity. (4) Non-linear effects in the dielectric. A systematic numerical study will give a better picture of these wake fields problem.

APPENDIX A  
THE MATHIEU EQUATIONS AND MATHIEU FUNCTIONS

### A. 1. Canonical Form of the Mathieu Equation

The Mathieu equation is the particular case of a linear type of the second order differential equation with periodic coefficients, which has a form

$$\frac{d^2y}{dz^2} + (a - 2q \cos 2z)y = 0, \quad (\text{A.1})$$

where the parameters  $a$  and  $q$  are limited to real number, but  $z$  is usually unrestricted. For the present, we shall confine our attention to solutions having period  $\pi$  or  $2\pi$  in  $z$ . If we write  $i\xi$  for  $z$  in eq. (A.1), it becomes

$$\frac{d^2y}{d\xi^2} - (a - 2q \cosh 2\xi)y = 0 \quad (\text{A.2})$$

### A. 2. Periodic Solution of $y'' + (a - 2q \cos 2z)y = 0$

We have two types of solutions. one is even and the other is odd function in  $z$ . These solutions may be expressed in series forms as:

$$ce_{2n}(z, q) = \sum_{r=0}^{\infty} A_{2r}^{(2n)} \cos 2rz, \quad (\text{A.3})$$

$$ce_{2n+1}(z, q) = \sum_{r=0}^{\infty} A_{2r+1}^{(2n+1)} \cos(2r+1)z, \quad (\text{A.4})$$

$$se_{2n+2}(z, q) = \sum_{r=0}^{\infty} B_{2r+2}^{(2n+2)} \sin(2r+2)z, \quad (\text{A.5})$$

$$se_{2n+1}(z, q) = \sum_{r=0}^{\infty} B_{2r+1}^{(2n+1)} \sin(2r+1)z, \quad (\text{A.6})$$

for  $n = 0, 1, 2, \dots$ . In these series, the coefficients  $A_r^{(m)}$  and  $B_r^{(m)}$  are functions of  $q$ . The function  $ce_m(z, q)$  and  $se_m(z, q)$  are respectively the even and odd type Mathieu functions of the first kinds of integral order  $m$ . A

few of the lowest-order Mathieu functions are plotted in figures A.1. and A.2.

### A. 3. Solution of $y'' - (a - 2q \cosh 2\xi)y = 0$

The first solutions of eq. (A.2) are derived by substituting  $i\xi$  for  $z$  in eqs. (A.3) - (A.6). Thus, we have

$$Ce_{2n}(\xi, q) = ce_{2n}(i\xi, q) = \sum_{r=0}^{\infty} A_{2r}^{(2n)} \cosh 2r\xi, \quad (\text{A.7})$$

$$Ce_{2n+1}(\xi, q) = ce_{2n+1}(i\xi, q) = \sum_{r=0}^{\infty} A_{2r+1}^{(2n+1)} \cosh(2r+1)\xi, \quad (\text{A.8})$$

$$Se_{2n+2}(\xi, q) = -i se_{2n+2}(i\xi, q) = \sum_{r=0}^{\infty} B_{2r+2}^{(2n+2)} \sinh(2r+2)\xi, \quad (\text{A.9})$$

$$Se_{2n+1}(\xi, q) = -i se_{2n+1}(i\xi, q) = \sum_{r=0}^{\infty} B_{2r+1}^{(2n+1)} \sinh(2r+1)\xi. \quad (\text{A.10})$$

These are defined to be modified Mathieu functions of the first kind of integral order, and the capital letters are used to denote the modified functions.

### A. 4. Orthogonality and Normalization of Mathieu Functions

The Mathieu functions of the first kinds have the property that for a given  $q$ ,

$$\int_0^{2\pi} ce_m(z, q) ce_p(z, q) dz = \int_0^{2\pi} se_m(z, q) se_p(z, q) dz = 0 \quad \text{for } m \neq p. \quad (\text{A.11})$$

With this orthogonal property, various normalizations are possible. Here,  $ce_m(z, q)$  and  $se_m(z, q)$  are normalized according to

$$\frac{1}{\pi} \int_0^{2\pi} ce_m^2(z, q) dz = \frac{1}{\pi} \int_0^{2\pi} se_m^2(z, q) dz = 1 \quad (\text{A.12})$$

for all real values of  $q$ . The normalization in (A.11) entails a mean square value of  $1/2$  over the interval  $(0, 2\pi)$ , which is the same as that for the circular functions. Under this normalization, the coefficients  $A_r^{(m)}$  and  $B_r^{(m)}$  are given by the relation

$$2[A_0^{(2n)}]^2 + \sum_{r=1}^{\infty} [A_{2r}^{(2n)}]^2 = 1, \quad (\text{A.13})$$

$$\sum_{r=0}^{\infty} [A_{2r+1}^{(2n+1)}]^2 = \sum_{r=0}^{\infty} [B_{2r+1}^{(2n+1)}]^2 = \sum_{r=0}^{\infty} [B_{2r+2}^{(2n+2)}]^2 = 1. \quad (\text{A.14})$$

## A. 5. Degenerate Forms of Mathieu Functions

### A. 5. 1. Mathieu Functions of the First Kind

When the fundamental ellipse tends to a circle by letting  $h \rightarrow 0$ , hence  $q \rightarrow 0$ ,  $A_r^{(m)}$  and  $B_r^{(m)}$  in the series tend to zero except that  $A_m^{(m)} \rightarrow 1$  and  $B_m^{(m)} \rightarrow 1$ , and the confocal hyperbolae become radii of the circle with  $\eta = \phi$ . So, we have

$$ce_m(\eta, q) \rightarrow \begin{cases} \cos m\eta = \cos m\phi & \text{for } m \geq 1 \\ A_0^{(0)} = 1/\sqrt{2} & \text{for } m = 0 \end{cases} \quad (\text{A.15})$$

$$se_m(\eta, q) \rightarrow \sin m\eta = \sin m\phi \quad \text{for } m \geq 1. \quad (\text{A.16})$$

### A. 5. 2. Modified Mathieu Functions

When a confocal ellipse of semi-major axis  $r$  tends to a circle with this radius by letting  $h \rightarrow 0$ ,  $\xi \rightarrow \infty$  while keeping the product  $h \cosh \xi \rightarrow r$ , then  $a \rightarrow m^2$  for a function of integral order  $m$ . Consequently, eq. (A.2) degenerate to the standard Bessel equation:

$$\frac{d^2y}{dr^2} + \frac{1}{r} \frac{dy}{dr} + (k_1^2 - \frac{m^2}{r^2})y = 0, \quad (\text{A.17})$$

where  $2q = h^2 k_1^2/2$ . Thus we have the following degenerate cases:

$$Ce_m(\xi, q) \rightarrow p_m J_m(k_1 r), \quad (\text{A.18})$$

$$Se_m(\xi, q) \rightarrow s_m J_m(k_1 r), \quad (\text{A.19})$$

$$\frac{d}{d\xi} Ce_m(\xi, q) \rightarrow p_m k_1 r J_m'(k_1 r), \quad (\text{A.20})$$

$$\frac{d}{d\xi} Se_m(\xi, q) \rightarrow s_m k_1 r J_m'(k_1 r), \quad (\text{A.21})$$

$$Fey_m(\xi, q) \rightarrow p_m Y_m(k_1 r), \quad (\text{A.22})$$

$$\frac{d}{d\xi} Fey_m(\xi, q) \rightarrow p_m k_1 r Y_m'(k_1 r), \quad (\text{A.23})$$

$$Ce_{2n}(\xi, -q) \rightarrow p_{2n} I_{2n}(k_1 r), \quad (\text{A.24})$$

$$Ce_{2n+1}(\xi, -q) \rightarrow s_{2n+1} I_{2n+1}(k_1 r), \quad (\text{A.25})$$

$$Se_{2n+1}(\xi, -q) \rightarrow p_{2n+1} I_{2n+1}(k_1 r), \quad (\text{A.26})$$

$$Se_{2n+2}(\xi, -q) \rightarrow s_{2n+2} I_{2n+2}(k_1 r), \quad (\text{A.27})$$

$$\pi Fek_{2n}(\xi, -q) \rightarrow p_{2n} K_{2n}(k_1 r), \quad (\text{A.28})$$

$$\pi Fek_{2n+1}(\xi, -q) \rightarrow s_{2n+1} K_{2n+1}(k_1 r), \quad (\text{A.29})$$

where  $p_m, s_m$  are constant multipliers, and  $f'(x) = df(x)/dx$ .  $Fey_m(\xi, q)$  is a linearly independent second solution for positive  $q$ . For negative  $q$ , the solution of the form  $Fek_m(\xi, -q)$  is usually used.

#### A. 6. Limiting Forms of $Fey_m(\xi, q)$ and $Fek_m(\xi, -q)$ as $q \rightarrow 0$

$$Fey_0(\xi, q) \rightarrow \frac{\sqrt{2}}{\pi} (\gamma - \ln 2 + \xi + \frac{1}{2} \ln q) (1 - \frac{1}{2} q \cosh 2\xi) \quad (\text{A.30})$$

$$\begin{aligned} 2 Fek_0(\xi, -q) \\ \rightarrow -\frac{\sqrt{2}}{\pi} [(\gamma - \ln 2 + \xi + \frac{1}{2} \ln q) (1 + \frac{1}{2} q \cosh 2\xi) - \frac{1}{2} \sinh 2\xi] \end{aligned} \quad (\text{A.31})$$

$$Fey_m(\xi, q) \rightarrow -2^{2m-1} \Gamma(m) \Gamma(m+1) \pi^{-1} q^{-m} e^{-m\xi} \quad \text{for } m \geq 1 \quad (\text{A.32})$$

$$Fek_m(\xi, -q) \rightarrow -\frac{1}{2} Fey_m(\xi, q) \quad \text{for } m \geq 1 \quad (\text{A.33})$$

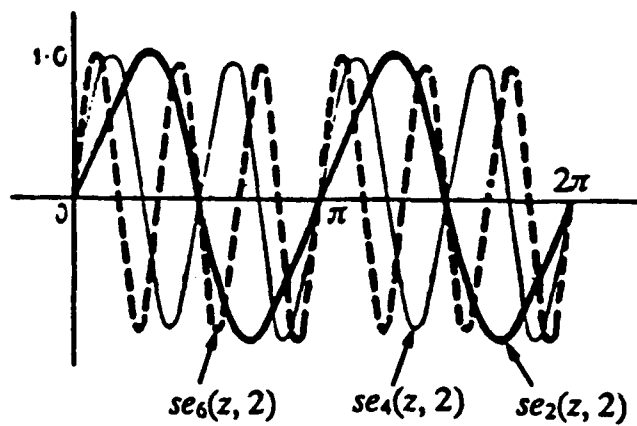
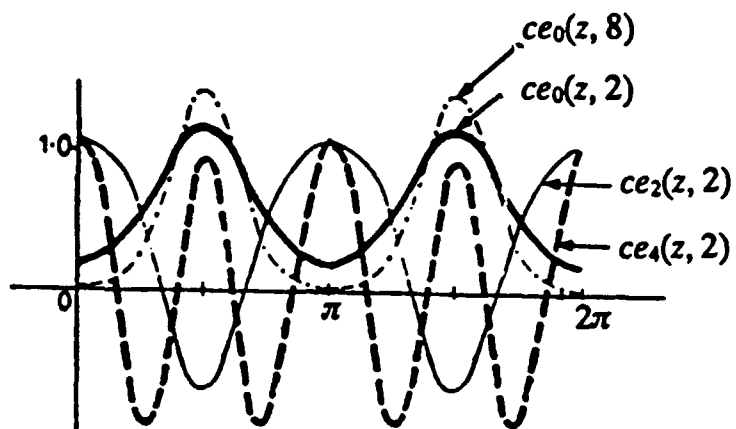


Figure A.1. Mathieu function of the first kind of even integral order  $ce_m(z, q)$  and  $se_m(z, q)$

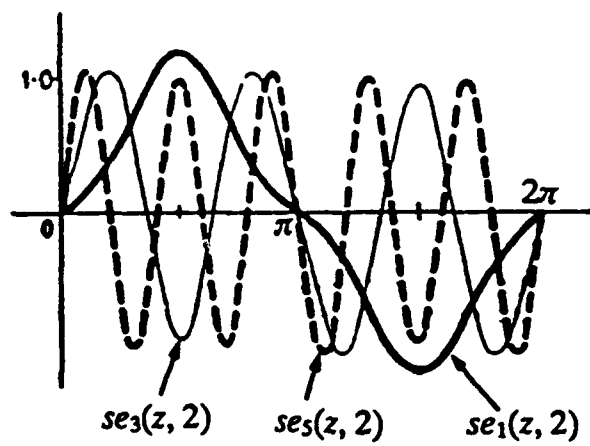
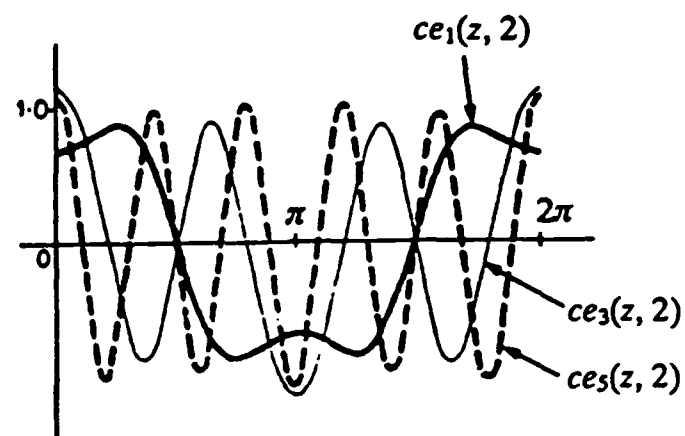


Figure A.2. Mathieu function of the first kind of odd integral order  $ce_m(z, q)$  and  $se_m(z, q)$

## REFERENCES

1. P. Sprangle, E. Esarey, A. Ting and G. Joyce, *Appl. Phys. Lett.* 53 (1988)
2. E. Esarey, A. Ting, P. Sprangle and G. Joyce, *Comments Plas na Phys. Controlled Fusion*, Vol 12, No. 4 (1989)
3. T. Tajima and J. M. Dawson, *Phys. Rev. Lett.* 43, 267 (1979)
4. T. Katsouleas and J. M. Dawson, *Phys. Rev. Lett.* 51, 392 (1983)
5. C. M. Tang, P. Sprangle and R. Sudan, *Appl. Phys. Lett.* 45, 375 (1984)
6. P. Chen, J. M. Dawson, R. W. Huff and T. Katsouleas, *Phys. Rev. Lett.* 54, 693 (1985)
7. R. Ruth, A. Chao, P. Morton and P. Wilson, *Particle Accelerators* 17, 171 (1985)
8. P. Chen and J. M. Dawson, in *Laser Acceleration of Particles, AIP Conf. Proceedings* No. 130, AIP, New York (1986)
9. J. B. Rosenzweig, D. B. Cline, B. Cole, H. Figueroa, W. Gai, R. Konecney, J. Norem, P. Schessow and J. Simpson, *Phys. Rev. Lett.* 61, 98 (1989)
10. G. A. Voss and T. Weiland, *DESY Publication* M82-010 (1982) and M82-074 (1982)
11. T. Weiland and B. Zotter, *Particle Accelerators*, Vol. 11, pp143-151 (1981)
12. K. L. F. Bane, P. B. Wilson and T. Weiland, in *Physics of High Energy Particle Accelerators, AIP Conf. Proceedings* No. 127, AIP, New York (1983)
13. K. W. Chen and S. H. Kim, *Proc. of 6th International Conference on High Power Particle Beams*, Kobe, Japan, June (1986)
14. H. Figueroa, W. Gai, R. Konecney, J. Norem, A. Ruggiero, P. Scoessow and J. Simpson, *Phys. Rev. Lett.* 60, 2144 (1988)

15. R. Keinigs, M. E. Jones and W. Gai, *Los Alamos Report*, No. LA-UR-88-1822 (1988), and *Argonne Report* ANL-HEP-PR-88-27 (1988)
16. W. Gai, P. Schoessow, B. Cole, R. Koncney, J. Norem, J. Rosenzweig and J. Simpson, *Phys. Rev. Lett.* 61, 2756 (1988)
17. G. Ruggiero, *Argonne Report*, ANL-HEP-CP-85-07 (1985)
18. K. L. F. Bane, P. Chen and P. B. Wilson, *IEEE Trans. on Nuclear Science*, NS-32, 3524 (1985)
19. S. H. Kim, *J. Plasma Phys.* 36, 195 (1986); Corrigendum 41, 577 (1989); *Phys. Rev. Lett.* 135A, 39 (1989)
20. J. S. Yang and K. W. Chen, "Closed Form Solution of Wake Potential in an Elliptic Pillbox Cavity by using Coordinate Transformation", *Proc. of 1989 Workshop on Advanced Accelerator Concepts*, Lake Arrowhead, Jan. (1989)
21. J. S. Yang and K. W. Chen, "Wakepotential in a Semi-Elliptic Pillbox Cavity", *Proc. of 1989 Workshop on Advanced Accelerator Concepts*, Lake Arrowhead, Jan. (1989)
22. Y. Chin, *KEK Report*, 83-19 (1983)
23. K. W. Chen and S. H. Kim, *SPIE* Vol. 875 (SPIE, Bellingham, WA 1988), pp. 223-233
24. J. D. Jackson, *Classical Electrodynamics*, John Wiley & Sons Inc.
25. P. L. Morton, V. K. Neil and A. M. Sessler, *J. Appl. Phys.* 37, 3875 (1966)
26. A. Chao, *AIP Conf. Proc.* No. 105, (AIP, New York, 1983), PP. 353-523
27. T. Weiland, *Particle Accelerators*, 15, pp. 245-292 (1984)
28. T. Weiland, *Proc. of 11th International Conf. on High Energy Accelerators*, Geneva, (1980) pp. 570-575
29. R. Klatt and T. Weiland, *SLAL Report*, SLAC-Report-303, pp. 282-285 (1986)
30. W. H. Panofsky and W. A. Wenzel, *Rev. Sci. Instrum.* 27, 967 (1956)

31. N. W. McLachlan, *Theory and Application of Mathieu Function*, Dover Pub. Inc.
32. *Tables of the Elliptic Cylinder Functions*, Proc. Royal Society, Edinburg, 52, 355 (1932)
33. *Handbook of Mathematical Functions*, Dover Pub. Inc.
34. G. Arfken, *Mathematical Methods for Physicists*, 3rd Edition, Academic Press, Inc.
35. B. M. Bolofovskii, *USP. Fiz. Nauk* 75, 295-350, Oct. (1961)
36. W. Gai, in *Advanced Accelerator Concepts*, AIP Conf. Proc. No. 193, 111, AIP, NY (1989)
37. P. B. Wilson, in *Physics of Particle Accelerators*, AIP Conf. Proc. No. 184, Vol. 1, AIP, NY (1989)

## GLOSSARY

$a$	Separation constant
$a_\lambda(\mathbf{x})$	vector eigenfunction
$A(\mathbf{x}, t)$	vector potential
$A_m$	Arbitrary constant
$A_i^{(m)}$	Coefficients for the series representation of $ce_m(\eta, q)$ and $Ce_m(\xi, q)$
$B(\mathbf{x}, t)$	Magnetic flux density
$B_m$	Arbitrary constant
$B_i^{(m)}$	Coefficients for the series representation of $se_m(\eta, q)$ and $Se_m(\xi, q)$
$c$	Speed of light
$ce_m(\eta, q)$	Even type Mathieu function of the first kind of integral order $m$
$Ce_m(\xi, q)$	Modified Mathieu function of the first kind of integral order $m$
$C_m$	Arbitrary constant
$C_{mn}$	Coefficient in the longitudinal wake potential
$\bar{C}_{mn}$	Coefficient in the transverse wake potential
$d$	Gap distance of an elliptical pillbox cavity
$D(\mathbf{x}, t)$	Electric flux density
$D_m(q)$	Wronskian relation $D_m(q) = Ce_m(0, -q)Fek_m'(0, -q) - Ce_m'(0, -q)Fek_m(0, -q)$
$e_c$	Eccentricity of the boundary ellipse

$E(\mathbf{x}, t)$	electric field
$Fey_m(\xi, q)$	Y-type Mathieu function of the second kind
$Fek_m(\xi, -q)$	K-type Mathieu function of the second kind
$h$	Semi-interfocal distance of an ellipse
$H(\mathbf{x}, t)$	Magnetic field
$i$	$\sqrt{-1}$
$\mathbf{J}$	Current density
$J_m(x)$	Bessel function of the first kind of integral order $m$
$\mathbf{k}$	Wave vector
$k_c$	Transverse component of wave vector $\mathbf{k}$
$k_z$	Longitudinal component of wave vector $\mathbf{k}$
$L$	length of a cavity
$\min(t, L/c)$	Minimum of $t$ and $L/c$
$\mathbf{n}$	Unit normal vector
$N_m(x)$	Bessel function of the second kind of integral order $m$
$p_m$	Constant multiplier
$q_\lambda(t)$	Time dependent coefficients of the vector potential $A(\mathbf{x}, t)$
$q_{mn}$	Parameters in the Mathieu functions
$Q$	Charge of a point source
$r_a$	Outer radius of dielectric-loaded circular cavity
$r_b$	Radius of dielectric-vacuum interface of dielectric-loaded circular cavity
$r_\lambda(t)$	Time dependent coefficient of the scalar potential $\varphi(\mathbf{x}, t)$

$r_0$	Transverse coordinate of the driving charge
$R_0$	Radius of a circular pillbox cavity
$\text{Re } z$	Real part of complex number $z$
$s$	Parameter related to the transverse wave number in dielectric
$se_m(\eta, q)$	Odd type Mathieu function of the first kind of integral order $m$
$Se_m(\xi, q)$	Modified Mathieu function of the first kind of integral order $m$
$s_m$	Constant multiplier
$S$	Cross sectional area of an elliptic pillbox cavity
$t$	Time
$T_\lambda$	Normalizing factor of the scalar eigenfunction $\phi_\lambda$
$u_\lambda$	Normalizing factor of the vector eigenfunction $\mathbf{a}_\lambda$
$U_\perp(z_0)$	Transverse wake potential of distributed charges
$U_z(z_0)$	Longitudinal wake potential of distributed charges
$v$	velocity of a particle
$V$	volume of a cavity
$V_\lambda(\mathbf{r})$	voltage induced by the driving charge at the transverse position $\mathbf{r}$
$W_\perp(z_0)$	Delta function transverse wake potential
$W_z(z_0)$	Delta function longitudinal wake potential
$\mathbf{x}$	Spatial coordinates
$(x, y, z)$	Cartesian Coordinates
$x_b$	Semi-major axis of the boundary ellipse

$y_b$	Semi-minor axis of the boundary ellipse
$\mathbf{z}$	Unit vector in z-direction
$z_0$	Delay distance between the driving and test charge
$\beta$	Normalized velocity $\beta = v/c$
$\chi_{0n}$	$n^{\text{th}}$ root of Bessel function $J_0(x)$
$\delta_{\mu\mu'}$	Kronecker delta
$\Delta$	Jacobian $\Delta = \left  \frac{\partial(x, y)}{\partial(\xi, \eta)} \right $
$\epsilon$	Permittivity of dielectric
$\epsilon_0$	Permittivity of vacuum
$\epsilon_p$	1/2 for $p = 0$ and 1 for $p \neq 0$
$\phi_\lambda(\mathbf{x})$	Scalar eigenfunctions
$\Phi_m(\xi, \omega)$	Scalar potential in the frequency domain
$\varphi(\mathbf{x}, t)$	Scalar potential
$\gamma$	Relativistic factor $\gamma = (1 - \beta^2)^{-1/2}$
$\lambda(z)$	Line charge density of the driving bunch
$\mu$	Permeability of dielectric
$\mu_0$	Permeability of vacuum
$\rho$	Charge density
$\sigma$	rms length of a Gaussian bunch
$\omega_\lambda$	Resonant frequencies
$(\xi, \eta, z)$	Confocal elliptical coordinates

$\xi_a$	$\xi$ at the boundary ellipse
$\xi_b$	$\xi$ at the dielectric-vacuum interface
$(\xi_0, \eta_0)$	Transverse coordinates of the driving charge